

**Remotely Sensed Data for High Resolution Agro-Environmental Policy Analysis**

Submitted in partial fulfillment of the requirements for

the degree of

Doctor of Philosophy

in

Engineering and Public Policy

**Paul Welle**

B.S., Environmental Engineering, Massachusetts Institute of Technology

Department of Engineering and Public Policy

Carnegie Mellon University

Pittsburgh, PA

August, 2017

## DEDICATION

*To Clara, of course*

## ACKNOWLEDGEMENTS

I would like to acknowledge support from my adviser, Meagan Mauter, for her indispensable advice and encouragement these last three years. I would also like to thank the other three members of my committee for their steadfast support— Granger Morgan, Jay Whitacre, and Nicholas Muller.

Besides the committee, I have very much benefited from collaborations with researchers from various institutions – Inês Lima Azevedo, Mitchell Small, Scott Doney, Sarah Cooley, Joshua Viers, Josue Medellín-Azuara, Siamak Ravanbakhsh, Barnabás Póczos, Karen Clay, and no doubt many others who took time to listen and give counsel.

I would also like to thank friends and student collaborators for their insights and in depth conversations, including Daniel Posen, Hassan Khan, Katherine McMahon, Stephanie Seki, Shuchi Talati, Leslie Abrahams, Kathrin Kirchen, Catherine Zhu, Momin Ghalib, and the entire We<sup>3</sup> lab for their support.

Lastly, this effort would not have been possible without my mother and siblings, who have been there for me always.

I have been very fortunate to have been funded by the Climate and Energy Decision Making Center (SES-0949710) for my first year and half, and then a National Science Foundation Graduate Research Fellowship Program under Grant No. (DGE-1252522) for the remainder of my degree. Additionally I was awarded a Bradford & Diane Smith Fellowship for 2014-2015. Research in this dissertation was also supported by the National Science Foundation under award number SEES-1215845 and CBET-1554117, as well as a gift from GreatPoint Ventures.

## COMMITTEE

### **Meagan Mauter, Ph.D. (chair)**

Associate Professor

Engineering and Public Policy & Civil and Environmental Engineering

Carnegie Mellon University

### **M. Granger Morgan, Ph.D.**

Hamerschlag University Professor of Engineering

Engineering and Public Policy, Electrical and Computer Engineering & Heinz College

Carnegie Mellon University

### **Nicholas Muller, Ph.D., MPA**

Associate Professor

Department of Economics and Environmental Studies Program

Middlebury College

### **Jay Whitacre, Ph.D.**

Professor

Engineering and Public Policy & Materials Science and Engineering

Carnegie Mellon University

## ABSTRACT

Policy analyses of agricultural and environmental systems are often limited due to data constraints. Measurement campaigns can be costly, especially when the area of interest includes oceans, forests, agricultural regions or other dispersed spatial domains. Satellite based remote sensing offers a way to increase the spatial and temporal resolution of policy analysis concerning these systems.

However, there are key limitations to the implementation of satellite data. Uncertainty in data derived from remote-sensing can be significant, and traditional methods of policy analysis for managing uncertainty on large datasets can be computationally expensive. Moreover, while satellite data can increasingly offer estimates of some parameters such as weather or crop use, other information regarding demographic or economic data is unlikely to be estimated using these techniques. Managing these challenges in practical policy analysis remains a challenge.

In this dissertation, I conduct five case studies which rely heavily on data sourced from orbital sensors. First, I assess the magnitude of climate and anthropogenic stress on coral reef ecosystems. Second, I conduct an impact assessment of soil salinity on California agriculture. Third, I measure the propensity of growers to adapt their cropping practices to soil salinization in agriculture. Fourth, I analyze whether small-scale desalination units could be applied on farms in California in order mitigate the effects of drought and salinization as well as prevent agricultural drainage from entering vulnerable ecosystems. And fifth, I assess the feasibility of satellite-based remote sensing for salinity measurement at global scale.

Through these case studies, I confront both the challenges and benefits associated with implementing satellite based-remote sensing for improved policy analysis.

## TABLE OF CONTENTS

Chapter 1: Introduction .....	12
Chapter 2: Estimating the effect of multiple environmental stressors on coral bleaching and mortality ...	17
2.1 Introduction.....	17
2.2 Methods .....	23
2.2.1 Data .....	23
2.2.2 Statistical Modelling .....	29
2.3 Results.....	30
2.3.1 Mortality.....	31
2.3.2 Bleaching.....	33
2.3 Discussion.....	37
References.....	38
Chapter 3: High-resolution model for estimating the economic and policy implications of agricultural soil salinization in California.....	41
3.1 Introduction.....	41
3.2 Methods .....	44
3.2.1 Disaggregated Approach for Estimating Yield and Revenue Losses from Soil Salinization	44
3.2.2 Aggregated Approach for Estimating Yield and Revenue Losses from Soil Salinization ....	45
3.2.3 Case study: California Yield and Revenue Losses from Soil Salinization .....	46
3.2.4 Statistical Analysis .....	47
3.3 Results.....	47
3.3.1 Results of Adopting a Disaggregated Approach for Estimating Yield and Revenue Losses from Soil Salinization in CA.....	47
3.3.2 Results of Adopting an Aggregated Approach to Estimating Yield and Revenue Losses from Soil Salinization in CA .....	50
3.4 Discussion.....	52
References.....	55
Chapter 4: Assessing the magnitude of crop switching due to salinity in the Central Valley of California .....	57
4.1 Introduction.....	57
4.2 Methods .....	59
4.2.1 Downscaling Land Use Data.....	60
4.2.2 Independent Variables .....	61
4.2.3 Modeling .....	62
4.2.4 Policy Analysis.....	63
4.3 Results and Discussion .....	65
4.3.1 Behavioral Results .....	65
4.3.2 Policy Scenario.....	68
References.....	70
Chapter 5: Economic and Policy Drivers of Agricultural Water Desalination in California’s Central Valley.....	72
5.1 Introduction.....	72
5.2 Methods .....	74

5.2.1	Private Costs.....	75
5.2.2	Private Benefits .....	76
5.2.3	Public Costs.....	79
5.2.4	Public Benefits .....	80
5.3	Results.....	81
5.3.1	Private Benefits of Improved Water Quality.....	82
5.3.2	Private Benefits of Improved Water Supply .....	82
5.3.3	Public Air Emissions Costs .....	84
5.3.4	Public Benefits of Agricultural Drainage Treatment .....	84
5.4	Discussion.....	85
	References.....	89
Chapter 6: Assessing the Feasibility of Remote Sensing of Soil Salinity at Global Scale .....		92
6.1	Introduction.....	92
6.2	Methods .....	96
6.2.1	Overview .....	96
6.2.2	Data .....	97
6.2.3	Modelling Approaches .....	99
6.3	Results.....	101
6.3.1	Ordinary Least Squares .....	101
6.3.2	Neural Networks .....	104
6.3.3	Model Comparison.....	105
6.4	Discussion.....	105
	References.....	108
Chapter 7: Conclusions.....		110
APPENDIX A: Chapter 2 .....		115
8.1	Spatial Distribution .....	115
8.2	Addressing Multi-Collinearity .....	115
8.3	Functional Forms for the Regressions .....	116
8.4	Using k-fold Cross-Validation to Identify the Best Model.....	117
8.5	Within-Region Correlation Tables.....	118
APPENDIX B: Chapter 3 .....		122
9.1	Data for Case Study .....	122
9.1.1	NASS County Commissioner Data.....	122
9.1.2	NASS Cropland Data Layer:.....	123
9.1.3	Gridded Soil Survey Geographic (gSSURGO) Database .....	124
9.1.4	Computing.....	127
9.2	Bias Removal.....	127
9.3	Uncertainty Analysis.....	128
9.4	Performance of Crop Classifier .....	130
9.5	Grower Adaptation.....	132
9.6	Estimating Calorie Losses Associated with Soil Salinization in California .....	134
9.7	Statistical Analysis.....	135
9.8	Symbols .....	138
APPENDIX C: Chapter 4 .....		140

APPENDIX D: Chapter 5 .....	143
11.1 Air Emission Damage Analysis .....	143
11.2 Defining Environmentally Sensitive Areas.....	146
11.3 Irrigation Salinity Data .....	147
11.3.1 Modelling Water Salinity .....	147
11.3.2 Averaged Modelling Results .....	148
11.3.3 Surface Water and Groundwater Estimates.....	149
11.3.4 Sensitivity of Results to Modelling Choices .....	150
11.4 List of Symbols .....	152
11.4.1 Variables .....	152
11.4.2 Subscripts: .....	153
References.....	154
APPENDIX E: Chapter 6.....	155

## LIST OF FIGURES

Figure 2-1. Temporal distribution of observations. Figures on the left column refer to bleaching, and those on the right refer to mortality. Figures 2-1A and 2-1B show the average DHW in the observed locations for the region of analysis between May 2005 and January 2007. Figures 2-1C and 2-1D show the number of observations,  $x$ , with 0%,  $0% < x < 30%$ , or  $x > 30%$  bleaching or mortality. Since the number of observed sites varies over time, in Figures 2-1E and 2-1F we show the share of observations in each distribution bin over time. The left and right panels for DHW, Figures 2-1A and 2-1B, differ because the observations available for mortality are a subset of those available for bleaching ..... 24

Figure 2-2. Population density in people per km<sup>2</sup> (in blue) and coral observations (red dots). Figure produced by the authors using data from the GPWv4 dataset. .... 26

Figure 2-3. Marine Ecoregions of the World (MEOW) regions. Red points represent coral observations. 29

Figure 2-4. Relative effects of temperature (DHW), solar radiation (PAR), depth, and distance from shore (DFS). In Figure 2-4A, the predicted coral mortality is displayed while holding each stressor at the 5<sup>th</sup> percentile and 95<sup>th</sup> percentile of its observed values in the sample (while all other stressors are held at their mean). The error bars represent plus/minus two standard errors of the expected value. In Figure 2-4B the analogous information is reported using bleaching as the dependent variable..... 36

Figure 3-1. Spatially resolved estimates of (A) soil salinity, (B) relative yield, (C) revenue lost per acre calculated with disaggregated data, and (D) revenue lost by county using aggregated data. .... 49

Figure 3-2. Aggregate and per crop relative yield and revenue losses. (A) Cumulative density function of revenue lost per acre and relative yield. (B) Relative yield by crop. (C) Total revenue lost by crop. Other High Uncertainty Crops (OHUC) include those crops that cannot be consistently estimated (see Figure S3 in Appendix B) using remote sensing. These include broccoli, carrots, celery, corn, lettuce, peaches and peppers. .... 50

Figure 4-1. Estimated marginal effects vs. crop groups ranked by salt tolerance for tree crops (A), vegetables (B), and a miscellaneous category (C). .... 68

Figure 4-2. Estimated revenue change from baseline values with salinity altered parametrically (A) and salinity set to its reported ‘low’, ‘mid’, and ‘high’ estimates according to the SSURGO data. .... 69

Figure 5-1. Marginal value of improved water quality and additional water supply. A) Marginal value of removing dissolved solids from a cubic meter of irrigation water, while holding the volume of irrigation water constant. B) Marginal value of an additional acre-ft of irrigation water at salinities equivalent to current irrigation water (490 ppm TDS)[1] under pre-drought (2010) and future climate (2050) scenarios. C) Marginal value of an additional cubic meter of irrigation water under drought scenarios represented by water availability in 2014. One acre-ft is equivalent to 1233 m<sup>3</sup>. .... 83

Figure 5-2. Private and public benefits and costs by crop and land area. A) CDF of private benefits for improved water quality and summed benefits of improved water quality and augmented supply in 2010 and 2014. B) Estimated air emission damages per unit of desalinated water for the gas powered thermal (GT), grid-powered reverse osmosis (RO), and solar-powered thermal systems (ST). C) CDF of private benefits minus social costs (the benefit gap) for GT, RO, and ST systems for 2010 and 2014 values of augmented supply. This benefit gap represents the minimum ecosystem valuation required for desalination technologies to have net societal benefits. .... 85

Figure 6-1. Visual representation of data preparation. Around the original salinity measurement (red dot) a grid of 32 x 32 Landsat 5 pixels are taken. This is done for all Landsat images taken within three years of the observation. The green squares indicate the data used in the ordinary least squares and artificial neural networks approach, while the entire image is used in the convolutional neural network approach. .... 96

Figure 6-2. Histogram of salinity observations. Blue bars represent all salinity values (n=3672) and green bars represent the agriculture only subset (n=1064). .... 99

Figure 6-3. In sample results from the ordinary least squares approach. A and B show the results from the agriculture only subset, while C and D show the results from all of the data. A and C show the regression of the natural log of electrical conductivity on Canopy Response Salinity Index (CRSI) using a univariate regression. B and D show the results of the multivariate regression using all parameters. CRSI performed the best of all the vegetation indices for each regression. .... 103

Figure 6-4. Out of sample results from the artificial neural network (A) and the convolutional neural network (B). In A, the results from the best-performing ANN which utilized all of the data and the 'average' formulation. Blue line represents perfect prediction. .... 104

## LIST OF TABLES

Table 2-1. Summary of variables.....	28
Table 2-2. Variables included in the estimation models, description, and units.....	31
Table 2-3. Results for the regression model of coral mortality as a function of different explanatory variables.....	33
Table 2-4. Results for the regression model of coral bleaching as a function of different explanatory variables.....	35
Table 4-1. Average Marginal Effects and Normalized Average Marginal Effects.....	67
Table 6-1. Out of sample measures of fit for OLS, ANN, and CNN models for full dataset.....	105

## Chapter 1: Introduction

The effectiveness of quantitative policy analysis is contingent on the availability of high-quality data that can illuminate the likely outcomes of different management alternatives. In agricultural and environmental systems, such data has typically been a limiting factor due to the vast spatial domains involved. While *in situ* sensors can act as point estimates which yield information in their immediate surroundings, they often fail to offer details regarding the system as a whole. For these reasons, data obtained by remote sensing from orbital sensors may offer a path to substantially improving policy analysis pertaining to agricultural and environment systems.

The first satellite launched for earth observation was the Earth Resource Technology Satellite, later renamed Landsat 1 in 1973. It imaged the Earth in eighteen day cycles across seven bands in the visible and near-infrared spectrum, producing images with a spatial resolution of 80 meters.

Since the launch of Landsat 1, hundreds of satellites have been placed in orbit in order to study the Earth system. There are currently 373 active satellites whose primary purpose is earth observation, and each has variety of capabilities and characteristics. Satellites such as Worldview-2 and Worldview-3 produce images with sub 1-meter spatial resolution. Other instruments, such as NASA's Moderate Resolution Imaging Spectroradiometer (MODIS), are capable of surveying the Earth every 1-2 days. And the Hyperion instrument aboard Earth Observing 1 catalogs data across 220 different spectral bands.

The net result of these data collection efforts is a rich archive that is continuously being collected on the Earth system. Information which was historically only available at aggregated scales (e.g. county, state, or country) are increasingly available at high-resolutions and global scales. For example, Burke et al. [1] were able to develop a method of measuring yields in maize from satellite data, allowing for new high-resolution data and increased crop data availability in parts of the world without strong conventional data collection routines. You et al. [2] developed an approach for generating crop area estimates with 10 km resolution at a global scale using a mixture of satellite data and crop modelling. Allen et al. [3] were able

to successfully measure crop water use from satellite data through an energy balance by estimating the latent heat of evaporation, an approach which produces data on crop water use at the field scale.

Famiglietti et al. [4] and Rodell et al. [5] were able to measure groundwater depletion in the Central Valley of California and India, providing measurements of resource drawdown in important agricultural regions. And Jean et al. [6] were able to predict poverty using machine learning techniques and nighttime satellite imagery, contributing data on household consumption and asset wealth in rural Africa.

Remotely sensed data supplies information that has higher resolution and broader spatial extent than traditional data sources. Each of the above datasets supplies new information which could be used to address difficult problems in the policy domain. High-resolution land cover data has wide applicability across agricultural and environmental analyses and can be used to monitor land use change with possible applications to biofuels or urbanization. Data on crop water use could have application to how farmers respond to drought. Data on yields, groundwater availability, and socioeconomic factors can aid agricultural researchers in disaggregating their analyses to the farm level. And data on meteorological variables can be used to map the relationship between changing climate and ecosystem disruption.

Policy analysis is likely to have particular benefit for agriculture, a key focus of this dissertation.

Agriculture is a resource-intensive industry under increasing production pressure and environmental concern. The United Nations (UN) Food and Agriculture Organization (FAO) estimated a 70% volumetric increase in food production beyond 2009 levels would be needed to feed in the world in 2050 [7]. Agriculture, meanwhile, already consumes 85% of the world's freshwater and 38% of the land area making it the dominant anthropological user in these arenas [8, 9]. Food production also uses considerable amounts of energy [10]; emits nonpoint source water pollution [11, 12], and is a key driver in carbon emissions due to land use change [13]. Expansion and continuation of current practices is becoming less feasible as food systems are increasingly forced to confront the opposing needs of augmenting production while decreasing resource use and limiting environmental degradation.

In this dissertation, I investigate how data derived from remote-sensing technologies might improve policy analysis in the agricultural and environmental domains through a series of case-studies. The goals of these case studies were to measure the impacts of climate change on the environment (Chapter 2), assess economic damages to agriculture from soil salinity (Chapters 3 and 4), analyze specific policy management alternatives to soil salinity and drought (Chapter 5), and develop techniques to measure soil salinity directly (Chapter 6).

In Chapter 2, I estimated the effects of climate change and anthropogenic stress on coral reefs during the 2005 mass bleaching episode in the Caribbean. This study moved beyond other studies in the literature by accounting for not just temperature, but also photosynthetically active radiation, depth, wind speed (as proxy for hurricane damage), and distance from shore and population density (as proxies for human interference). Different regression techniques are employed, and an optimal model formulation is developed using cross-validation. In this study, each of the explanatory variables relies on satellite observations, and accurate assessment of the coral-climate response would not be possible without such data.

In Chapter 3, I assess the likely effects of soil salinization on agriculture in the state of California. This study makes use of a satellite-based crop classifier and high resolution soils data to account for the lost revenues due to salinity at the field-scale. This approach gives better understanding of the spatial distribution of damages, but also results in higher accuracy reporting of net damages across the state. Resolution is particularly important in assessing the effects of salinity, because salinity can change over relatively small spatial scales, and so conventional county-level resolution datasets would introduce large error into the estimation of salinity damages.

In Chapter 4, I investigate the behavioral response of farmers to extant salinity levels. The modelling efforts developed in Chapter 3 rely on current cropping patterns, and so implicitly assume that growers do not adjust their cropping practices given different levels of salinity. In Chapter 4 I test the importance of this assumption by modelling how growers change cropping patterns in response to salinity levels. To do

this, I employ a cross-entropy downscaling technique that uses a satellite-based crop classifier as well as county-level cropping data to produce an intermediate scale dataset of 56,043 spatial polygon observations. I then create a regression model to predict which crops will be planted within these polygons, and assess the impact of salinity on cropping decisions.

In Chapter 5, I assess the possibility of employing small-scale desalination units in agricultural settings for combatting the effects of salinization and drought. By capturing drainage or other waste sources, these systems can (1) supply a new source of water in water scarce regions, (2) increase the quality of existing water supplies and thus decrease salinization, and (3) prevent harmful contaminants from entering the ecosystem. The benefits are measured using high-resolution data to model the value of decreasing salinity. The value of augmented water supply is estimated using positive mathematical programming, a technique to assess farmer decision making. These benefits are compared to the system's fixed and operational costs, as well as the likely human health damages from air emissions associated with the energy use of such systems as estimated by the Air Pollution Emission Experiments and Policy Version 2 (AP2) model.

In Chapter 6, I assess the feasibility of monitoring soil salinity directly using satellite-based remote sensing. There have been recent successes in the literature to relate soil salinity to vegetation indices, those these efforts often use data from small spatial domains and relatively rudimentary statistical techniques. Recent advances in machine learning may offer more sophisticated ways of enhancing prediction. In this study I use a global dataset of salinity measurements and create a complimentary set of explanatory variables (including satellite measurements, temperature, precipitation, and elevation) to predict salinity using ordinary least squares, artificial neural networks, and convolutional neural networks.

These case studies explore how high-resolution data can contribute to novel impact and policy assessments in the agricultural and environmental domains, where data availability is often limited. In each of the case studies techniques are employed to manage the technical challenges and uncertainty inherent in satellite derived data products. Where practical, traditional policy techniques such as

sensitivity analyses are performed on key parameters. By combining high-resolution data with traditional economic and policy analysis toolsets, this thesis demonstrates the value of such technologies for application to policy.

## References

- [1] Burke M and Lobell D B 2017 Satellite-based assessment of yield variation and its determinants in smallholder African systems *Proceedings of the National Academy of Sciences* **114** 2189-94
- [2] You L Z, Wood S, Wood-Sichra U and Wu W B 2014 Generating global crop distribution maps: From census to grid *Agr Syst* **127** 53-60
- [3] Allen R G, Tasumi M, Morse A, Trezza R, Wright J L, Bastiaanssen W, Kramber W, Lorite I and Robison C W 2007 Satellite-based energy balance for mapping evapotranspiration with internalized calibration (METRIC)—Applications *Journal of Irrigation and Drainage Engineering* **133** 395-406
- [4] Famiglietti J S, Lo M, Ho S L, Bethune J, Anderson K J, Syed T H, Swenson S C, de Linage C R and Rodell M 2011 Satellites measure recent rates of groundwater depletion in California's Central Valley *Geophys Res Lett* **38**
- [5] Rodell M, Velicogna I and Famiglietti J S 2009 Satellite-based estimates of groundwater depletion in India *Nature* **460** 999-U80
- [6] Jean N, Burke M, Xie M, Davis W M, Lobell D B and Ermon S 2016 Combining satellite imagery and machine learning to predict poverty *Science* **353** 790-4
- [7] Food and Agricultural Organization of the United Nations 2009 *How to Feed the World in 2050*.
- [8] Shiklomanov I A 2000 Appraisal and assessment of world water resources *Water international* **25** 11-32
- [9] Food and Agricultural Organization of the United Nations 2013 *FAO Statistical Yearbook* (FAO: Rome) p 34
- [10] Beckman J, Borchers A and Jones C A 2013 Agriculture's Supply and Demand for Energy and Energy Products *USDA-ERS Economic Information Bulletin* **112**
- [11] Environmental Protection Agency 2000 *National Water Quality Inventory 2000 Report*
- [12] Ongley E D, Xiaolan Z and Tao Y 2010 Current status of agricultural and rural non-point source pollution assessment in China *Environmental Pollution* **158** 1159-68
- [13] Guo L B and Gifford R 2002 Soil carbon stocks and land use change: a meta analysis *Global change biology* **8** 345-60

## **Chapter 2: Estimating the effect of multiple environmental stressors on coral bleaching and mortality**

This chapter is based on the following published work:

Welle P D, Small M J, Doney S C, and Azevedo I L 2017 Estimating the effect of multiple environmental stressors on coral bleaching and mortality *PloS One* **12** e0175018.

### **2.1 Introduction**

Coral reefs provide important ecosystem services, such as sustaining fisheries, coastal protection, and social and cultural services such as recreation and tourism [1]. Worldwide, the goods and services provided by coral reefs are estimated to contribute nearly \$30 billion US dollars annually [2]. Coral biodiversity and cover have been decreasing over the last three decades, and the trend is projected to accelerate as ocean temperatures continue to rise [3,4].

Environmental and climate change related stressors, such as temperature, solar radiation, and human interference are affecting these ecosystems, and the magnitude of such stressors will increase in the near future. The extent to which different stressors may contribute to bleaching and mortality of corals, however, is still largely unknown and uncertain.

A consensus is emerging that the warming of the oceans caused by anthropogenic climate change is leading to coral habitat destruction and will continue to do so into the future with likely very serious consequences [3–5]. Higher ocean temperatures have led to increased coral bleaching. As carbon dioxide concentrations increase, ocean pH can be expected to decline, retarding the corals' ability to produce their calcium carbonate exoskeleton [6] and affecting larval settlement and recruitment [7]. Temperature and pH have been seen to act in a synergistically destructive manner, each amplifying the others' effect to cause increased bleaching and mortality [8,9]. Solar radiation arriving at corals is also likely to change with the climate, due to its sensitivity to aerosol and cloud concentrations [10].

Undoubtedly, the most studied driver of habitat loss has been anomalously high temperatures. Elevated temperatures have consistently been seen to correlate with coral bleaching and death [11–15]. Results carried out from controlled laboratory experiments have confirmed these findings [8,16], and future increasing temperatures can be seen to be a major threat to corals worldwide. However, studies focusing on site condition, rather than controlled laboratory experiments, are still lacking.

Coral bleaching, defined as the loss of coral pigmentation from algal symbionts, was first observed nearly a century ago. It has recently become an issue of much concern as sea temperatures rise and mass bleaching episodes become more common [17]. Bleaching leaves corals less able to generate energy from algal photosynthesis, more vulnerable to diseases, and less able to engage in spawning and reproduction [18]. Temperature anomaly has been widely identified as the chief driver in this phenomenon. However, the marginal sensitivity of coral health to temperature changes is still fairly uncertain. In addition, there are other contributors that are likely to intensify in the near future due to shifting climate and increased human interference. Variations in solar radiation, sedimentation, and abundance of herbivorous fish have been seen to affect coral health and can be linked to human action [19].

Solar radiation, either in the form of ultraviolet (UV) or photosynthetically active radiation (PAR), has been seen to cause damage to exposed corals, in some cases bleaching a number of corals without presence of elevated temperatures [20,21]. Sudden increases in the amount of radiation received by corals have also been linked to bleaching [22]. In laboratory experiments, elevated radiation coupled with elevated temperature caused additional bleaching beyond that of temperature alone [8], further evidence of which was provided by Downs et al. [23] by using molecular biomarkers.

Humans often play a more direct role in harming coral ecosystems beyond affecting stressors driven by anthropogenic climate change. Improper diving and boating can lead to direct damage, which is becoming a significant problem in the Red Sea [24,25]. Overfishing, another anthropogenic stressor, reduces predation of the major coral competitor, macroalgae, and can cause increased likelihood of ecosystem phase shifts [26]. Proximity to land can leave corals at risk to fertilizer runoff and resultant

eutrophication, adding more pressure to the ecosystem to shift to an algal dominated state [27].

Population density has been found to be a strong indicator of anthropogenic stress, and has been successfully used in the literature as a proxy variable for such stress [28,29]. Marine protected areas (MPAs) and land-use regulation are common techniques used to address these problems (e.g. [30–33]).

The depth at which corals are located has also been postulated to be important, as temperature and radiation attenuate with depth, but the direction of this effect is still fairly uncertain. For example, Mumby et al. [34] found an increased survival with deeper corals in French Polynesia, supporting results from earlier studies in Myrmidon Reef [35] and for a global analysis [36]. Deeper corals tend to be larger, slower growing, and more resistant to bleaching. The effect of depth is not always clear and will depend on several other factors, such as coral biology. For example, Marshall and Baird [37] found a significant spatial variation in bleaching, with some shallow sites reporting less bleaching than deeper ones. Williams and Bunkley-Williams [38] observe that “in the Florida Keys and Puerto Rico, bleaching started in the shallows and moved deeper; in Jamaica and St. Croix, the opposite was observed.” It is of great interest to develop an understanding of how all the above-identified stressors interact to impact coral health, so that this information can be combined with climate predictions to create a holistic understanding of the fate of coral reefs.

Thermal bleaching has been attributed to an overproduction of protons during the light reaction of the photochemical process [20]. Increased light and temperature accelerate the chemical processes associated with these reactions to the point where the dark reaction is unable to make use of all the energy and free radicals of oxygen are created, that are hypothesized to subsequently damage the host coral. Thermal bleaching is the expulsion of the algal symbionts, or zooxanthallae, presumably as protection against the various dangerous forms of oxygen [17]. In support of this theory, it has been observed empirically that free radicals are produced before bleaching occurs [39,40]. It also appears that bleaching may occur less in corals that have recently bleached, causing their levels of zooxanthallae to be lower than would

otherwise be the case [21]. Additionally, the threshold for coral bleaching was found to be 1°C lower in winter when symbiont concentration is lowest [14].

Using tank experiments, Anthony et al. [8] sought to understand the interaction between temperature, light, and sedimentation, and found that increased turbidity protects corals from bleaching. While it is well-established in the literature that sedimentation is damaging to reefs [41], it is likely that in these tank experiments the turbid water shielded the corals from radiative damage or a radiation-temperature interaction effect [8]. The studies by Anthony et al. [8], Brown et al. [21], and others indicate that the biological pathway through which bleaching occurs indeed relies on excess solar radiation and temperature.

The National Oceanographic and Atmospheric Administration's (NOAA's) Coral Reef Watch (CRW) uses Degree Heating Weeks (DHW) to generate real-time warnings for areas at risk for bleaching. DHWs are computed by summing the number of degrees above maximum climatological monthly mean (MMM) for each week across the preceding twelve weeks (<http://coralreefwatch.noaa.gov/>), and therefore represent an estimate of how far above 'typical' values recent temperatures have strayed. Weeks with anomalies less than 1°C are considered to be non-anomalies and rounded to zero. Moderate bleaching is expected when DHW is larger than 4, and severe bleaching may occur with a DHW larger than 8. These data are made available in near real-time at a global scale.

A number of studies have attempted to explain the effect of temperature on coral bleaching using the DHW formulation and statistical models for regression analysis [42–46]. Existing analyses of coral bleaching typically involve one of two approaches: predicting the probability of being in a categorical stage of bleaching or resilient state (e.g., “high” or “low”) or predicting the fraction of corals bleached with an ordinary least squares (OLS) model. For example, McWilliams et al. [42] used the ReefBase (<http://www.reefbase.org>) data to predict bleaching severity and spatial extent using DHW, and found a log-linear increasing relationship, and Eakin et al. [43] performed a similar analysis with data exclusively

from the 2005 bleaching event in the Caribbean, regressing bleaching on DHW using ordinary least squares (OLS).

Two major studies used metrics similar to degree heating weeks to assess what coral cover might look like in the future as temperatures rise. Hoegh-Guldberg [11] predicted the Degree Heating Months (DHM, similar to DHW) into the future, showing that DHM would rise beyond triple the levels currently experienced by as early as 2080. More importantly, DHM exceeding the worst values observed to date would become yearly events before the end of the century. Another study used similar metrics in the Caribbean to show that the DHM associated with the 2005 mass bleaching episode would reoccur roughly every other year by 2030-2050, depending on adaptation [5].

A few of these studies [42,43] use only temperature in predicting coral bleaching, but no study to date has attempted to predict coral mortality. Those studies that include additional predictor variables [44–46] find that variables such as PAR, depth, and wind speed lead to significant improvement in predicting coral health outcomes.

While a few of the above mentioned studies have attempted to determine the effect of temperature on coral bleaching using statistical and regression analyses [42–46], these studies have generally used an ordinary least-square (OLS) regression. There are several reasons why an OLS regression may not be an appropriate way to describe coral behavior in light of stressors, further elaborated upon in the methods. These studies have useful first order implications, but it is important to consider carefully whether temperature alone is sufficient for predicting future coral mortality. Theory and biological experimentation suggest that pH and radiation arriving at the corals will also be important in driving the photosynthesis reaction. If regressions of past temperature events are to be taken as predictive of future bleaching and mortality rates, it is important to consider the magnitude of the roles that each driver plays. Satellite radiation data available in the form of PAR or ultraviolet radiation (UVR) should be included as well as other environmental variables that might be relevant.

Yee, Santavy, and Barron [44] and Yee and Barron [45] extended the traditional analysis to include PAR taken from Moderate Resolution Imaging Spectroradiometer (MODIS) aboard NASA's Terra satellite. The authors found that adding PAR (as well as other environmental variables and community taxonomic composition) increased  $R^2$  as well as resulted in lower corrected Akaike Information Criterion ( $AIC_c$ ). These studies fit models to understand the probability of bleaching events. These early results, combined with data from the empirical work discussed above, indicate it may be crucial to incorporate a wider variety of environmental variables to understand coral health.

In this study, we use the observations of coral bleaching, mortality, and depth from a dataset compiled by Eakin et al. [43], which we describe in more detail in the data and methods section. The dataset includes 2945 measurements of coral health taken during the Caribbean summer of 2005 and is the most thorough measurement of basin-scale bleaching ever recorded. Major coral losses were observed in the Caribbean during the period for which measurements were made. During this period, record temperatures were set across the basin. In some reefs measured bleaching rates were as high as 95% [47]. We complement the dataset with weather data, specifically DHWs data from NOAA CRW and photosynthetically active radiation (PAR) from MODIS Aqua satellite, as well as distance from each coral reef to the nearest coastline, population density, wind speed and information about biogeographic regions. We provide more details regarding these data in the data and methods section and in the SI.

The work presented in this paper contributes to the literature by developing and using a novel regression approach, where the fraction of corals bleached and fraction of corals dead are estimated using a parametric non-linear model that controls for unobserved time invariant effects. Two separate models are created, one to predict coral bleaching, and the other to predict near-term mortality. A large ensemble of supporting data is assembled to control for omitted variable bias and improve fit, resulting in a significant improvement in predictive capacity.

## 2.2 Methods

### 2.2.1 Data

We collect data from a variety of sources and combine them into a comprehensive statistical analysis of the coral death and bleaching process. The final dataset included observations on coral bleaching and mortality, temperature in the form of degree heating weeks, photosynthetically active radiation, and distance from shore. The following sections provide additional detail on these data.

#### 2.2.1.1 Coral Bleaching and Mortality

A dataset from Eakin et al. [43] is used to quantify the negative ecosystem effects observed in Caribbean reefs, with a total of 2,945 observations measured between May 2005 and January 2007. In Section 8.1 of Appendix A we include more information on the data used and limitations associated with the dataset. Figure S1 in Appendix A reports the spatial distribution of the observations, while the temporal distribution is reported in Figure 2-1. Figure 2-1A shows the average observed degree heating weeks (DHW) for the observations in that time period, and can be used to visualize the intensity of the temperature anomaly over time. The middle plots report the frequency of observations over time and are color coded to show the fraction of corals with different bleaching or mortality levels. Most observations were taken at the end of the summer of 2005, when temperatures were highest. The bottom graph illustrates the same information as the second graph with each bar normalized so trends in bleaching and mortality can be seen more clearly. Qualitatively, bleaching appears to be relatively stable while mortality increases with time.

The outcome measures of interest are coral bleaching and coral mortality. Each can be measured as a percentage of cover affected or colonies affected. *Cover bleached* represents the fraction of coral bleached in the observed area, while *colonies bleached* represent the fraction of bleached coral organisms relative to healthy organisms. Likewise, *cover dead* is the fraction dead per area and *colonies dead* is the fraction dead to living organisms. Eakin et al. [43] showed that these two measures, fractional area and

fractional number of colonies, used independently give statistically indistinguishable results and uses this to justify selecting the average of the two as the dependent variable. In this study the same approach is followed and the average of the two measurement strategies is used, yielding one composite measure for bleaching and one for mortality.

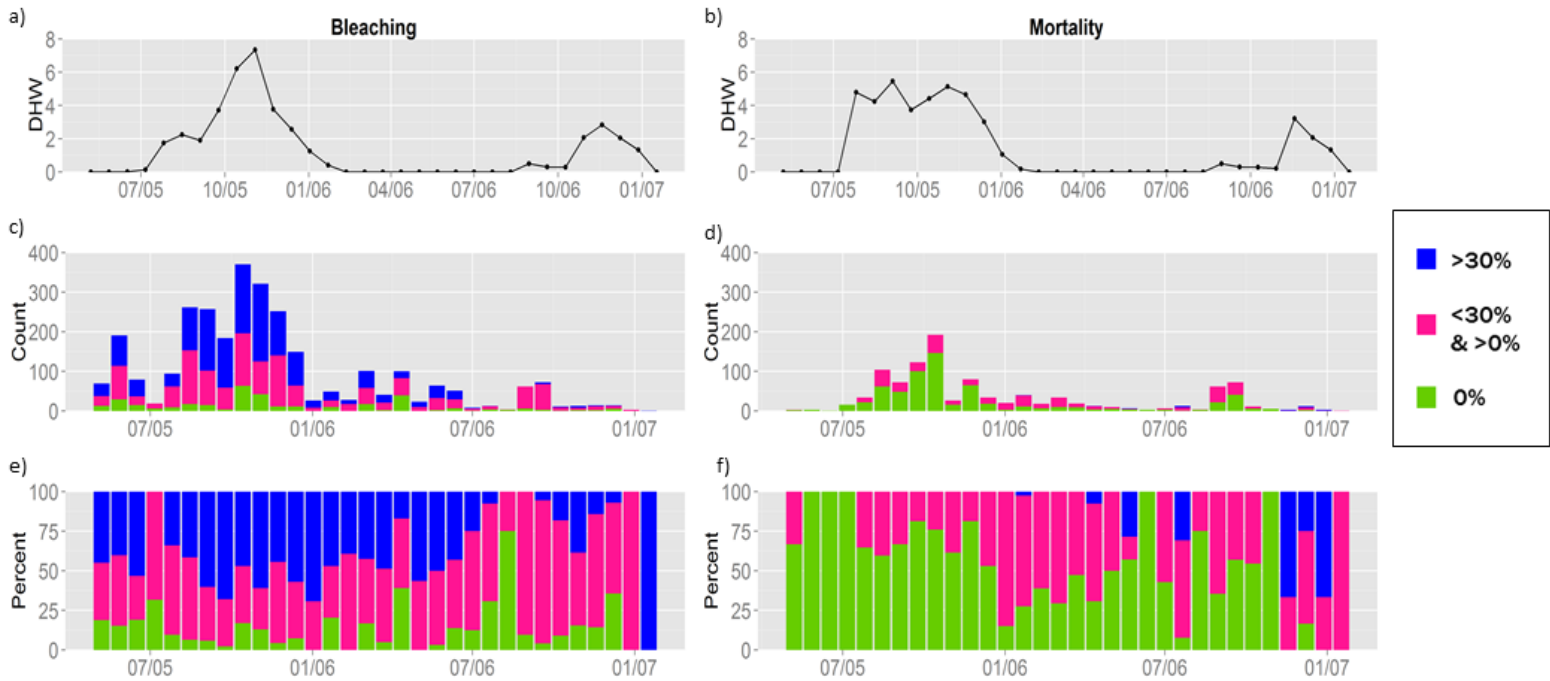


**Figure 2-1. Temporal distribution of observations. Figures on the left column refer to bleaching, and those on the right refer to mortality. Figures 2-1A and 2-1B show the average DHW in the observed locations for the region of analysis between May 2005 and January 2007. Figures 2-1C and 2-1D show the number of observations,  $x$ , with 0%,  $0% < x < 30%$ , or  $x > 30%$  bleaching or mortality. Since the number of observed sites varies over time, in Figures 2-1E and 2-1F we show the share of observations in each distribution bin over time. The left and right panels for DHW, Figures 2-1A and 2-1B, differ because the observations available for mortality are a subset of those available for bleaching.**

It is not possible to assure that all bleaching and mortality are directly attributable to thermal stress (as opposed to, for example, disease or hurricanes). To address this concern, a measurement is included in the analysis only if it occurs after the first issuance of a thermal stress warning and before the 90<sup>th</sup> day following the last no stress alert, as defined in the CRW Bleaching Alert System (<http://coralreefwatch.noaa.gov>). All bleaching identified in our data, therefore, occurred under the

presence of thermal stress. As noted in Table 2-1, the spatial variation in temperature is still sufficient during the study period to yield a relatively wide range of DHW values, enabling its effects to be determined by the regression analysis.

Lastly, it should be noted that the sampling campaign did not follow a strict probabilistic approach, meaning that the corals measured may not perfectly represent the distribution of corals in the wider Caribbean. The sample itself is unique, however, in its size and extent and thus offers valuable insight into how changing climate and anthropogenic stress may be affecting coral health outcomes.

#### *2.2.1.2 Temperature*

Temperature is expressed in degree heating weeks, DHW. All temperature measures are calculated using data from NOAA's Coral Reef Watch (CRW). CRW maintains a historical database of observed and maximum DHW values, which were used in this analysis. All data are available at a 50km resolution. DHW are matched with observations based on time and location.

#### *2.2.1.3 Photosynthetically active radiation (PAR)*

We utilize satellite-derived estimates of the daily-averaged, photosynthetically available radiation (PAR) (400-700nm) just below the sea surface. PAR is a standard data product from NASA MODIS Aqua (<http://modis.gsfc.nasa.gov/data/dataproduct/>). MODIS Aqua is a moderate resolution satellite that images the Earth every 1-2 days, with data collected in 36 spectral bands. We use PAR data from the MODIS Level 3 8-day binned files. In order to calculate PAR anomaly, climatology data was used in order to establish a baseline. PAR variations are calculated using two different methods. The first is as an average of 12 satellite weeks of raw data. The second follows a method similar to the one for DHW, in which each weekly average is subtracted from the baseline maximum monthly PAR. In Table 2-1 the second measure is titled 'PAR anomaly.' As with DHW, a PAR anomaly value of 0 indicates no stress and increasingly positive numbers indicate increasing stress.

#### 2.2.1.4 Dual formulations for DHW and PAR

For each of these stressors (DHW, PAR, and PAR anomaly), observed and maximum values are calculated. Observed DHW, for instance, represents the DHW calculated over the 12 weeks immediately preceding the observation (and therefore the stress observed up to the date of measurement). Maximum DHW represents the 12-week window between the January 1<sup>st</sup>, 2005 and the date of observation that records the highest DHW value. Maximum DHW, by construction, must be greater than or equal to observed DHW. We have used these two metrics to contrast continuous (or near-term) stress versus stress induced by past peak temperature or PAR events.

#### 2.2.1.5 Population Density

The maximum population density within a 50 kilometer radius from the site of coral observation was calculated using the UN-Adjusted Gridded Population of the World v4 (GPWv4) dataset estimates for 2005 (see Figure 2-2).

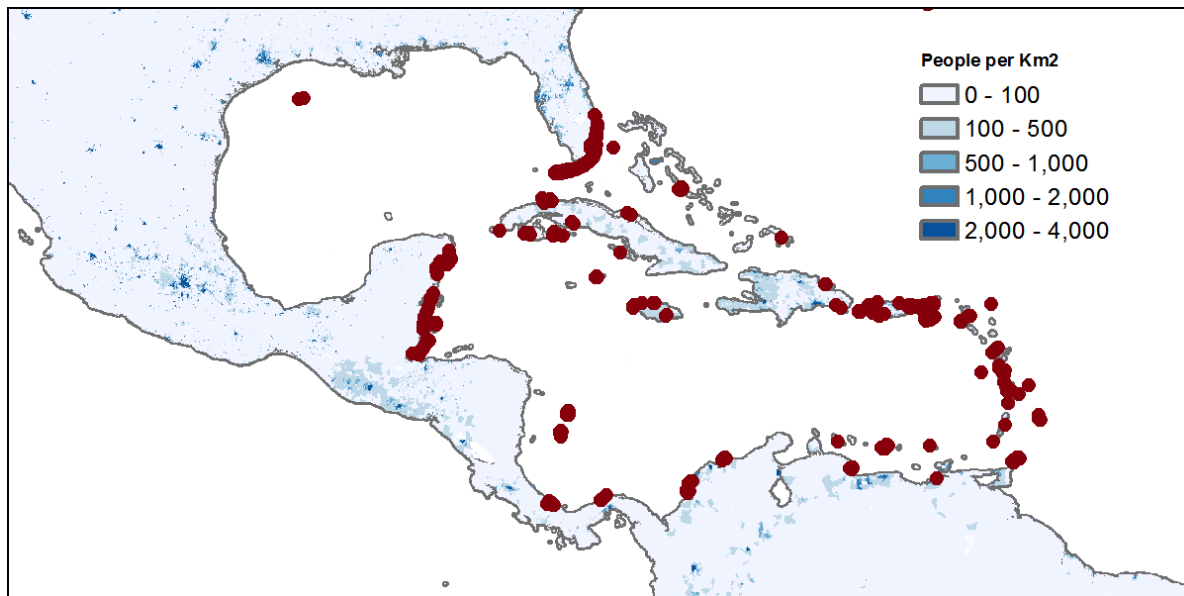


**Figure 2-2. Population density in people per km<sup>2</sup> (in blue) and coral observations (red dots). Figure produced by the authors using data from the GPWv4 dataset.**

#### *2.2.1.6 Distance from Shore (DFS)*

Distance from the reef location to shore was calculated using ArcGIS and is defined as the minimal distance from each coral observation to land as measured in kilometers.

#### *2.2.1.7 Wind speed as a proxy for hurricane and storm intensity*

Since 2005 was an active hurricane year in the Caribbean, it is important to control for possible mortality associated with storms. Maximum wind speed was used as a proxy for storm and hurricane stress. The parameter was calculated by finding the maximum wind speed that occurred between Jan 1, 2005 and the date of coral observation. Data was sourced from the NCEP-DOE Atmospheric Model Intercomparison Project (AMIP-II) reanalysis (R-2) project, and represents wind speed at 10 meters above sea level.

AMIP-II is available at global scale, is reported twice-daily, and has a spatial resolution of 2.5 degrees.

Table 2-1 provides the summary statistics for the variables in the dataset. While a certain few locations report high mortality (maximum = 68%), the majority reported none at all (median = 0%; mean = 2%). In contrast, the median bleaching was nearly 26%. For temperature, it can be seen that almost half of the observations reported no temperature stress on the date of measurement (Observed DHW), and the typical location experienced what NOAA CRW would consider ‘mild bleaching’ at least once during the summer (Maximum DHW).

**Table 2-1. Summary of variables.**

<b>Variable</b>	<b>Min</b>	<b>Median</b>	<b>Mean</b>	<b>Max</b>
<b>Bleaching [%]</b>	0	26	33	100
<b>Mortality [%]</b>	0	0	2	68
<b>Maximum DHW [°C]</b>	0	3.6	4.6	17.2
<b>Observed DHW [°C]</b>	0	0.5	2.8	16.6
<b>Maximum PAR [Einstein / m<sup>2</sup>]</b>	35.6	47.7	47.9	53.7
<b>Maximum PAR Anomaly</b>	1.6	16.0	17.9	56.0
<b>[Einsteins / m<sup>2</sup>]</b>				
<b>Observed PAR</b>	26.3	39.8	40.4	52.4
<b>[Einsteins / m<sup>2</sup>]</b>				
<b>Observed PAR Anomaly</b>	0	0.75	4.7	36.5
<b>[Einsteins / m<sup>2</sup>]</b>				
<b>Base PAR [Einsteins / m<sup>2</sup>]</b>	42.3	51.1	50.4	54.2
<b>Distance from Shore [°]</b>	0	0.014	0.062	1.79
<b>Depth [m]</b>	0.9	9.2	10.0	42.7

### *2.2.1.8 Controlling for spatial correlations*

We control for spatial correlation between observations by introducing spatial fixed effects, using the ecoregional boundaries from the Marine Ecoregions of the World (MEOW). The data includes nine regions, as shown in Figure 2-3. The Northern Gulf of Mexico and Western Caribbean regions were lumped together since the Northern Gulf of Mexico region only contained 5 observations.

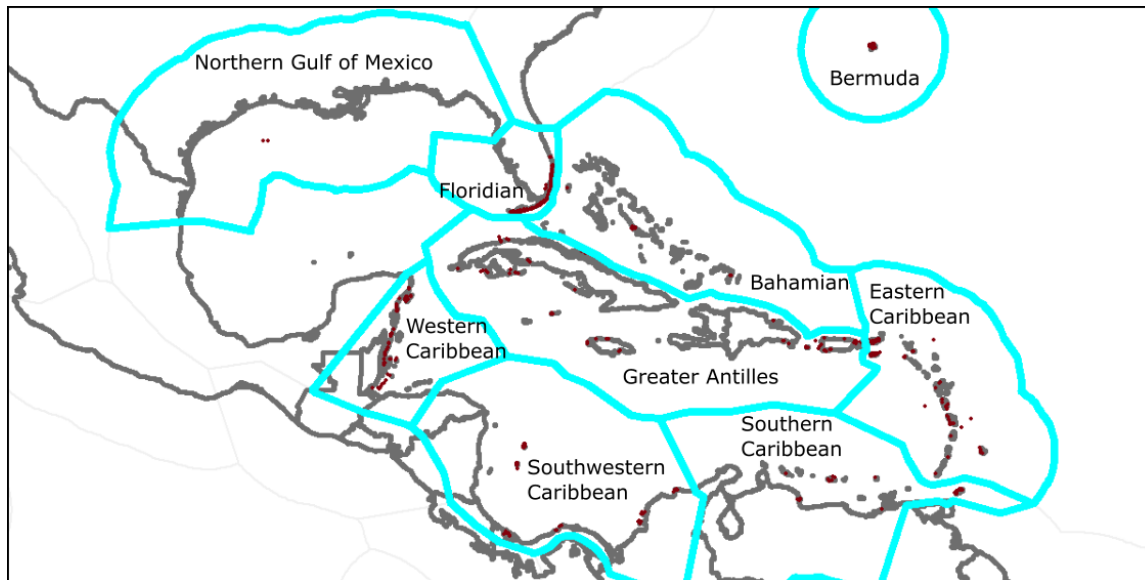


**Figure 2-3. Marine Ecoregions of the World (MEOW) regions. Red points represent coral observations.**

### 2.2.2 *Statistical Modelling*

As a part of the study, three major model specifications were tested – OLS, Tobit, and Fractional Logit. In the SI, section S1B we explain the assumptions that go with each of these modeling approaches. Here, and in the results, we present the results for the Fractional Logit model, since it performed best according to our selection criteria. While typical logit models are used to predict binary outcomes, by using a quasi-likelihood approach it is possible to repurpose the functional form so as to be able to use a continuous and bounded dependent variable [48]. It has been argued that Fractional Logit is more appropriate when the values outside the censored range are infeasible, and indeed this model best fits our results.

When considering spatial data, it is important to recognize that nearby observations will not be independent of one another. For example, due to larval dispersion in the water column, there is likely to be biological connectivity and similarity between nearby corals and reefs, as well as correlation between unobservable factors. To address this issue, we employ a fixed-effect regression that controls for spatial correlation. We include a spatial dummy for each of the nine ecoregions that span our data in the Caribbean as defined by the Marine Ecoregions of the World (MEOW) dataset. The fixed effects

Fractional Logit model can be stated in a general form as follows, with  $j$  stressors ( $x$ ) and  $k$  spatial dummies ( $d$ ):

$$y_i = \frac{1}{1 + e^{-(\beta_0 + \sum_j \beta_j x_{ij} + \sum_k \beta_k d_{ik} + \epsilon_i)}} \quad (1)$$

where  $y_i$  denotes that fraction of coral sampled at location  $i$  exhibiting mortality (Model 1) or bleaching (Model 2). As noted above, the dependent variables are calculated following Eakin et al. [43], as the average of the fraction of the area covered and the fraction of the colonies affected by mortality and bleaching, respectively. The exact model formulation was selected according to performance in a  $k$ -fold cross-validation. In  $k$ -fold cross-validation, the data is partitioned into  $k$  distinct groups, with each group acting as the test data set while the other  $k - 1$  groups act to train the model. This process is repeated many times, and the reported model fit represents the average MSE across 1000 simulations.

### 2.3 Results

The selected models for bleaching and mortality employ the same functional form as well as spatial controls (Equation 1), differing only in the included interaction terms and on whether average or maximum observed values are used in the independent variables. Mortality or bleaching,  $y$ , is predicted using a function of explanatory variables,  $x_j$ , and spatial controls,  $d_k$ . We find that different explanatory variables affect bleaching and mortality, and thus the variables used in the two models are highlighted in Table 2-2.

**Table 2-2. Variables included in the estimation models, description, and units.**

3	Variable	Description	Units	Included in the mortality estimation model	Included in the bleaching estimation model
	Bleaching	Composite of cover bleached and colonies bleached	%		X
	Mortality	Composite of cover dead and colonies dead	%	X	
	Maximum <sup>†</sup> DHW,	Temperature anomaly	°C	X	
	Observed <sup>‡</sup> DHW	Temperature anomaly	°C		X
	Maximum PAR Anomaly	Radiation anomaly	Einstein / m <sup>2</sup> ·day	X	X
	Distance from Shore (DFS)	Shortest Euclidean path to shoreline	Kilometers		X
	Population Density	Maximum population density within 50km of observation	1000 people per km <sup>2</sup>	X	X
	Wind	Maximum wind speed before observation date	Meters / second	X	X
	Depth	Depth of coral below surface	Meters	X	X
	Depth x MaxPAR	Interaction terms between coral depth and maximum PAR anomaly	Meters x Einstein / m <sup>2</sup> ·day	X	X
	Depth x MaxDHW	Interaction terms between coral depth and maximum DHW	Meters x °C	X	
	Depth x ObsDHW	Interaction terms between coral depth and observed DHW	Meters x °C		X

<sup>†</sup>Maximum stress is the most extreme values recorded since the beginning of the event (January, 2005). <sup>‡</sup>Observed stresses are the values observed on the day of measurement

### 3.2.1 Mortality.

In Table 2-3 we show the estimated coefficients for mortality, as well as the marginal effects averaged across all data points in the sample. We find that maximum DHW, coral depth, and a coral depth-PAR Anomaly interaction term are all statistically significant in explaining coral mortality. Increases in maximum DHW lead to increased mortality, with an increase of 10 DHW leading to an approximate 4.9 percentage point increase in mortality. Similarly, an increase in PAR anomaly of 10 Einstein/m<sup>2</sup>·day would be associated with an increase in 0.8 percentage points in mortality, and an increase in 10 meters of the depth of a coral reef is associated with 9.7 percentage points less mortality. While population and wind speed are not statistically significant in the model, we find that their inclusion improved performance during cross-validation. Both parameters were positively correlated with mortality.

Finally, we do find a significant difference in coral survival across regions, as seen in the regional marginal effects in Table 2-3. These effects can be interpreted as the change in expected mortality from a

reference region, which has been set as the Western Caribbean / Northern Gulf of Mexico joint region. For example, according to the model the Eastern Caribbean region is expected to experience 4.7 percentage points less mortality than the reference given the same level of stress, while the Greater Antilles are expected to experience 4.9 percentage points more mortality. One region, Bermuda, shows itself to be an outlier. This indicates the corals in Bermuda showed themselves to be more robust than corals in other regions given the same level of stress, however it should be noted that this region reports the least data in the aggregate dataset with just 41 observations.

**Table 2-3. Results for the regression model of coral mortality as a function of different explanatory variables.**

<i>Variables</i>	<i>Coefficients</i>	<i>Average Marginal Effect</i>
Maximum DHW	0.304*** (0.050)	0.492*** (0.071)
Maximum PAR Anomaly	-0.0073 (0.015)	0.0808*** (0.018)
Population	0.0373 (0.031)	0.0679 (0.057)
Wind	0.00114 (0.040)	0.00207 (0.073)
Depth	-0.143*** (0.056)	-0.0969*** (0.023)
Depth × Maximum PAR Anomaly	0.00517*** (0.0012)	
Depth × Maximum DHW	-0.00328 (0.0040)	
Bermuda	-10.9*** (0.46)	-93.1*** (5.8)
Bahamian	1.56** (0.77)	-6.2* (3.5)
Eastern Caribbean	0.474 (0.35)	-4.7*** (1.6)
Greater Antilles	0.896** (0.42)	4.9** (2.3)
Southern Caribbean	-2.08** (1.03)	-7.4*** (2.6)
Southwestern Caribbean	-0.380 (0.35)	-19.5*** (2.2)
Floridian	-1.23*** (0.47)	-12.3*** (2.2)
Constant	-5.74*** (0.89)	
<i>Log Likelihood</i>	-64.34	
<i>Cross-validated MSE</i>	30.64	
<i>Cross-validated RMSE</i>	5.53	
<i>Cross-validated R<sup>2</sup></i>	0.325	
<i>Number of Observations</i>	1,045	

Estimated coefficients and average marginal effects using a fractional logit model, where coral mortality is explained as a function of environmental stressors. Robust standard errors are shown in parentheses (\*\*\*)  $p < 0.01$ , \*\*  $p < 0.05$ , \*  $p < 0.1$ ).

### 3.2.2 Bleaching.

In Table 2-4 we show the estimated coefficients for bleaching, as well as the marginal effects averaged across all data points in the sample. The marginal effect of temperature on bleaching is far larger than those of the other effects included in the model. Distance from shore, which is used as a proxy for coastal

environmental stressors from human activities, is negatively associated with bleaching, indicating that, as expected, corals found further from land (and therefore stressors such as runoff or land use) are less likely to experience bleaching. Likewise, as with the mortality model, population density and wind speed were found to be positively associated with coral bleaching.

NOAA indicates that ‘mild bleaching’ can occur at DHW values larger than 4, and ‘severe bleaching’ at values of DHW larger than 8. The bleaching model suggests that an average DHW of 4 would be associated with a bleaching fraction of 37%, and an average DHW of 8 is associated with a bleaching of 53%. These high levels of bleaching may indicate an increasing sensitivity in the Caribbean to temperature. Lastly, PAR is found to be associated with increased bleaching, but only when phrased in terms of PAR anomaly, or radiation above baseline. This result indicates that corals adapt to their local microclimates with radiation as well as temperature.

Spatial variation across the Caribbean continues to significantly affect model results. Bermuda continues to report anomalous results, 19.8 percentage points below the reference region. The other regions report a 5.6 percentage point spread, the Southern Caribbean reporting the least bleaching tendencies and the Bahamian region the most. Accounting for separate spatial fixed effects is therefore crucial in maintaining unbiased estimates of the effects of stressors on coral health outcomes.

**Table 2-4. Results for the regression model of coral bleaching as a function of different explanatory variables.**

<i>Variables</i>	<i>Coefficients</i>	<i>Average Marginal Effect</i>
Observed DHW	0.201*** (0.014)	3.31*** (0.16)
Maximum PAR Anomaly	0.0268*** (0.0054)	-0.0274 (0.059)
Distance from Shore	-0.0363*** (0.0137)	-0.72*** (0.27)
Population	0.0311*** (0.0059)	0.618*** (0.12)
Wind	0.0132 (0.0085)	0.263 (0.17)
Depth	0.0734*** (0.011)	0.375*** (0.085)
Depth × Observed DHW	-0.00336** (0.0010)	
Depth × Maximum PAR Anomaly	-0.00246*** (0.00049)	
Bermuda	0.114 (0.137)	-19.8*** (1.7)
Bahamian	1.05*** (0.245)	2.8** (1.4)
Eastern Caribbean	0.0185 (0.156)	0.86 (0.64)
Greater Antilles	0.325* (0.188)	1.6** (0.77)
Southern Caribbean	1.16*** (0.148)	-3.8** (1.9)
Southwestern Caribbean	0.605*** (0.148)	-0.69 (0.63)
Floridian	0.476** (0.176)	-2.2** (0.89)
Constant	-2.421*** (0.198)	
Log-likelihood	-1299	
Cross-validated MSE	607.0	
Cross-validated RMSE	24.6	
Cross-validated R <sup>2</sup>	0.29	
Number of Observations	2,945	

Estimated coefficients and average marginal effects using a fractional logit model, where coral bleaching is explained as a function of environmental stressors. Robust standard errors are shown in parentheses (\*\*\* p<0.01, \*\* p<0.05, \* p<0.1).

When assessing the final bleaching and mortality models, it is important to assess which elements have not been selected. For instance, while, as noted in the introduction, the literature suggests that a DHW – PAR interaction term has biological and laboratory support, it was not found to be superior in tests performed during the cross-validation. Likewise, in the bleaching model, maximum PAR Anomaly was

selected over observed PAR anomaly, indicating that exposure to anomalous levels of radiation before the 12-week window is important in predicting current levels of bleaching.

To illustrate the sensitivity to the different stressors, in Figure 2-4 we show the difference between the predicted coral outcome when each of the stressors is varied between the 5<sup>th</sup> and 95<sup>th</sup> percentile of observed values in the sample (while all other variables are held at their means). Temperature is the major driver of both the bleaching and the mortality responses. Population density, the proxy for anthropogenic stress included in both models, plays a secondary effect in both models. For instance, in both the bleaching and mortality models the temperature effect is ~4 times larger than that for population density. Hurricane stress, as measured by wind speed, plays a minor role in both models across the observed range. This tepid response is perhaps due to the cancelling out of the dual effects of hurricanes on coral health outcomes – hurricanes may increase stress on corals either directly or through increased runoff, or they may lessen stress due to upwelling [43,49].

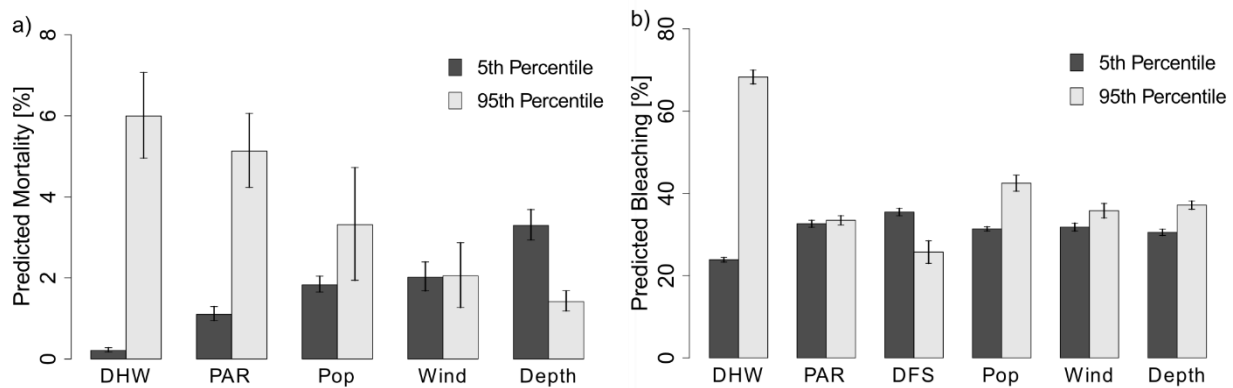


**Figure 2-4. Relative effects of temperature (DHW), solar radiation (PAR), depth, and distance from shore (DFS). In Figure 2-4A, the predicted coral mortality is displayed while holding each stressor at the 5<sup>th</sup> percentile and 95<sup>th</sup> percentile of its observed values in the sample (while all other stressors are held at their mean). The error bars represent plus/minus two standard errors of the expected value. In Figure 2-4B the analogous information is reported using bleaching as the dependent variable.**

## 2.3 Discussion

In this study, we present further evidence of the effects from climatic and anthropogenic influences on coral reef ecosystem health. These effects are robust across a range of modeling strategies, and show that even after controlling for confounding mechanisms sea surface temperature plays a dominating role in controlling coral bleaching and mortality. Predictions indicate that in the Caribbean and across the world anomalous temperature events will rise in severity and become more frequent [11]. If, as estimated in Donner et al. [5], events of the magnitude of the 2005 Caribbean warming episode become bi-annual events in the next few decades, reef systems will degrade at accelerating rates.

Of note is that we find significant spatial differences between different geographic locales indicating varying ability of corals to respond to climate change. We also find interesting regional differences in correlations between stressors. For example, the correlation between distance from shore and depth varies across eco-regions, in some instances being high and positive, as is the case in the Southwestern Caribbean ( $\rho=0.21$ ), sometimes high and negative (for example, Bahamian, where  $\rho=-0.39$ ), and in other instances a low correlation. More detail is included in the supplementary information. However, barring rapid and drastic biological acclimation, our results show that Caribbean reefs will face mounting existential pressure as the ocean continues to warm.

In conclusion, we find that that temperature and radiation far outweighed direct anthropogenic stressors in driving coral health outcomes during the 2005 Caribbean event. While selecting models based on performance using cross-validation decreases the risk of over-fitting, caution still must be used in generalizing the model to the modern Caribbean. Catastrophic events fundamentally change the nature of ecosystems, and it must be noted that the Caribbean of today cannot be completely represented by the Caribbean of 2005. However, the analysis presented in this paper provides additional evidence for the effect of temperature and other environmental stressors on coral health using a large sample of corals, and can be taken as suggestive of future trends both in the Caribbean and across the world. Indeed, the approach developed here can be used by other modelers and researchers to assess the effects for other

locations, times and conditions, and it also provides a first order estimate that modelers can use in climate models to assess the effects of future environmental stressor states on coral health.

## References

- [1] Moberg F, Folke C 1999 Ecological goods and services of coral reef ecosystems *Ecol. Econ.* **29** 215–33.
- [2] Cesar H, Burke L, and Pet-Soede L 2003 *The economics of worldwide coral reef degradation.*
- [3] Hughes T P, Baird A H, Bellwood D R, Card M, Connolly S R, Folke C, et al. 2003 Climate change, human impacts and resilience of coral reefs *Science* **301** 929–33.
- [4] Hoegh-Guldberg O, Mumby P J, Hooten A J, Steneck R S, Greenfield P, Gomez E, et al. 2007 Coral reefs under rapid climate change and ocean acidification *Science* **318** 1737–42.
- [5] Donner S D, Knutson T R, and Oppenheimer M 2007 Model-based assessment of the role of human-induced climate change in the 2005 Caribbean coral bleaching event. *Proc. Natl. Acad. Sci. U S A* **104** 5483–8.
- [6] Anthony K N, Maynard J A, Diaz-Pulido G, Mumby P J, Marshall P A, Cao L, et al. 2011 Ocean acidification and warming will lower coral reef resilience *Glob. Chang. Biol.* **17** 1798–808.
- [7] Albright R, Mason B, Miller M, and Langdon C. Ocean acidification compromises recruitment success of the threatened Caribbean coral *Acropora palmata* *Proc. Natl. Acad. Sci. U S A.* **107** 20400–4.
- [8] Anthony K N, Connolly S R, and Hoegh-Guldberg O 2007 Bleaching, energetics, and coral mortality risk: Effects of temperature, light, and sediment regime *Limnol. Oceanogr.* **52** 716–26.
- [9] Nagelkerken I, Connell S D 2015 Global alteration of ocean ecosystem functioning due to increasing human CO<sub>2</sub> emissions. *Proc. Natl. Acad. Sci. U S A.* **112** 13272–77.
- [10] Ramanathan V, Crutzen P J, Kiehl J T, and Rosenfeld D 2001 Aerosols, climate, and the hydrological cycle *Science* **294** 2119–24.
- [11] Hoegh-Guldberg O 2000 The future of coral reefs: Integrating climate model projections and the recent behaviour of corals and their dinoflagellates. *Proc. Ninth Int. Coral Reef Symp. Bali.* **2** 23–7.
- [12] Donner S D, Skirving W J, Little C M, Oppenheimer M, Hoegh-Guldberg O 2005 Global assessment of coral bleaching and required rates of adaptation under climate change *Glob. Chang. Biol.* **11** 2251–65
- [13] Sheppard C R C 2003 Predicted recurrences of mass coral mortality in the Indian Ocean *Nature* **425** 294–7.
- [14] Berkelmans R, Willis B 1999 Seasonal and local spatial patterns in the upper thermal limits of corals on the inshore Central Great Barrier Reef *Coral Reefs* **18** 219–28.
- [15] Glynn P W, D’Croz L D 1990 Experimental evidence for high temperature stress as the cause of El Nino-coincident coral mortality *Coral Reefs* **8** 181–191.
- [16] Jokiel P, Coles S 1990 Response of Hawaiian and other Indo-Pacific reef corals to elevated temperature *Coral Reefs* **8** 155–162.
- [17] Coles S L, Brown B E 2003 Coral bleaching--capacity for acclimatization and adaptation *Adv Mar Biol.* **46** 183–223.
- [18] Szmant A, Gassman N 1990 The effects of prolonged “bleaching” on the tissue biomass and reproduction of the reef coral *Montastrea annularis* *Coral Reefs* **8** 217–24.
- [19] Dunne R, Brown B 2001 The influence of solar radiation on bleaching of shallow water reef corals in the Andaman Sea, 1993–1998 *Coral Reefs* **20** 201–210.

- [20] Fitt W, Brown B, Warner M, and Dunne R 2001 Coral bleaching: interpretation of thermal tolerance limits and thermal thresholds in tropical corals *Coral Reefs* **20** 51–65.
- [21] Brown B, Dunne R, Goodson M, and Douglas A. 2002 Experience shapes the susceptibility of a reef coral to bleaching *Coral Reefs* **21** 119–126.
- [22] Hoegh-Guldberg O, Smith G J 1989 The effect of sudden changes in temperature, light and salinity on the population density and export of zooxanthellae from the reef corals *Stylophora pistillata* Esper and *Seriatopora hystrix* Dana *J. Exp. Mar. Bio. Ecol.* **129** 279–303.
- [23] Downs CA, Mueller E, Phillips S, Fauth J E, and Woodley C M 2000 A Molecular Biomarker System for Assessing the Health of Coral (*Montastraea faveolata*) During Heat Stress *Mar Biotechnol.* **2** 533–44.
- [24] Davenport J, Davenport J L 2006 The impact of tourism and personal leisure transport on coastal environments: A review. *Estuar. Coast Shelf Sci.* **67** 280–92.
- [25] Jameson S, Ammar M, Saadalla E 1999 A coral damage index and its application to diving sites in the Egyptian Red Sea *Coral Reefs* 1999 **18** 333–9.
- [26] Hughes T P, Rodrigues M J, Bellwood D R, Ceccarelli D, Hoegh-Guldberg O, McCook L, et al. 2007 Phase shifts, herbivory, and the resilience of coral reefs to climate change *Curr. Biol.* **17** 360–5.
- [27] Fabricius K E 2011 Factors determining the resilience of coral reefs to eutrophication: A review and conceptual model *Coral Reefs: An Ecosystem in Transition* ed Z Dubinsky and N Stambler (Dordrecht: Springer Netherlands). pp. 493–505.
- [28] Mora C 2008 A clear human footprint in the coral reefs of the Caribbean *Proc. Biol. Sci.* **275** 767–73
- [29] Maire E, Cinner J, Velez L, Huchery C, Mora C, Dagata S, et al. 2016 How accessible are coral reefs to people? A global assessment based on travel time *Ecol Lett.* **19** 351–60.
- [30] Richmond R H, Rongo T, Golbuu Y, Victor S, Idechong N, Davis G, et al. 2007 Watersheds and Coral Reefs: Conservation Science, Policy, and Implementation *Bioscience* **57** 598–607.
- [31] Christie P, White A T 2007 Best practices for improved governance of coral reef marine protected areas *Coral Reefs* **26** 1047–56.
- [32] Rehr A P, Small M J, Bradley P, Fisher W S, Vega A, Black K, et al. 2012 A decision support framework for science-based, multi-stakeholder deliberation: A coral reef example *Environ. Manage.* **50** 1204–18.
- [33] Leenhardt P, Low N, Pascal N, Micheli F, and Claudet J 2015 The Role of Marine Protected Areas in Providing Ecosystem Services *Aquatic Functional Biodiversity – an Ecological and Evolutionary Perspective* ed A Belgrano, G Woodware, and U Jacob pp. 211–39.
- [34] Mumby P, Chisholm J, Edwards A, Clark C, Roark E, Andrefouet C, et al. 2001 Unprecedented bleaching-induced mortality in *Porites* spp. at Rangiroa Atoll, French Polynesia *Mar Biol.* **139** 183–9.
- [35] Fisk D, Done T 1985 Taxonomic and bathymetric patterns of bleaching in corals, Myrmidon Reef *Proc. 5th Int Coral Reef Congr.*
- [36] Williams E, Willaims L 1990 The world-wide coral reef bleaching cycle and related sources of coral mortality. *Atoll Res Bull.* 1–72.
- [37] Marshall P A, Baird A H 2000 Bleaching of corals on the Great Barrier Reef: differential susceptibilities among taxa *Coral Reefs* **19** 155–63.
- [38] Williams E H, Bunkley-Williams L. Bleaching of Caribbean coral reef symbionts in 1987-1988 *Proc. 6th Int. Coral Reef Symp.* **3** 313–8.
- [39] Lesser M P, Stochaj W R, Tapley D W, and Shick J M 1990 Coral Reefs effects of irradiance, ultraviolet radiation, and temperature *Coral Reefs* **8** 225–32.
- [40] Lesser M P 1997 Oxidative stress causes coral bleaching during exposure to elevated temperatures *Coral Reefs* **16** 187–92.
- [41] Erftemeijer P L, Riegl B, Hoeksema B W, and Todd PA 2012 Environmental impacts of dredging and other sediment disturbances on corals: a review *Mar. Pollut. Bull.* **64** 1737–65.

- [42] McWilliams J, Côté I, and Gill J 2005 Accelerating impacts of temperature-induced coral bleaching in the Caribbean *Ecology* **86** 2055–60.
- [43] Eakin C M, Morgan J A, Heron S F, Smith T B, Liu G, Alvarez-Filip L, et al. 2010 Caribbean corals in crisis: record thermal stress, bleaching, and mortality in 2005 *PLoS One* **5** e13969.
- [44] Yee S H, Santavy D L, Barron M G 2008 Comparing environmental influences on coral bleaching across and within species using clustered binomial regression. *Ecol Modell.* **218** 162–74.
- [45] Yee S H, Barron M G. 2010 Predicting coral bleaching in response to environmental stressors using 8 years of global-scale data. *Environ Monit Assess.* **161** 423–38.
- [46] Maina J, Venus V, McClanahan T R, and Ateweberhan M. 2007 Modelling susceptibility of coral reefs to environmental stress using remote sensing data and GIS models. *Ecol Modell.* **212** 180–99.
- [47] Wilkinson C, Souter D 2008 *Status of Caribbean coral reefs after bleaching and hurricanes in 2005.*
- [48] Papke L, Wooldridge J 1996 Econometric methods for fractional response variables with an application to 401 (k) plan participation rates. *J. Appl. Econom.* **11** 619–32.
- [49] DeBose J L, Nuttall M F, Hickerson E L, and Schmahl G P 2013 A high-latitude coral community with an uncertain future: Stetson Bank, northwestern Gulf of Mexico *Coral Reefs* **32** 255–67.

# **Chapter 3: High-resolution model for estimating the economic and policy implications of agricultural soil salinization in California**

This chapter is based on the following work currently under review at *Environmental Research Letters*:

Welle P D, and Mauter, M S High-Resolution Model for Estimating the Economic and Policy Implications of Agricultural Soil Salinization in California. *Environmental Research Letters*, *accepted but not yet published*.

## **3.1 Introduction**

Maintenance and intensification of agricultural practices will be critical to meeting the nutritional demands of the world's growing population. One widely practiced method of intensification, crop irrigation, can also lead to unintentional soil degradation and reduced crop yield when the total dissolved solids (TDS) concentration of the irrigation water is high or a substantial fraction of water is lost to direct evaporation [1, 2]. Quantifying the economic and social costs of soil salinization is critical to assessing conditions under which technology or policy intervention is necessary to correct market inefficiencies.

Soil salinization, the process by which dissolved solids in the irrigation water accumulate in the root zone as irrigation water evaporates or transpires, is problematic in arid regions, in regions dependent on groundwater, in regions that have adopted water-conserving irrigation practices, and in regions with shallow, impermeable soil layers [3]. In the last case, the applied water forms a perched water table, from which salts can be transported back to the surface through capillary action [4]. Once salinized, agricultural soils become less productive due to the combination of osmotic and ionic stress exerted on the plant [5, 6]. Growers may choose to fallow salinized land, leading to land use change [7] and greenhouse gas emissions [8, 9], or continue to cultivate less productive salinized land by switching crops and/or adjusting management practices, leading to reduced revenues and intensification of agricultural inputs (e.g. water).

Best management practices for mitigating the effects of soil salinization in high-risk agricultural areas have largely been derived from laboratory and field-scale experiments which elucidate the mechanisms by which soil salinization diminishes crop yield. These studies have probed the relationship between irrigation water quality and soil salinity, have provided yield reduction models that relate expected yield to soil salinity for a specific crop [6, 10-12] and have evaluated the efficacy of various remediation strategies. The most prevalent remediation strategy is salinity leaching, or the excess application of irrigation water to drain soils of existing salt content. Field experiments over a range of soil and crop types have been used to identify leaching fractions capable of maintaining soil salinity at moderate levels, but these leaching guidelines may not be implemented due to practical constraints on water availability or environmental discharge [13-16].

In addition to the work seeking to identify best practices for managing saline soils at the farm-scale, a separate body of literature has quantified the regional extent of soil salinization. Combining local inventories of affected land area with expert judgment, the UN Global Assessment of Human-induced Soil Degradation (GLASOD) program estimated that 76 million hectares, an area larger than France, were affected by human-induced salinization in 1991 [1]. More recent data compilation efforts suggest that China, Australia, and Pakistan are all experiencing the negative impacts of agricultural soil salinization [4, 17, 18]. Beyond land inventories, hydrological models have estimated the rate of salt flux over large areas [19] and informed predictions about future salt accumulation under current management practices. These regional assessments of soil salinity also serve as the basis for work quantifying the future social and economic impacts of soil salinization. Typically formulated as an optimization problem in which individual agents maximize their profits given constraints and costs of the inputs to production, these studies estimate changes in the economic output of a region relative to a baseline year. Examples include estimated revenue losses due to inefficient management of 14.5% in the Tungabhadra project in western India [20]; additional profit losses of \$1.8 to \$3.6 billion annually by 2030 over 2008 levels in the Central Valley of California [21]; and annual profit losses of 44-87% in the Murray-Darling Basin due to the

combined effects of climate change and salinity [22]. Each of these approaches quantifies losses relative to a baseline scenario, rather than the total current losses incurred, making it difficult to assess the full value of soil remediation efforts.

These loss estimation approaches typically rely on aggregated data for either crop or soil parameters, while yields are determined by field-scale processes. Unfortunately, using aggregated data can introduce bias into the estimate, as demonstrated in the climate adaptation and downscaling literature [23].

Similarly, it has been seen that when multiple spatial resolutions are available the selection of which characteristic resolution can have large impacts on the final output of the analysis [24, 25]. While these effects have seldom been studied with regards to agricultural optimization models employed to assess soil salinization, there are examples of these effects within agricultural models in general [26].

The present work makes three contributions. First, we develop a novel method for quantifying the absolute yield and revenue losses attributable to soil salinization. Integrating high-resolution satellite data, interpolated ground measurements, and county level yields and prices, we extend grower models traditionally applied to field-scale processes to understand regional-scale trends in the productivity of critical agricultural regions. Salinity and crop data are analyzed at the pixel scale (30 m by 30 m resolution), allowing precise modeling of specific soil conditions and avoiding the use of regional averages for spatially sensitive parameters. Second, we incorporate techniques to remove bias from our satellite-based estimates using coarse resolution validation data as a basis for quantifying classifier accuracy. This step is important in achieving correct results, and is documented in Appendix B Sections 9.2 and 9.4. Finally, we compare the model output to results from an analogous model using coarser resolution data to assess the influence of data resolution on the magnitude of the estimated salinity impacts. We apply these models to estimate 2014 yield and revenue losses from soil salinization in the State of California and to study the effects of spatial aggregation in model estimation.

## 3.2 Methods

We assess the costs of salinization by analyzing high resolution pixel-level data. These costs are quantified by calculating yield and revenue losses relative to a hypothesized non-salinized baseline state. After analyzing the model with high-resolution data sources, we apply the same approach to data aggregated at the regional level. We then assess the advantages of using the computationally intensive disaggregated data in comparison with more aggregated data sources.

### 3.2.1 Disaggregated Approach for Estimating Yield and Revenue Losses from Soil Salinization

We quantify current losses due to soil salinization in terms of yield (tons) and revenue (dollars). Yield loss at each pixel is calculated using Equation 1.

$$Y_p^L = \sum_c P_{c^*,c} * (1 - F_{p,c}) * \bar{Y}_c^M \quad (1)$$

where  $Y_p^L$  is the yield lost ( $Y^L$ ) due to salinity at pixel  $p$ .  $P_{c^*,c}$  is the probability that given the satellite based crop classifier indicates that a pixel contains a particular crop  $c^*$ , the pixel actually contains crop  $c$ . This term is used in order to remove bias from the estimate; a procedure further discussed in Appendix B Section 9.2.  $F_{p,c}$  is the fraction of maximum yield achieved given existing levels of salinity and choice of crop, estimated in Equation 2.  $\bar{Y}_c^M$  is the theoretical maximum yield, or the estimated crop-specific yield in the absence of soil salinity, and is estimated in Equation 3.

$$F_{p,c} = 1 - b_c(S_p^S - a_c) \quad (2)$$

$$\bar{Y}_c^M = Y_{r,c} \cdot \left( \frac{1}{n} \sum_{p \in c} F_{p,c} \right)^{-1} \quad (3)$$

Equation 2 models the crop salt tolerance response, as originally developed in Maas and Hoffman [11] where  $S_p^S$  is the soil salinity at a particular pixel and  $a_c$  and  $b_c$  represent the crop-specific threshold and slope response. The function is piecewise linear, with  $F_{p,c}$  equaling 1 until  $S_p^S$  reaches  $a_c$ , then linearly

decreasing at rate  $b_c$  until reaching 0. In Equation 3 the theoretical maximum yield,  $\bar{Y}_c^M$ , is calculated by dividing observed regional data on yields ( $Y_{r,c}$ ) by regionally averaged  $F_{p,c}$  values, where  $n$  represents the number of pixels in region  $r$ . This results in a single estimate of average maximum yield  $\bar{Y}_c^M$  for each crop in each region, which captures differences in soil fertility, climate, and technology between regions. Following this method, we estimate total area wide yield losses  $Y^{TL}$  (tons) using Equation 4, where  $k$  is a coefficient that converts the intensity of yield from acre<sup>-1</sup> to pixel<sup>-1</sup>.

$$Y^{TL} = \sum_p k * Y_p^L \quad (4)$$

Similarly, revenue loss  $R_p^L$  is obtained by estimating the fraction of theoretical maximum revenue  $R_{p,c}^M$  that is realized given the salinity impacted yields (Equations 5 and 6). The formulation for revenue loss parallels that of yield lost in Equation 1, with the addition of regional prices  $p_{r,c}$  to convert maximum yield to maximum revenue.  $R_p^L$  is translated into total revenues lost  $R^{TL}$  by summing over all pixels in the study and multiplying by the correction factor  $k$ .

$$R_p^L = \sum_c P_{c*,c} * (1 - F_{p,c}) * R_{p,c}^M \quad (5)$$

$$R_{p,c}^M = R_{r,c}^M = p_{r,c} \bar{Y}_c^M \quad (6)$$

### 3.2.2 Aggregated Approach for Estimating Yield and Revenue Losses from Soil Salinization

The aggregated approach mimics the disaggregated approach, but substitutes regionally aggregated estimates in place of pixel-level crop acreage estimates and salinity values. First, regional salinity values  $S_r^S$  are calculated by averaging pixel level salinity values across the region. Next, the fraction of maximum yield achieved is estimated Equation 7. Regional yield losses are calculated by estimating the theoretical maximum yield  $Y_c^M$  in Equation 8 and assessing the impact of salinity  $S_r^S$  on yields and revenues (Equations 9 and 10). Lastly, estimates of total yields lost  $Y^{TL}$  and revenues lost  $R^{TL}$  are

obtained by multiplying the per acre revenue and yield losses ( $Y_{r,c}^L$ ,  $R_{r,c}^L$ ) by regional crop acreages ( $A_{c,r}$ ) and summing over all crops and regions.

$$F_{r,c} = 1 - b_c(S_r^S - a_c) \quad (7)$$

$$Y_c^M = Y_{r,c} \cdot (F_{r,c})^{-1} \quad (8)$$

$$Y_{c,r}^L = (1 - F_{r,c}) * Y_c^M \quad (9)$$

$$R_{c,r}^L = (1 - F_{r,c}) * p_{r,c} * Y_c^M \quad (10)$$

$$Y^{TL} = \sum_c \sum_r Y_{c,r}^L * A_{c,r} \quad (11)$$

$$R^{TL} = \sum_c \sum_r R_{c,r}^L * A_{c,r} \quad (12)$$

### 3.2.3 Case study: California Yield and Revenue Losses from Soil Salinization

We apply these methods to assess the effects of soil salinization on yields and revenues in the State of California. California is the highest grossing agricultural state in the United States, with 2013 cash receipts of \$46.4 billion, or 12% of US agricultural totals [27]. Growers in the arid Central Valley of California are dependent on irrigation to sustain agricultural output and have long been plagued with soil salinization issues. Reduced yields from soil salinity are likely to be exacerbated during periods of drought, when application of leaching water is curtailed.

We combine statewide agricultural statistics from the California Department of Water Resources (DWR) with national statistics from the National Agricultural Statistics Service (NASS) to populate the yield reduction model, with county-level data serving as regions. We use the top twenty most profitable (highest gross revenues) crops in California for participation in the study (Table S1 in Appendix B). When combined, these crops account for over 95% of the non-livestock agricultural cash receipts in the state [28]. In addition to these twenty crops we account for fallowed land, bringing the total crop

categories to twenty-one. Crop data are released as 30 m square pixels, which define the characteristic resolution of the case study.

The data are sourced from a variety of agencies that publish on intermittent intervals, requiring the combination of data from 2013 and 2014 in the loss analysis. The two driving data sources, crop patterns and salinity, are both for 2014. Prices and yields are for 2013, but have low year-to-year variation. We thus consider the year of analysis to be 2014. Estimating rehabilitation potential also requires information on crop water use intensity and leaching practices, which was last reported in 2010. Full detail on data sources is given in Appendix B Section 9.1.

### *3.2.4 Statistical Analysis*

We perform a statistical analysis to determine the magnitude of the linear correlation between salinity and four parameters: crop marginal value, crop salt tolerance, estimated yield reduction, and estimated revenue losses per acre (Table S4). To perform the regression, we use the vector salinity data and aggregate the four parameters up to the same scale using zonal averages. The regression is estimated using a generalized additive model (GAM) to control for latitude and longitude using a thin plate spline regression. See Appendix B Section 9.7 for additional detail.

## **3.3 Results**

This method provides the first quantitative estimate of lost yields and revenues to salinity at a sufficiently high resolution (30 m) for both field and region-level decision making. We demonstrate the value of these methods using the State of California as a case study, calculating the losses due to salinity.

### *3.3.1 Results of Adopting a Disaggregated Approach for Estimating Yield and Revenue Losses from Soil Salinization in CA*

We find that higher salinity soils in California (Figure 3-1A) are spatially correlated with low crop yield (Figure 3-1B;  $r = -0.84$ ), high revenue losses (Figure 3-1C;  $r = 0.33$ ), the cultivation of salt tolerant crops (Figure S4B in Appendix B;  $r = 0.26$ ), and the cultivation of lower revenue crops ( $r = -0.30$ ). When

regressing each of these four parameters of interest on salinity, we observe a statistically significant response for each variable's coefficient (see Table S4). We find that salinity is correlated with lower relative yields ( $\beta = -5.38$ ), higher revenue losses ( $\beta = 364.9$ ), higher crop tolerance ( $\beta = 0.034$ ), and lower crop revenues ( $\beta = -304.46$ ). Each of these coefficients are significant at the  $p < 0.001$  level.

Salinity values are highest in the Imperial Valley (located in southeast California along the border with Mexico) and the southern Central Valley. Relative yield is driven by two parameters: soil salinity and crop salt sensitivity (Table S1 in Appendix B). Although we observe that growers compensate for elevated levels of soil salinity by planting salt tolerant crops on salinity-impaired fields (Figure S5A in Appendix B), relative yield remains lowest where salinity values are highest.

The spatially resolved data from Figure 3-1B is re-plotted in Figure 3-2B as a cumulative density function (CDF) which relates the fraction of agricultural land in California to the percentage of relative yield.

According to the Cropland Data Layer published by USDA, approximately 1.7 million acres of California farmland are fallowed and produce no agricultural output, encoded with a relative yield of zero. Another 1.6 million acres have reduced agricultural yield, reporting salinity in excess of the tolerance threshold of the current crop mix. The existing salinity levels on the final 4.8 million acres of agricultural land are unlikely to affect yield for the current crop mix. Aggregating across all agricultural farmland in California, we estimate that soil salinization reduces crop yields by 8.0 million tons annually.

Reduced agricultural yields result in lost revenue. Revenue losses (Figure 3-1C) are highest in the western San Joaquin Valley, with losses as high as \$3000 per acre on select fields. While yield losses are higher in the Imperial Valley, revenue losses are less substantial as growers are primarily planting lower revenue crops, such as alfalfa. The CDF of revenue lost per acre is reported in Figure 3-2A. At the state level, we estimate that soil salinization reduced grower revenues by \$3.7 billion, or 7.9% of CA agricultural output, in 2014. We find that this value likely ranges between \$1.4 billion and \$7.0 billion and that nearly all the uncertainty in our data can be attributed to uncertainty in the salinity measurements (Figure S2 in Appendix B).

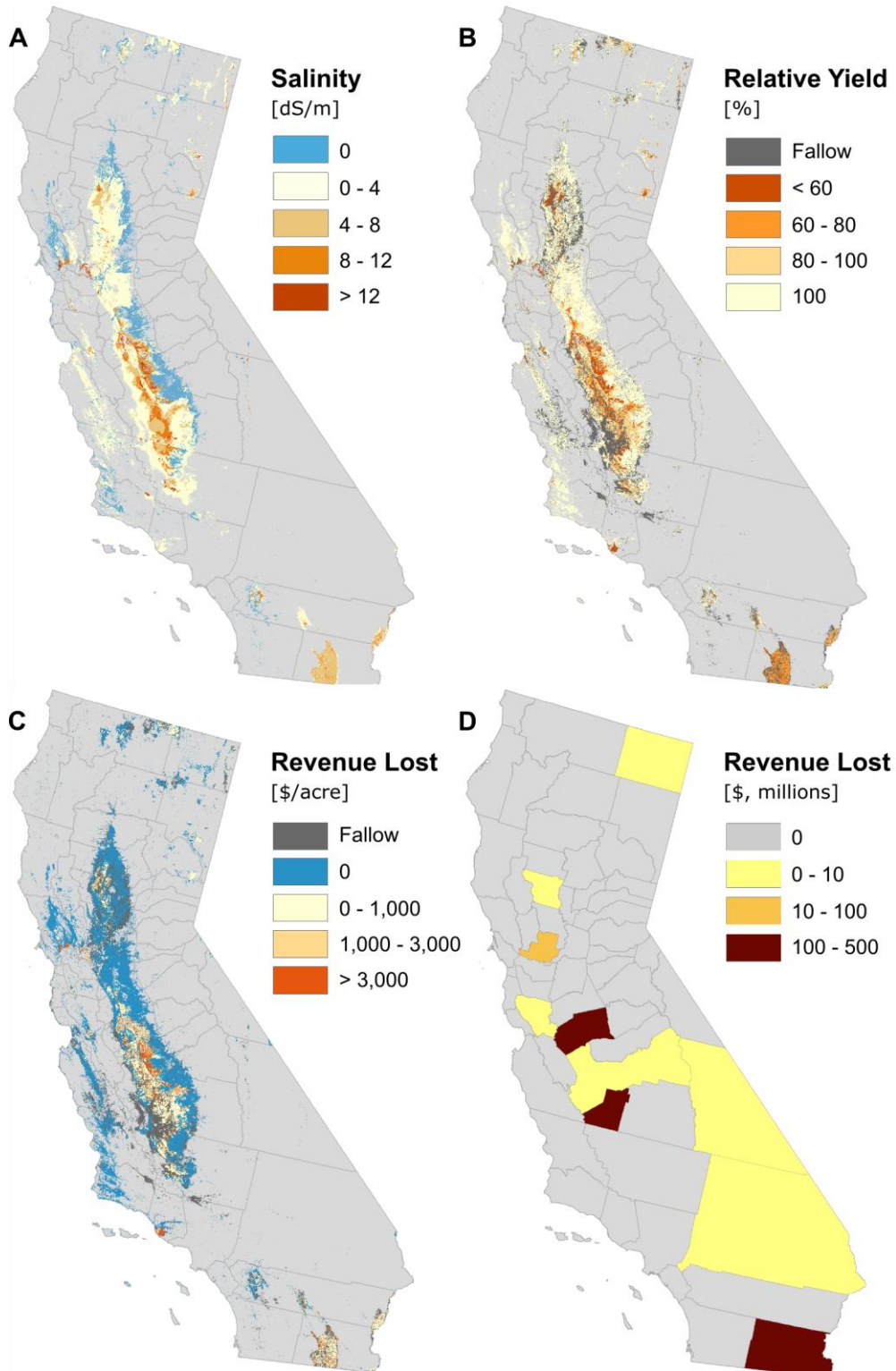


**Figure 3-1. Spatially resolved estimates of (A) soil salinity, (B) relative yield, (C) revenue lost per acre calculated with disaggregated data, and (D) revenue lost by county using aggregated data.**

Lost yield and lost revenue for individual crops are plotted in Figure 3-2. The Other High Uncertainty Crops (OHUC) category is an amalgamation of the seven crops that could not reliably be identified using remote sensing techniques (Figure S3 in Appendix B). Together, almonds, strawberries, grapes, and alfalfa account for approximately half (49.5%) of the total \$3.7 billion in annual revenue loss. Revenue lost is a function of soil salinity, crop sensitivity, crop marginal revenue, and total crop acreage. While these four crops account for a large percentage of total acreage, they also experience higher yield reductions on a per acre basis. Relative yield averages 85% for these crops, compared to a 94% average yield for all other crops.

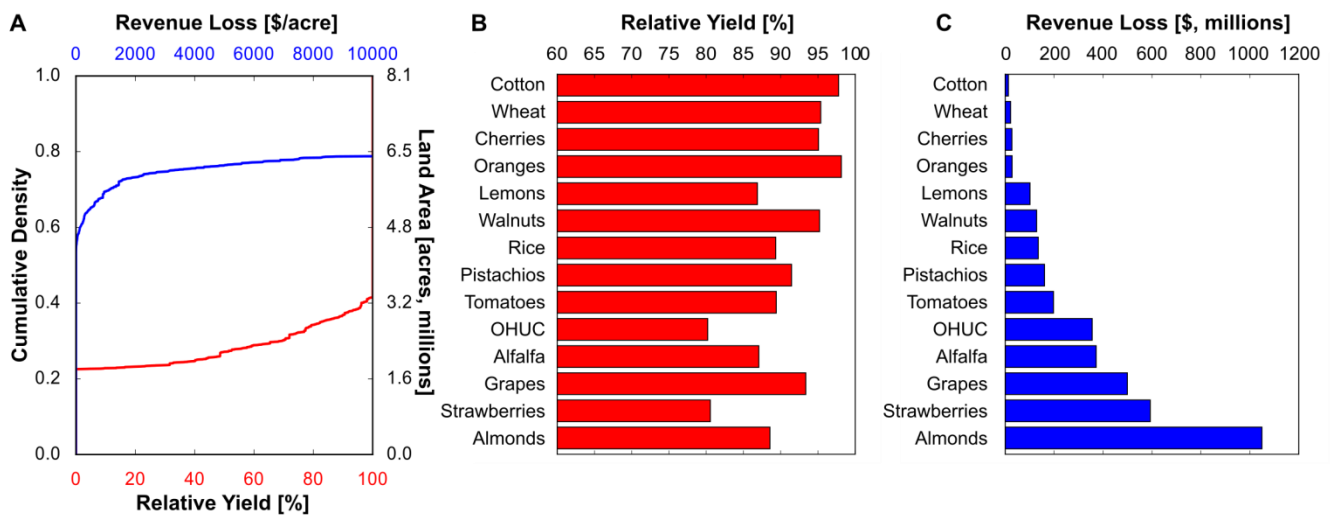


**Figure 3-2. Aggregate and per crop relative yield and revenue losses. (A) Cumulative density function of revenue lost per acre and relative yield. (B) Relative yield by crop. (C) Total revenue lost by crop. Other High Uncertainty Crops (OHUC) include those crops that cannot be consistently estimated (see Figure S3 in Appendix B) using remote sensing. These include broccoli, carrots, celery, corn, lettuce, peaches and peppers.**

### 3.3.2 Results of Adopting an Aggregated Approach to Estimating Yield and Revenue Losses from Soil Salinization in CA

A similar approach is applied using regional data. Cropping data comes from county-level statistics (see Section 9.1 in Appendix B for detail), while salinity data are aggregated to the county level (Figure 3-1D).

There are several prominent differences between results from the aggregate and disaggregate analyses. The first is that all of the estimated lost revenues occur in just 10 counties, compared with the 40 counties with estimated revenue loss using the disaggregated approach. Of the 10 counties with lost revenues, 97% of the losses occur in three counties (Imperial, Kings, and Merced). This contrasts with the wider distribution of losses that are estimated by the disaggregated model.

Two effects are driving the differences between the aggregated and disaggregated approaches. The first is that salt-sensitive, high revenue crops are not likely to be grown on soils with salinity levels equal to the county average. Indeed, the spatially resolved satellite data shows a negative relationship between salinity and crop marginal revenue and a positive relationship between salinity and salt tolerance (Section 9.5 in Appendix B). This causes an upward bias in loss estimates.

The second effect is that if elevated salinity is confined to a small geographic area within the county then the average salinity for the county may be low. While models based on disaggregated data estimate damages in the area with elevated salinity, models based on aggregated data inherently smooth over variability in field-level soil salinity. As a result, these aggregated modeling approaches may miss salinity losses if the county average salinity is below the threshold for the cultivated crops. This effect will cause a downward bias in the final estimate.

After aggregating both approaches to the state level, we find that the aggregated model suggests that estimated annual lost revenues in the state of California due to salinity are \$1.0 billion, compared with the \$3.7 billion estimated in the disaggregated approach. This number lies outside the \$1.7 - \$7.0 billion determined in the uncertainty analysis (Section 9.3 of Appendix B).

The differences in the two estimates may result from either the different crop data sources (i.e. satellite vs regional surveys) or the spatial resolution of the analysis. To eliminate the effect of the differing crop data sources, we perform a third analysis where we run the aggregated model using pixel-level satellite data that has been aggregated at the county level to estimate regional crop acreage. When we perform

this analysis, we find that the aggregated satellite data results in similar cumulative damages (\$1.2 billion) to the those estimated using regional cropping data (\$1.0 billion) and leaves Figure 3-1D unchanged. Thus, the lower yield and revenue loss estimates stem directly from performing the analysis at the county, rather than pixel, scale.

### **3.4 Discussion**

In analyzing agricultural systems there has historically been a tradeoff between the scale of the analysis and its resolution. Field measurements are highly accurate, but can be costly to collect at sufficient density over large regions. Regional estimates provide data at broader scales, but are typically limited in their ability to describe a variable's spread and correlation with other variables, factors which are of critical importance in assessing spatially distributed processes such as salinization. Recent improvements in remote sensing, combined with modern data storage and processing, are helping to circumvent the scale / resolution tradeoff. By continuously collecting measurements with both high spatial and temporal resolution, orbital sensors are capable of describing a variable's entire distribution as well as its spatial correlation with other covariates. As the accuracy and availability of remotely sensed data increase, effectively integrating this information with more traditional, regional data sources offers significant promise for improving the accuracy of regional level agricultural policy analysis.

In this study, we present a novel method that integrates high-resolution satellite data, interpolated ground measurements, and county level yields and prices to estimate the regional effects of soil salinization on agricultural productivity. The estimates are performed at the field-scale, allowing the model to capture the local variation inherent in agricultural systems. The method has broad applicability for testing alternative management practices and policies at the regional level, as illustrated in our case study of California where we evaluate leaching as a best-management practice for addressing soil salinization. Moreover, the generalized approach may serve as a template for integrating multi-modal data to assess the economic effects of phenomena on agriculture at high resolution over regional scales.

While the general approach is valid, the proposed methods are limited by their inability to predict crop switching, as well as their continued reliance on regional averages for a number of the inputs. The model quantifies losses based on current cropping patterns and does not account for how producers might adjust their production practices given changes in resource availability, soil quality, or other factors. For example, as salinity levels decrease, growers are likely to switch from lower value, salt tolerant species to higher value, salt sensitive crops. The current analysis does not account for the theoretical gain of revenue that growers would accrue due to switching crops, meaning the current model is likely to underestimate the revenue losses from soil salinity. In order to address this limitation, we would need to expand to a spatially resolved, multi-year data set. Applying panel data methods to such data would allow for the estimation of switching costs, and accounting for these costs could provide an avenue for estimating the likely change in crop mix as salinity levels decrease.

Second, the model is limited by the available data. The salinity data are sourced from interpolated ground measurements which are smoothed through time and space, increasing the probability that reported values deviate from actual field conditions. Emerging techniques for remotely collecting soil salinity data, which rely on either airborne electromagnetic surveys or salinity estimates from orbital sensors [29-31], will further enhance the resolution of soil salinity estimates and reduce uncertainty in yield reduction analyses. Lastly, the formulas approximating the relationship between leaching fraction, soil salinity, and crop yield represent average responses of each crop class. They do not account for variation in other soil parameters or management practices that influence yield in specific fields, including irrigation practices, soil organic carbon and micronutrient concentrations, or the use of salt tolerant cultivars. To account for this underlying variability, we perform extensive uncertainty analysis on the yield response function as described in Section 9.3 of Appendix B. Future improvements in the remote sensing of soil quality parameters and crop yield may enable stronger statistical prediction of yield response. If successful, revised yield response functions would be easily incorporated into this analysis framework.

The limitations of the method are critical for interpreting the results of the case study. The estimated yield and revenue losses for California are calculated directly from current cropping patterns and do not account for crop switching. Accounting for crop switching are likely to increase the estimated revenue losses, though the effect on relative yield is less clear. The effect of incorporating local estimates for salinity, yield, and water use in place of regional ones is also uncertain, and depends on underlying correlations between the data. For instance, it is possible that theoretical maximum yield is correlated within region to areas with either lower or higher salinity levels, an effect that would cause our results to be biased upwards or downwards, respectively. Directly measuring these correlations and accounting for their effects is a significant motivation for seeking higher resolution data.

Despite these limitations, multi-modal models for estimating the effects of soil salinization on agricultural productivity offer valuable insight into the magnitude of yield and revenue losses in vulnerable regions. The estimated 2014 losses of 8.0 million tons of yield and \$3.7 billion in 2014 are a significant fraction of state agricultural outputs of 69 million tons with a combined worth \$32 billion. To put this in perspective, these estimates suggest that the yearly economic damages due to soil salinization are of comparable scale to the yearly damages associated with the California drought in 2014 and 2015 [32, 33]. While the uncertainty analysis accounts for multiple years of data, the results presented are for 2014 and may differ under non-drought conditions.

We have shown that salinity has large impacts on Californian agriculture. Leaching, the primary strategy for managing soil salinity, is likely to be further constrained in California as a result of the high selenium content of this agricultural drainage discharge [34]. At the same time, drought and reduced snowpack water storage is expected to limit the water supply critical to leaching practices. Alternatives to salinity leaching include land fallowing or the application of lower salinity irrigation water, leading to climate impacts [8, 9] or the need for costly water treatment systems [35]. In short, salinization is likely to remain a significant societal and technological challenge in arid regions such as California. Successful

management will rely on accurate monitoring and assessment coupled with impact analyses that are performed at a spatial scale that captures the underlying mechanisms of yield loss.

## References

- [1] Oldeman L 1994 The global extent of soil degradation *Soil Resilience and Sustainable Land Use* ed D J Greenland and I Szabolcs (Wallingford, UK: CAB International) pp 99–118
- [2] Ghassemi F, Jakeman A J, and Nix H A 1995 *Salinisation of land and water resources: human causes, extent, management and case studies* (Wallingford, UK: CAB International)
- [3] Hillel D 2000 *Salinity management for sustainable irrigation: integrating science, environment, and economics* (Washington, D.C.: World Bank Publications)
- [4] Rengasamy P 2006 World salinization with emphasis on Australia. *J. Exp. Bot.* **57** 1017-23.
- [5] Hasegawa P M, Bressan R A, Zhu J K, and Bohnert H J 2000 Plant cellular and molecular responses to high salinity *Annu. Rev. Plant Biol.* **51** 463-99.
- [6] Maas E 1984 Crop tolerance *California Agriculture* **38** 20-21.
- [7] United Nations Environment Program 2014 Assessing Global Land Use: Balancing Consumption with Sustainable Supply. A Report of the Working Group on Land and Soils of the International Resource Panel Bringezu S, Schütz H, Pengue W, O'Brien M, Garcia F, Sims R, Howarth R W, Kauppi L, Swilling M, and Herrick J
- [8] Houghton R A 2003 Revised estimates of the annual net flux of carbon to the atmosphere from changes in land use and land management 1850–2000. *Tellus B* **55** 378-90.
- [9] Tilman D, Balzer C, Hill J, and Befort B L 2011 Global food demand and the sustainable intensification of agriculture. *Proc. Natl. Acad. Sci. USA* **108**, 20260-64.
- [10] Maas E 1993 Testing crops for salinity tolerance *Proc. Workshop on Adaptation of Plants to Soil Stresses* p 247.
- [11] Maas E V, and Hoffman G J 1977 Crop salt tolerance - current assessment *J. Irrig. Drain. Div. ASCE* **103** 115-34.
- [12] Van Genuchten M T and Gupta S 1993 A reassessment of the crop tolerance response function *Indian Soc. Soil. Sci* **41** 730-7.
- [13] Hanson B, Grattan S R, and Fulton A 1999 *Agricultural salinity and drainage* (Davis, CA: University of California, Davis)
- [14] Hoffman G J and Van Genuchten M T 1983 Soil properties and efficient water use: water management for salinity control *Limitations to efficient water use in crop production* ed Taylor HM *et al* (Madison, WI: American Society of Agronomy) pp 73-85.
- [15] Rhoades J and Merrill S 1976 Assessing the suitability of water for irrigation: theoretical and empirical approaches. *FAO Soils Bulletin 31* (Rome, Italy: Food and Agriculture Organization of the United Nations) pp 69-109
- [16] Ayers R S and D W Westcot 1985 *Water quality for agriculture* (Rome, Italy: Food and Agriculture Organization of the United Nations)
- [17] LADA Project Team 2010 *China National Level Report of Land Degradation Assessment in Drylands (LADA)*
- [18] Qureshi A S, McCornick P G, Qadir M, Aslam Z 2008 Managing salinity and waterlogging in the Indus Basin of Pakistan *Agr. Water Manage.* **95** 1-10
- [19] Schoups G, Hopmans J W, Young C A, Vrugt J A, Wallender W W, Tanji K K, and Panday S 2005 Sustainability of irrigated agriculture in the San Joaquin Valley, California. *Proc. Natl. Acad. Sci. USA* **102** 15352-6.

- [20] Janmaat J 2004 Calculating the cost of irrigation induced soil salinization in the tungabhadra project. *Agr. Econ.* **31** 81-96.
- [21] Howitt R, Kaplan J, Larson D, MacEwan D, Medellín-Azuara J, Horner G and Lee, N 2009 *The economic impacts of Central Valley salinity: Final Report to the State Water Resources Control Board*
- [22] Connor J D, Schwabe K, King D and Knapp K 2012 Irrigated agriculture and climate change: the influence of water supply variability and salinity on adaptation. *Ecol. Econ.* **77** 149-57
- [23] Baron C, Sultan B, Balme M, Sarr B, Traore S, Lebel T, Janicot S, and Dingkuhn M 2005 From GCM grid cell to agricultural plot: scale issues affecting modelling of climate impact. *Philos. T. Roy. Soc. B.* **360** 2095-108.
- [24] Pontius Jr R G, Chen H, Thontteh O 2005 Multiple scale pattern recognition and the foundation of observation-free statistics. *Proc Amer Soc Photogramm Rem S.* Baltimore MD
- [25] Fotheringham A S and Wong D W 1991 The modifiable areal unit problem in multivariate statistical analysis. *Environ Plann. A.* **23** 1025-44
- [26] Medellín-Azuara J, Harou J J and Howitt R E 2010 Estimating economic value of agricultural water under changing conditions and the effects of spatial aggregation. *Sci. Total Environ.* **408** 5639-48.
- [27] National Agricultural Statistics Service, U.S. Department of Agriculture 2015 *California Agricultural Statistics 2013 Annual Bulletin*
- [28] National Agricultural Statistics Service, U.S. Department of Agriculture 2013 County Ag Commissioners' Data Listing [http://www.nass.usda.gov/Statistics\\_by\\_State/California/Publications/AgComm/Detail](http://www.nass.usda.gov/Statistics_by_State/California/Publications/AgComm/Detail) (accessed August 15, 2015).
- [29] Metternicht G and Zinck A 2008 *Remote sensing of soil salinization: Impact on land management* (Boca Raton, Florida: CRC Press)
- [30] Allen R G, Tasumi M and Trezza R 2007 Satellite-based energy balance for mapping evapotranspiration with internalized calibration (METRIC)—Model *J. Irrig. Drain. E-ASCE* **133** 380-94
- [31] Lobell D B, Ortiz-Monasterio J I, Asner G P, Naylor R L and Falcon W P 2005 Combining field surveys, remote sensing, and regression trees to understand yield variations in an irrigated wheat landscape *Agron. J.* **97** 241-9
- [32] Howitt R, MacEwan D, Medellín-Azuara J, Lund J and Sumner D 2015 *Economic analysis of the 2015 drought for California agriculture*
- [33] Howitt R, Medellín-Azuara J, MacEwan D, Lund J and Sumner D 2014 *Economic analysis of the 2014 drought for California agriculture*
- [34] 2015 *Westlands v. The United States* United States District Court Eastern District of California
- [35] Stuber M D 2016 Optimal design of fossil-solar hybrid thermal desalination for saline agricultural drainage water reuse *Renew. Energ.* **89** 552-63

# **Chapter 4: Assessing the magnitude of crop switching due to salinity in the Central Valley of California**

This chapter is currently in preparation for publication. It is being co-authored with Meagan Mauter, Nicholas Muller, and Momin Ghalib.

## **4.1 Introduction**

It is important that methods which assess the impacts of policy changes on agriculture account for farmer behavioral response. One key response available to growers seeking to adapt to new conditions is crop switching – namely the practice of cultivating crops better suited to expected future conditions. From a theoretical perspective, impact assessment methods which do not account for crop switching are only appropriate if relevant shocks are unexpected and, thus, farmers are not able to adjust their crop mix to the new circumstances. Since policy changes are typically implemented with lead-in time, accurately predicting how farmers change their cropping decisions is a key research task for those seeking to estimate policy effects on agriculture.

Approaches to model crop switching include both theoretical and empirical techniques. Positive mathematical programming (PMP) is a deductive technique based on assumed profit maximizing behavior [1-3], of which the Statewide Agricultural Production (SWAP) model is an example. The grower in a PMP model receives revenues according to the mix of crops planted, while their cost curve is calibrated to data from the region in which it is implemented. After calibration, the model can be used in policy exercises while accounting for the change in cropping patterns. Empirical approaches, on the other hand, seek to model behavioral response using regression techniques. For example, in their work to estimate the effects of climate change on US agriculture, Mendelson et al. [4] regress land value on climatic, economic, and soil parameters and use this regression to estimate the change in long term profits under climate change. Such a model assumes that farmers will modify their crop choice to maximize their property value, and so incorporates crop switching. The approach outlined in Mendelson et al. [4] has

been both extended and implemented in other contexts [5-14]. Other researchers have sought to apply discrete choice models (e.g. multinomial logit) to estimate crop switching directly. Discrete choice models use regression based approaches to predict what growers will cultivate directly, and have been applied to agriculture related to a variety of questions including adoption of conservation tillage practices [15], irrigation choice [16], as well as population expansion and industrial development [17].

Often theoretical and empirical models are applied to aggregated data (e.g. county or state-level) due to data availability, even though aggregated data may limit the accuracy of policy analyses. Measurements conducted at the farm-scale are costly and so government agencies typically rely on survey data to inform parameters such as yield and cropping patterns. However, applying policy analysis on aggregated data may limit accuracy for several reasons. First, aggregated data (e.g. county or country level) can result in inaccurate estimation if there is significant within-region variation in the parameters of interest [18, 19]. While county-level data may have sufficient resolution for models which seek to measure the impact of spatially smooth parameters such as climatic variables, variables which change over small spatial scales such as soil parameters require higher resolution data. Second, if the phenomenon of interest has a small spatial extent, relying on aggregated data may result in a small number of independent observations. And third, biophysical data are increasingly available at higher resolutions, and this increased information cannot be taken into account in models estimated using aggregated data.

Spatial disaggregation techniques can be used to generate estimates of land use at high resolution from aggregate data when using aggregate data directly is not appropriate and disaggregated data are not available. One method for spatial disaggregation is termed cross-entropy minimization, which seeks to minimize the Kullback-Liebler divergence between a prior and final estimate subject to constraints. The key challenge to retrieving accurate estimates from cross-entropy minimization is constructing an accurate prior. Howitt et al. [20] use a Dynamic Markov model based on disaggregated data in order to generate priors. Chakir [21] proposes an econometric approach, using aggregated data as well as higher-resolution biophysical data to generate priors at higher resolution. You et al. [22] and You et al. [23]

develop an framework which uses a variety of data on agronomic crop suitability as well as population density to generate priors at global scale.

In this study, we model farmer behavioral response to salinity in the Central Valley (CV) of California by estimating a discrete choice model on a cross-sectional dataset from the year 2015. First, we statistically downscale county-level crop acreage estimates using cross-entropy to 56,043 soil polygon regions using a satellite based crop classifier as our prior. Next, we construct a rich set of explanatory variables for each soil polygon including salinity, other soil parameters, temperature, precipitation, topographical features, crop prices, expenses, as well as spatial fixed effects which demarcate local administrative boundaries. We use this econometric model to gain insight as to how farmers modify their cropping patterns in response to different salinity levels. Lastly, we conduct policy exercises to determine the likely change in revenue given changes in extant salinity levels.

## **4.2 Methods**

In this study we model producer crop choice in order to assess behavioral response to soil salinity in the CV. The CV is a productive agricultural region in California spanning 19 counties - Butte, Colusa, Glenn, El Dorado, Fresno, Kern, Kings, Madera, Merced, Placer, San Joaquin, Sacramento, Shasta, Stanislaus, Sutter, Tehama, Tulare, Yuba, and Yolo. We select for the analysis the top 20 crops according to gross revenue in 2015, and cluster these crops into 10 categories by their crop type and salt tolerance (tolerance and revenue by crop category is reported in Table S1 in Appendix C). These categories are Sensitive Nuts, Tolerant Nuts, Other Trees, Feed (Hay), Grain, Field, Vineyard, Sensitive Vegetable, Vegetable, and Tolerant Vegetable.

The general methodological approach involves downscaling land use data (Section 4.2.1), constructing a set of independent variables (Section 4.2.2), regressing downscaled land use data on explanatory variables (Section 4.2.3), and utilizing the regressions to conduct policy exercises (Section 4.2.4).

### 4.2.1 Downscaling Land Use Data

A critical step in the analysis is downscaling land use data from county-level to the level of soil polygon regions (see Section 4.2.2 for details on soil polygons) using cross-entropy minimization. This procedure requires two sets of data – (1) regional level data at the aggregate scale and (2) priors at the disaggregated scale.

For regional-level data we use crop area estimates reported at the county level by the National Agricultural Statistics Service (NASS) [24]. These data are released annually and contain estimates of price, yield, and gross acreage by crop.

For the priors at the disaggregated scale, we aggregate up 30-meter pixel estimates of crop land use as reported by the Cropland Data Layer (CDL) [25]. While we could utilize the CDL directly for land use estimates, it was found in Welle and Mauter [26] that even after conducting bias correction procedures there can still be considerable difference between the CDL and county-level estimates of certain crops. The CDL has net accuracy of 84.9% at the pixel level, and thus serves as an excellent prior. For each soil polygon within an individual county the prior  $\pi_{cr}$  is formulated as the estimated area fraction of crop  $c$  in region  $r$ , where region in this context refers to the soil polygons. It is calculated in Equation 1, where  $Satellite_{rc}$  is the estimated acreage from the satellite based crop classifier for crop  $c$  in soil polygon region  $r$ .

$$\pi_{rc} = \frac{Satellite_{rc}}{\sum_r Satellite_{rc}} \forall r, c \quad (1)$$

Once the prior is constructed, the minimization problem can be executed as described in Equations 2-5, where a separate optimization problem is resolved for each county. The decision variable,  $s_{rc}$ , is the fraction of a crop's land area to be allocated to particular soil polygon region. The optimization problem is subject to three constraints. Equation 3 ensures that the land fractions sum to 1 for each crop. Equation

4 restricts each value of  $s_{rc}$  to the unit interval. Equation 5 prevents more acreage being assigned to a region than its geographic size ( $Size_r$ ), where  $Area_c$  is the number of acres for crop  $c$  in a county.

$$\text{minimize} \quad CE(s_{rc}) = \sum_c \sum_r s_{rc} \ln s_{rc} - \sum_c \sum_r s_{rc} \ln \pi_{rc} \quad (2)$$

$$\text{subject to} \quad \sum_r s_{rc} = 1 \quad \forall c \quad (3)$$

$$0 \leq s_{rc} \leq 1 \quad \forall r, c \quad (4)$$

$$\sum_r s_{rc} \cdot Area_c \leq Size_r \quad \forall r \quad (5)$$

It should be noted that if the prior satisfies the constraints in Equations 3-5, then the solution to the objective function in Equation 2 will be  $s_{rc} = \pi_{rc}; \forall c \forall r$ . Using this intuition, the procedure can be understood as one that attempts to disaggregate cropped area at the county level ( $Area_c$ ) to the regional level according to regional-level priors, making small adjustments to the priors when they result in an infeasible solution.

#### 4.2.2 Independent Variables

The land use data disaggregated in section 2.1 is regressed on a set of explanatory variables, including salinity, other soil parameters, temperature, precipitation, topographical features, crop prices, expenses, as well as dummy variables which demarcate local administrative boundaries.

Soil parameters are sourced from the Soil Survey Geographic Database (SSURGO) for the year 2015, which is a vector dataset of 456,249 soil polygon regions across California [27]. The SSURGO database is first clipped to the 156,315 polygons which intersect the 19 counties of the Central Valley, of which 56,043 contain agricultural crops as measured in the CDL. Soil polygons contain information on salinity, soil permeability, water capacity, sand, and clay. Polygons have median size of 0.12 km<sup>2</sup>.

Weather and topographical parameters include temperature, precipitation, and elevation. Surface temperature is sourced from the National Centers for Environmental Prediction (NCEP) / National Center for Atmospheric Research (NCAR) Reanalysis project [28], while precipitation data come from the

Climate Hazards Group InfraRed Precipitation with Station data (CHIRPS). Both datasets are included in the regression as four monthly averages, representing seasons – January, April, July, and October.

Elevation data are sourced from the National Elevation Dataset (NED) and have a spatial resolution of 1/3 arc-second, or approximately 10 meters. All three datasets are averaged within the soil polygons.

Crop prices and expense data are included as predictors in the regression, though the only available data are sourced from county level surveys. Prices for each of the crops are established using NASS county-level data [24]. Expenses, including agriculture services, chemicals, fertilizers, depreciation, fuels, interest, labor, rent, seed and supplies, supplies and repairs, and taxes are available at the county level from the 2012 Census of Agriculture conducted by NASS.

Lastly, since there are likely unobserved parameters which affect crop choice (e.g. state water contracts, groundwater, et cetera), we include spatial dummy variables for administrative districts. The administrative regions used are the California Department of Water Resources (DWR) Detailed Analysis Units (DAUs). DAUs are based on a combination of hydrologic and administrative boundaries (e.g. irrigation districts, county borders), and represent the smallest unit at which DWR releases data. There are a total of 355 DAUs in California, 89 of which intersect our study area.

#### *4.2.3 Modeling*

The land use of each crop cluster is related to explanatory variables through a fractional multinomial logit (FMNL) model, which is the multinomial generalization of the fractional logit model presented in Papke and Wooldridge [29]. Fractional multinomial logit allows for the prediction of values that are represented as a share or a percentage, and is thus suited to predicting farmer crop allocation. It is estimated by applying a quasi-maximum likelihood approach. An important assumption implicit in the FMNL framework is the independent of irrelevant alternatives (IIA) assumption, which implies that the ratio of fractional cropping area of any two categories is independent of all other categories. Because of this feature of model, we cluster the 20 study crops into 10 individual crop groupings.

The general model is presented in Equations 6-8. Equation 6 shows the model for predicting the share  $Y_{rj}$  of each of the ten crop categories  $j$  in soil polygon region  $r$ . As with multinomial logistic regression, one of the categories is withheld as the pivot against which the other categories are estimated, here represented as crop group  $K$ . Equation 7 shows the implied crop share of the pivot crop category, derived using  $\sum_j Y_{rj} = 1$ . The independent variables in our analysis are displayed in Equation 8, and include the salinity parameter  $Salinity_r$ , 4 soil parameters  $Soil_{ra}$ , 20 price parameters  $CountyPrice_{r,c}$ , 89 DAU parameters  $DAU_{r,d}$ , 4 temperature parameters  $Temp_{r,season}$ , 4 precipitation parameters  $Precip_{r,season}$ , and altitude parameter  $Altitude_r$ .

$$E[Y_{rj}|z_{rj}] = \frac{e^{z_{rj}}}{1 + \sum_{k=1}^{K-1} e^{z_{rk}}} \quad (6)$$

$$E[Y_{rj}|z_{rj}] = \frac{1}{1 + \sum_{k=1}^{K-1} e^{z_{rk}}} \quad (7)$$

$$z_{rj} = \beta_{0j} + \beta_{1j}Salinity_r + \sum_a \alpha_{aj}Soil_{ra} + \sum_c \delta_{c,j}CountyPrice_{r,c} + \sum_d \theta_{d,j}DAU_{r,d} + \sum_{season} \vartheta_{season,j}Temp_{r,season} + \sum_{season} \mu_{season,j}Precip_{r,season} + \beta_{2j}Altitude_r \quad (8)$$

#### 4.2.4 Policy Analysis

We apply the fitted model to assess grower response to soil salinity. Specifically, we parametrically adjust the soil salinity and use the trained regression to predict the new crop mix for each soil polygon region.

Using the new crop mix we calculate the predicted total revenue across all polygons under the new salinity set while allowing the growers to adjust their crop choice.

The analysis is based upon the empirical yield reduction equation presented in Hoffman [30]. Each individual crop is measured through field experimentation for two parameters – a threshold and a slope.

The threshold (parameter  $a_j$  in Equation 9) is the salinity above which a crop begins to experience yield losses. The slope (parameter  $b_j$  in Equation 9) determines the rate at which salinity impacts yields. The result of Equation 9 is the relative yield,  $Yield_{rj}^{Rel}$ , which lies on the unit interval and represents the fraction of theoretical maximum yield that a crop receives while being cultivated at a specific salinity value.

First, we estimate the theoretical maximum yield from many observations of  $Yield_{rj}^{Rel}$ . The finest resolution yield data that are available are at the county level, represented by  $Yield_j$ . The relative yield parameters within that county are averaged over the soil polygon regions, resulting in an average estimate of yield reduction for the county  $\overline{Yield_j^{Rel}}$ . The theoretical maximum yield  $Yield_j^{Max}$  is calculated by dividing  $Yield_j$  by  $\overline{Yield_j^{Rel}}$ . Theoretical maximum yield is assumed to be constant within each county, so the maximum yield at a polygon  $Yield_{rj}^{Max}$  is simply set to the county level value  $Yield_j^{Max}$ .

For the policy analysis, soil salinity is varied by multiplying extant salinity by a multiplicative factor, as in Equation 11. The parameter  $\alpha$  is varied from -0.8 to 0.8, and a new crop mix  $Y_{rj}$  is predicted for each soil polygon region in Equation 12. Lastly, revenue is calculated in Equation 13.

$$Yield_{rj}^{Rel} = 1 - b_j(Salinity_r - a_j) \quad (9)$$

$$Yield_j^{Max} = \frac{Yield_j}{\overline{Yield_j^{Rel}}} \quad \forall county \quad (10)$$

$$NewSalinity_r = (1 + \alpha) \cdot Salinity_r \quad (11)$$

$$Y_{rj} = f(NewSalinity_r, \dots) \quad (12)$$

$$Revenue = \sum_r \sum_j Area_r \cdot Y_{rj} \cdot price_{rj} \cdot Yield_{rj}^{Rel} \cdot Yield_{rj}^{Max} \quad (13)$$

## 4.3 Results and Discussion

### 4.3.1 Behavioral Results

Following Mendelsohn et al. [4], two models are estimated with different weighting schemes. The first regression uses cropland weights, which weigh each observation based on the total cropped area in that particular region. Revenue weights, likewise, weigh the observations based on total current revenue being generated in that soil polygon region.

The average marginal effects from these regressions are reported in Table 4-1. Marginal effects represent the increased share in percentage points for each crop that would result from a one unit increase in salinity, where salinity is expressed in dS/m. Average marginal effects are the computed marginal effects at each observation averaged over all of the observations. While the interpretation of the beta coefficients in a FMNL model are interpreted relative to the pivot category, average marginal effects can be interpreted as stand-alone estimates.

The cropland and revenue weighted regressions report largely similar marginal effects across the ten crop groups, both by significance and magnitude across. Of note is that all of the coefficients are relatively small; the largest being the negative coefficient for vineyards. The value of -0.25 in the cropland weighted regression for vineyards indicates that an additional unit of salinity would result in a decrease in one quarter of one percentage point of vineyard coverage.

The parameter estimates for three crop groups are robustly significant over the different weighting schemes: tolerant vegetables, tolerant nuts, and vineyards. Tolerant vegetables and nuts have a significantly positive coefficient, indicating that as salinity rises so does their relative crop share. Vineyards, meanwhile, have a significantly negative coefficient. The fact that the more tolerant cultivars experience increased crop share under higher levels of salinity provides evidence for grower adaptation. Likewise, the decrease in relatively salt-sensitive high-revenue vineyards shows evidence that growers take salinity into account when making crop choice. The signs of the parameter estimates are robust to the

different weighting schemes employed. The one exception is for grain. However, the parameter estimate for this crop category is not significantly different from zero at conventional levels.

Also reported are the normalized average marginal effects. Average marginal effects can be misleading if there are large differences in baseline group measurement. Sensitive nuts, for example, cover on average 35% of the fractional share of each polygon, while vegetables cover just 2% (full baseline cropping is presented in Table SI1 in Appendix C). Normalized average marginal effects, also presented in Table 4-1, are calculated by simply dividing the average marginal effects by the average baseline cropped area. The values can be interpreted as the percent increase or decrease of fractional crop area relative to baseline levels. The value of -2.0 for vineyards in the cropland weighted regression, for example, indicates that 2.0% less vineyards will be planted relative to 2015 levels given an increase in one unit of salinity. Clearly, the sign and significance of the normalized average marginal effects are the same as the average marginal effects by construction.

**Table 4-1. Average Marginal Effects and Normalized Average Marginal Effects.**

Variables	Average Marginal Effects		Normalized Average Marginal Effects	
	Cropland Weights	Revenue Weights	Cropland Weights	Revenue Weights
Nuts, Sensitive	-0.06055 0.08509	-0.13824 0.08646	-0.175 0.246	-0.400 0.250
Nuts, Tolerant	0.18275 *** 0.04127	0.24430 *** 0.05845	3.262 *** 0.737	4.360 *** 1.043
Other Tree	0.04679 0.04366	0.04334 0.04307	0.479 0.447	0.444 0.441
Feed (Hay)	-0.01685 0.04469	-0.03720 0.04143	-0.086 0.228	-0.189 0.211
Grain	-0.02150 0.04937	0.01175 0.06916	-0.278 0.638	0.152 0.894
Field	0.01137 0.03110	0.01005 0.03124	0.517 1.413	0.457 1.419
Vineyard	-0.25191 *** 0.06239	-0.21035 *** 0.05062	-2.023 *** 0.501	-1.689 *** 0.407
Vegetable, Sensitive	-0.00001 0.00004	-0.00003 0.00006	-0.068 0.194	-0.145 0.273
Vegetable	0.01084 0.00953	0.00189 0.01108	0.598 0.526	0.104 0.612
Vegetable, Tolerant	0.10866 *** 0.02984	0.08850 *** 0.02607	1.746 *** 0.480	1.422 *** 0.419
DAU Dummies	X	X	X	X
Soil Parameters	X	X	X	X
Weather and Elevation	X	X	X	X
Crop Prices	X	X	X	X
Expenses	X	X	X	X

\*\*\* p<0.01, \*\* p<0.05, \* p<0.1

Next, we compare the marginal effects reported in Table 4-1 with the theoretical salt tolerance of each of the individual crop clusters. Tolerance is computed using the  $a$  and  $b$  parameters in Equation 9 by calculating  $Yield^{Rel,50}$ , the salinity at which a crop's yield is estimated to decrease by half. In Figure 4-1, the average marginal effects are plotted alongside the crop groups which are clustered according to crop type (tree, vegetable, and other) and then sorted in increasing order by  $Yield^{Rel,50}$ . A positive slope

indicates that as the tolerance of the crop group increases, so do the marginal effects. This trend is seen in each of the crop clusters, showing agreement between the regression and the agronomic literature.

In plotting all of the crop groups together (see Figure S1A in Appendix C) the slope is still generally positive, although less apparent than when the crop groups are clustered by crop type. This may indicate an increased ability of growers to change crops within group as salinity shifts, perhaps indicating lower switching costs (e.g. equipment, training) between crops of a similar type.

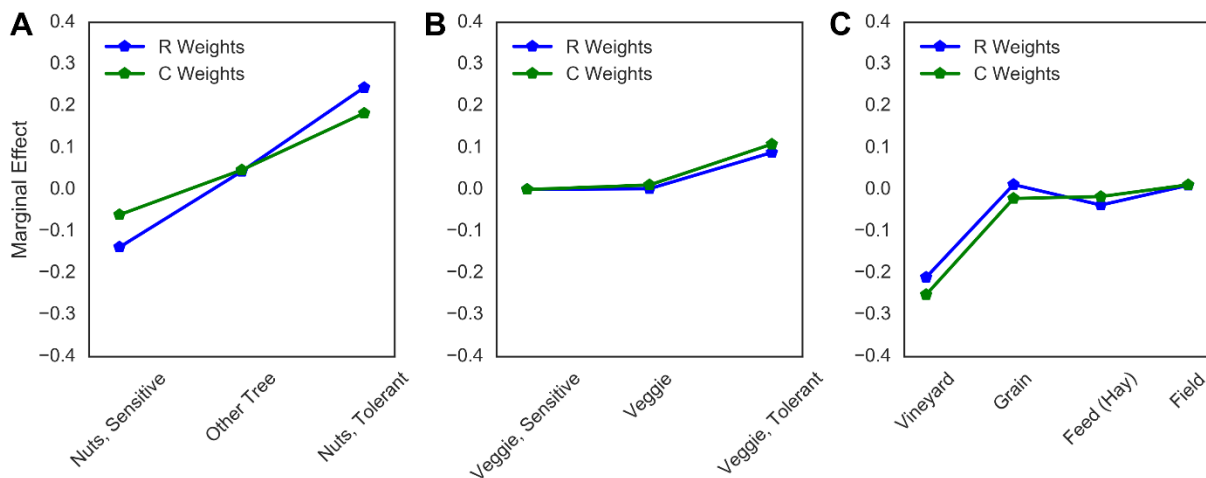


**Figure 4-1. Estimated marginal effects vs. crop groups ranked by salt tolerance for tree crops (A), vegetables (B), and a miscellaneous category (C).**

#### 4.3.2 Policy Scenario

Figure 4-2 reports the results of the policy analysis. In Figure 4-2A, we vary the salinity levels between -80% and 80% of the original values. It should be noted that due to the multiplicative formulation, we are only modulating salinity in areas where salinity is nonzero. We do this for two policy scenarios – one in which crop fraction is fixed at 2015 levels and the other which allows for crop switching in accordance with the regression results. The outcome shows that, as expected, increasing and decreasing salinity result in decreased and increased revenues, respectively. The difference between the two scenarios is small, reflecting the small magnitude of response to salinity identified in the regression results.

In Figure 4-2B we conduct a similar exercise to compare the effects of crop switching to uncertainty inherent in the data. The SSURGO salinity data reports an estimated ‘high’ and ‘low’ value for salinity along with the midpoint estimate. We calculate the change in revenue that would occur if all soil polygon regions would receive their ‘low’ or ‘high’ values, and find a difference of \$1 billion. When we account for crop switching in accordance with the regression model this estimate remains largely unchanged.

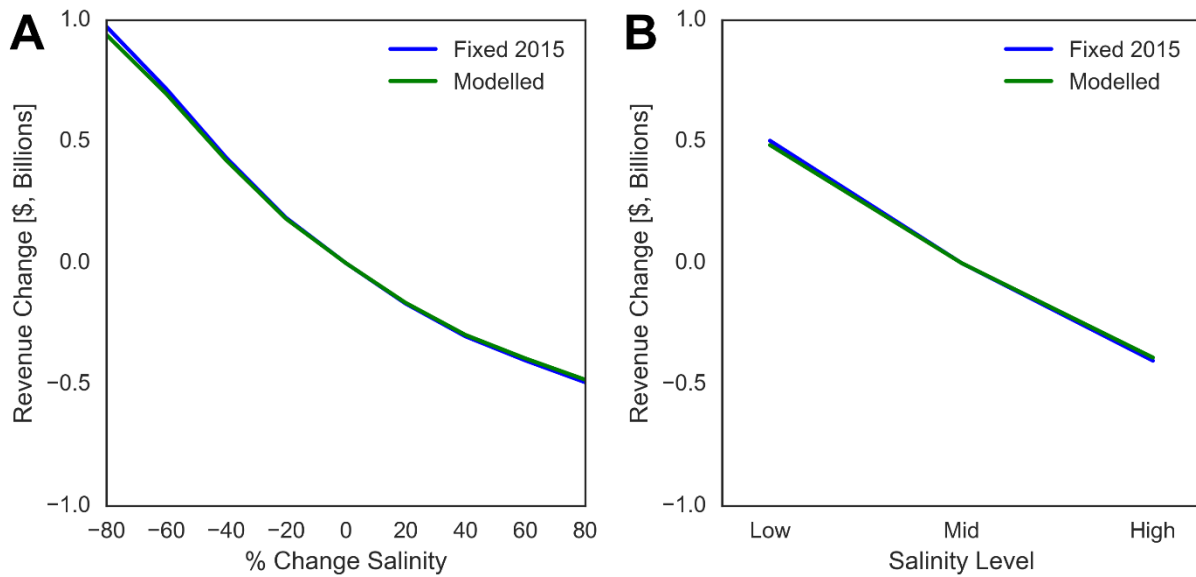


**Figure 4-2. Estimated revenue change from baseline values with salinity altered parametrically (A) and salinity set to its reported ‘low’, ‘mid’, and ‘high’ estimates according to the SSURGO data.**

The approach as implemented has several limitations. First, the regression results are estimated from a cross-section of 2015 data, meaning the response is identified from growers in different parts of the state choosing to grow different crops. While we collect a large ensemble of explanatory data, there are heightened risks of omitted variable bias when employing such a design. Moreover, the regression results are not likely to be accurate in predicting crop share under salinity conditions that differ substantially from current levels.

Second, the policy analyses rely on empirical relationships from Hoffman [30] in order to compute revenues under different salinity domains. The regression results indicate that farmers are relatively

insensitive to salinity, suggesting that they may have other management techniques to prevent yield loss. Because of this, our results offer evidence that there may be limitations in using the agronomic approach as developed in Hoffman [30] for salinity impact assessment.

Despite these limitations, we believe the approach as implemented offers evidence that growers are modifying their cropping patterns according to the levels of salinity found in their soils, but that the general magnitude of this effect is small. When we implement crop switching in policy scenarios we find little difference in economic performance between portfolios optimized for 2015 salinity levels and those in which growers are allowed to modify their crop choice according to the regression results. These results support a conclusion that accounting for crop switching due to salinity levels may be a second-order modelling concern.

## References

- [1] Howitt R E, Medellin-Azuara J, MacEwan D and Lund J R 2012 Calibrating disaggregate economic models of agricultural production and water management *Environmental Modelling & Software* **38** 244-58
- [2] Howitt R E 1995 Positive Mathematical-Programming *Am J Agr Econ* **77** 329-42
- [3] Merel P and Howitt R 2014 Theory and Application of Positive Mathematical Programming in Agriculture and the Environment *Annu Rev Resour Econ* **6** 451-70
- [4] Mendelsohn R, Nordhaus W D and Shaw D 1994 The Impact of Global Warming on Agriculture: A Ricardian Analysis *The American Economic Review* **84** 753-71
- [5] Mendelsohn R and Reinsborough M 2007 A Ricardian analysis of US and Canadian farmland *Climatic Change* **81** 9-17
- [6] Weber M and Hauer G 2003 A Regional Analysis of Climate Change Impacts on Canadian Agriculture *Canadian Public Policy / Analyse de Politiques* **29** 163-80
- [7] Polsky C 2004 Putting space and time in Ricardian climate change impact studies: agriculture in the US Great Plains, 1969–1992 *Annals of the Association of American Geographers* **94** 549-64
- [8] Gbetibouo G A and Hassan R M 2005 Measuring the economic impact of climate change on major South African field crops: a Ricardian approach *Global and Planetary Change* **47** 143-52
- [9] Kurukulasuriya P and Mendelsohn R 2008 Crop switching as a strategy for adapting to climate change *African Journal of Agricultural and Resource Economics* **2** 105-26
- [10] Seo S N and Mendelsohn R 2008 Measuring impacts and adaptations to climate change: a structural Ricardian model of African livestock management *Agricultural Economics* **38** 151-65
- [11] Seo S N, Mendelsohn R, Dinar A, Hassan R and Kurukulasuriya P 2009 A Ricardian Analysis of the Distribution of Climate Change Impacts on Agriculture across Agro-Ecological Zones in Africa *Environmental and Resource Economics* **43** 313-32
- [12] Massetti E and Mendelsohn R 2011 Estimating Ricardian models with panel data *Climate Change Economics* **02** 301-19
- [13] Seo S N, Mendelsohn R and Munasinghe M 2005 Climate change and agriculture in Sri Lanka: a Ricardian valuation *Environment and Development Economics* **10** 581-96

- [14] Kabubo-Mariara J and Karanja F K 2007 The economic impact of climate change on Kenyan crop agriculture: A Ricardian approach *Global and Planetary Change* **57** 319-30
- [15] Ding Y, Schoengold K and Tadesse T 2009 The impact of weather extremes on agricultural production methods: Does drought increase adoption of conservation tillage practices? *Journal of Agricultural and Resource Economics* 395-411
- [16] Pfeiffer L and Lin C Y C 2014 Does efficient irrigation technology lead to reduced groundwater extraction? Empirical evidence *Journal of Environmental Economics and Management* **67** 189-208
- [17] Yin R S, Xiang Q, Xu J T and Deng X Z 2010 Modeling the Driving Forces of the Land Use and Land Cover Changes Along the Upper Yangtze River of China *Environ Manage* **45** 454-65
- [18] Just R E 2000 Some Guiding Principles for Empirical Production Research in Agriculture *Agricultural and Resource Economics Review* **29** 138-58
- [19] Just R E and Pope R D 1999 Implications of Heterogeneity for Theory and Practice in Production Economics *Am J Agr Econ* **81** 711-8
- [20] Draper A J, Jenkins M W, Kirby K W, Lund J R and Howitt R E 2003 Economic-engineering optimization for California water management *Journal of water resources planning and management* **129** 155-64
- [21] Chakir R 2009 Spatial Downscaling of Agricultural Land-Use Data: An Econometric Approach Using Cross Entropy *Land Economics* **85** 238-51
- [22] You L Z, Wood S and Wood-Sichra U 2009 Generating plausible crop distribution maps for Sub-Saharan Africa using a spatially disaggregated data fusion and optimization approach *Agr Syst* **99** 126-40
- [23] You L Z, Wood S, Wood-Sichra U and Wu W B 2014 Generating global crop distribution maps: From census to grid *Agr Syst* **127** 53-60
- [24] National Agricultural Statistics Service, U.S. Department of Agriculture 2015 County Ag Commissioners' Data Listing [http://www.nass.usda.gov/Statistics\\_by\\_State/California/Publications/AgComm/Detail](http://www.nass.usda.gov/Statistics_by_State/California/Publications/AgComm/Detail).
- [25] National Agricultural Statistics Service, U.S. Department of Agriculture 2015 CropScape cropland data layer. <http://nassgeodata.gmu.edu/CropScape>
- [26] Welle P and Mauter M High-Resolution Model for Estimating the Economic and Policy Implications of Agricultural Soil Salinization in California *Environmental Research Letters* Under Review
- [27] Natural Resources Conservation Service, U.S. Department of Agriculture 2015 Soil Survey Geographic (SSURGO) Database <http://sdmdataaccess.nrcs.usda.gov/>.
- [28] Kalnay E, Kanamitsu M, Kistler R, Collins W, Deaven D, Gandin L, Iredell M, Saha S, White G, Woollen J, Zhu Y, Leetmaa A, Reynolds R, Chelliah M, Ebisuzaki W, Higgins W, Janowiak J, Mo K C, Ropelewski C, Wang J, Jenne R and Joseph D 1996 The NCEP/NCAR 40-Year Reanalysis Project *Bulletin of the American Meteorological Society* **77** 437-71
- [29] Papke L E and Wooldridge J M 1996 Econometric methods for fractional response variables with an application to 401(k) plan participation rates *Journal of Applied Econometrics* **11** 619-32
- [30] Maas E V and Hoffman G J 1977 Crop salt tolerance - current assessment *Journal of the irrigation and drainage division* **103** 115-34

# **Chapter 5: Economic and Policy Drivers of Agricultural Water**

## **Desalination in California's Central Valley**

This chapter is based on the following work currently under review at *Agricultural Water Management*:

Welle, P, Medellin-Azuara J, Viers J H and Mauter M S Economic and Policy Drivers of Agricultural Water Desalination in California's Central Valley *Agricultural Water Management*, submitted for publication.

### **5.1 Introduction**

The twin stressors of water scarcity and soil salinization diminish agricultural yields and grower profitability in arid regions [1]. Climate models project expansion of arid regions and increased probability of drought in both the western United States and the majority of agricultural regions worldwide [2-4]. In these water-stressed regions, growers often augment water supply with alternative sources including brackish groundwater and agricultural drainage water. The application of these lower quality water sources can lead to the accumulation of salts and, in areas with insufficiently permeable soil, to the development of shallow saline water tables [5]. Recent studies estimate the cost of soil salinization in California at billions of dollars per year [1, 6]. As a result, improving the sustainability of food production systems in arid, drought prone, and salinizing regions is a high environmental and policy priority [7].

Traditional responses to the diminished yields associated with soil salinization increase agricultural land area, intensify agricultural water consumption, and impose downstream environmental impacts. Local land fallowing reduces agricultural production and drives land-use change, which is often associated with increased greenhouse gas emissions [8]. The second response, salinity leaching from salt-impaired fields via the excess application of irrigation water, consumes scarce water resources, raises elevated groundwater tables, and often leads to the discharge of saline tile drainage to sensitive environmental ecosystems [9]. While alternative drainage management schemes include re-application of tile drainage

to salinity tolerant crops or storage in evaporation ponds, most tile drainage is discharged to the environment [9, 10]. Specific contaminants found in this agricultural drainage, notably selenium and boron, impair reproduction, inhibit growth, suppress the immune system, and cause mutagenesis in fish and birds [11, 12]. Thus, conventional salinity management practices force tradeoffs in agricultural productivity and environmental sustainability [13].

Water treatment technologies offer a potential remedy to this issue by allowing farmers to treat existing irrigation waters or access new impaired water sources, including saline groundwater or agricultural tile drainage. Drainage water leached from agricultural soils and discharged through tile drains can be deionized and beneficially reused as a source of irrigation water, while the residual brine concentrate may be disposed of through subsurface injection or crystallized and disposed of as solid waste. Desalination of tile drain discharge would simultaneously minimize ecosystem damages, limit soil salinization, reduce agricultural water intensity (acre-feet / acre-year), and offer a new source of irrigation supply.

Technologies potentially applicable to agricultural water desalination are distinct from conventional seawater desalination technologies for municipal water treatment in requiring higher water recovery, tolerance of highly variable feed streams, and cost-effectiveness at small to medium scales. The cost-effectiveness of these technologies will also be facilitated by limited requirements for pre-treatment, low operator oversight, and resiliency to intermittent or variable water quality. Several technologies for distributed agricultural water desalination have been piloted or installed commercially, including thermal desalination (e.g. multi-effect distillation), membrane-based desalination (e.g. reverse osmosis), and electrochemical desalination (e.g. electrodialysis)[14-16]. In each case, the technology is capable of reducing the total dissolved solids concentration of the product water to effectively zero.

Growing demand for drought mitigation and agricultural drainage treatment has motivated a number of studies assessing the technical feasibility and cost of specific agricultural water desalination technologies [14, 15, 17-20]. These studies have generated estimates of water treatment cost, but we are unaware of complementary work assessing the private benefits of technology adoption or the broader consequences

of technology adoption for integrated food, energy, and water systems. There remains significant uncertainty about the implications of widespread water desalination for agricultural management practices such as soil leaching, the energy consumption of water desalination technologies and any associated air emission impacts, or the ecosystem services benefits of reduced discharge salinity. Explicitly quantifying these benefits and costs is critical for assessing the likelihood of technology diffusion and the role for policy interventions that maximize public benefits.

The present work quantifies the marginal public and private costs and benefits of agricultural water desalination under a range of future precipitation and climate scenarios in the Central Valley (CV) of California. We present the first assessments of the marginal private benefits of water desalination, realized as improved agricultural yields, using high-resolution multi-modal soil salinity and crop data. We then assess private adoption at the field-level by comparing private benefits to current desalination costs. Next, we contribute the first assessment of potential marginal public costs associated with adoption of agricultural water desalination. Public costs in the form of human health and climate damages are estimated for three different desalination technologies that use renewable, grid, and fossil energy sources. Finally, we back out the effective value of human health and environmental benefits in watersheds impaired by agricultural drainage that would be required for the technology to have net positive effects from a societal perspective.

## **5.2 Methods**

We quantify the public and private costs and benefits associated with desalination systems in the CV, a region of high agricultural value, severe water scarcity, and impaired air and water quality. The most agriculturally productive region in the US, the CV includes about 9 million acres of cropped land producing the majority of California growers' \$46 billion USD of revenue in 2013 [21]. Water availability for irrigation is often scarce due to the aridity of the region, persistent drought conditions exacerbated by a warming climate [4], unsustainable groundwater withdraws [22, 23], and suboptimal market mechanisms for water transfers [24]. In addition to water scarcity, soil salinization has required

widespread installation of tile drains that enable salinity leaching. Discharging this tile drainage into surrounding ecosystems has impaired surface water throughout the CV [25].

A complete system analysis that incorporates the regulatory, legal, economic, and technical factors that impact water use and allocation is beyond the scope of the present work. Instead, this analysis is framed in marginal terms, and therefore limits the decision space by assuming that present-day regulatory environment, legal conditions, and management practices remain constant. Additionally, on the technological modeling side, we limit the analysis to that of a theoretical desalination system capable of reducing water salinity to 0 ppm TDS with 100% recovery for a cost of \$0.78–\$1.33 per m<sup>3</sup> of feed. This cost includes the financial costs of brine disposal, but assumes no environmental externalities associated with brine management. While no desalination system is capable of providing this service, it reduces the need to model all possible desalination system design choices. As a result of these assumptions, the analysis provides an upper bound estimate on the marginal benefits of actual desalination systems.

### *5.2.1 Private Costs*

While the costs of large-scale seawater desalination have decreased to nearly \$0.5/m<sup>3</sup> [26] distributed, inland, brackish water desalination systems do not benefit from the same economies of scale or ease of concentrate disposal. Instead, inland desalination systems must adopt brine management techniques, which typically range from \$0.40 - \$1.80 per m<sup>3</sup> of concentrate [17, 27, 28]. Finally, minimizing these brine volumes requires high water recovery, which can lead to membrane scaling and increased maintenance costs. As a result, the total system lifecycle costs of inland brackish water desalination are often significantly higher than seawater desalination systems.

This analysis utilizes existing estimates of the lifecycle costs of distributed desalination costs sourced from the peer-reviewed literature. These estimates include the costs associated with pretreatment, desalination processes, and concentrate management, as well as amortized fixed costs. Recent estimates of lifecycle water desalination costs in the CV by McCool et al. [17] and Stuber [14] are consistent with

an earlier review of small scale desalination system costs ranging between \$0.78–\$1.33 per m<sup>3</sup> of feed [19]. In most instances, we perform our analysis across this same range of amortized system costs. When calculating the benefit gap, we simplify our calculations by selecting a mid-range value of \$1/m<sup>3</sup> of feed. The lifecycle system costs may reduce as desalination technologies mature [26].

### 5.2.2 *Private Benefits*

The private benefits of increased agricultural revenue from reduced soil salinity and additional water supply are developed by extending two existing modeling approaches described elsewhere [1, 29]. Both estimates are developed as marginal quantities with units of [\$/acre-ft] or [\$/m<sup>3</sup>], which represent the marginal revenues of improved quantity (an additional unit of water) or quality (a completely desalinated unit of water). Due to the marginal nature of the calculations, these benefits do not account for any potential benefits associated with switching from lower value to higher value crops, a theme more fully addressed in the discussion section.

Additionally, the two models for water quality and water quantity operate at different levels of spatial aggregation. Modeling improved water quality is highly dependent on local estimations of crop types and soil salinity, and so this model is resolved at a 30-meter pixel (referred to in this paper as field-scale) resolution. Modeling the value of improved water supply is performed over hydrologic regions (referred to as regional-scale) with an average size of 2040 km<sup>2</sup>. This approach allows estimation of a use value of water absent detailed water pricing data.

#### 5.2.2.1 *Improved Water Quality*

Reducing the total dissolved solids (TDS) concentration of irrigation water reduces the soil salinity, increases agricultural yields, and confers higher revenues to the producer. Revenues are assessed marginally according to Equation 1.

$$\frac{dR}{dW^T} = \frac{dR}{dS^S} \cdot \frac{dS^S}{dS^W} \cdot \frac{dS^W}{dW^T} \quad (1)$$

The value  $\frac{dR}{dW^T}$  is the increased revenue  $R$  per unit of water treated  $W^T$  on the margin, which is further decomposed into three components – (1) the change in revenue per change in soil salinity  $\frac{dR}{dS^S}$ , (2) the change in soil salinity per change in salinity of applied water  $\frac{dS^S}{dS^W}$ , and (3) the change in salinity of applied water per change in quantity of water treated  $\frac{dS^W}{dW^T}$ . These three components are represented in Equations 2, 3, and 4 respectively.

$$\frac{dR}{dS^S} = \begin{cases} 0 & ; S^S \leq t_1 \text{ or } S^S \geq t_2 \\ b \cdot p \cdot Y^M; & S^S > t_1 \text{ and } S^S < t_2 \end{cases} \quad (2)$$

$$\frac{dS^S}{dS^W} = \frac{1}{L} + \frac{0.2}{L} \cdot \ln(L + (1 - L))e^{-5} \quad (3)$$

$$\frac{dS^W}{dW^T} = -\frac{S_0^W}{W} \quad (4)$$

Equation 2 is developed through differentiating the yield reduction model presented in Maas and Hoffman [30]. The parameter  $b$ , which is negative for all crops in the study, is the crop-specific sensitivity parameter, which determines how quickly yield decreases as salinity increases. The two parameters  $p$  and  $Y^M$  are crop-specific county level values of price and theoretical maximum yield (for non salt-affected crops). The expression  $\frac{dR}{dS^S}$  is zero when salinity is less than the salinity threshold ( $t_1$ ) at which relative yield is 100% or above the threshold ( $t_2$ ), where the yield is 0%.

The equilibrium relationship between soil salinity and the salinity of applied water is provided in Equation 3. The model, originally presented in Hoffman and Van Genuchten [31], is calculated as a single function of the leaching fraction,  $L$ . The leaching fraction is the fraction of total water that percolates through the soil column, and determines how quickly soil salinity changes as the salinity of the applied water shifts.

Finally, we employ a simple dilution model in Equation 4 to calculate the salinity of the applied water when mixed with desalinated water, which throughout this analysis is modeled as water with no dissolved

solids. The two parameters  $S_0^W$  and  $W$  represent the salinity of the applied water and the total water applied, respectively. In the absence of high-resolution data on the salinity or relative volumes of surface water, groundwater, and precipitation applied to crops during the growing season, the present analysis assumes that the salinity of the irrigation water before being mixed with desalinated water is constant at an average value of 490 ppm TDS (approximated in dS/m by assuming  $TDS = 640 \cdot EC$ ). Section 11.3 of Appendix D provides further detail on the estimation of the salinity of the applied water as well as sensitivity to final results of changing assumptions on which this estimation is based. Equation 4 thus represents the change in water salinity from 490 ppm that results when a marginal amount of 0 ppm TDS desalinated water is introduced.

Each of these equations is resolved at a 30 meter pixel resolution across the CV. Crop type is detected according to a satellite-based crop classifier, and all other parameters are measured locally at the county level [1].

#### *5.2.2.2 Augmented Water Supply*

We employ the Statewide Agricultural Production (SWAP) model to estimate the economic value of water to agricultural producers under historical and future warm and dry climate scenarios [29]. SWAP uses the deductive Positive Mathematical Programming (PMP) technique to estimate the economic value of irrigation water over hydrologic regions assuming that growers seek to maximize net returns to land and management in irrigating crops [32]. PMP consists of a four-step procedure described in detail in Howitt, Medellín-Azuara, MacEwan and Lund [33]. The basic method can be outlined as follows: (1) a linear program with Leontief technology is solved to obtain marginal values on a calibration constraint; (2) a PMP exponential cost function is parameterized; (3) a constant elasticity of substitution (CES) production function is calibrated which makes use of the Lagrange multiplier on the calibration constraint in the first step; and (4) a non-linear program that includes the CES production function and the PMP cost function is solved. The model specified by this four-step procedure calibrates exactly to the base dataset. SWAP uses four production inputs (land, water, labor, and supplies) and a 20-crop group set compatible

with the California Department of Water Resources classification. The fully calibrated program is provided by the set of Equations 5 through 7:

$$\max \Pi = \sum_g \sum_i (v_{gi} Y_{gi}) - \delta_{gi} e^{\gamma_{gi} X_{gi,land}} - \sum_{j \neq land} \omega_{gij} X_{gij} \quad (5)$$

where,

$$Y_{gi} = \tau_{gi} \left( \sum_j \beta_{gij} X_{gij}^\rho \right)^{v/\rho} \quad \forall g, i \quad (6)$$

$$\sum_i X_{gi,land} \leq \sum_{ws} W_{g,ws} \quad \forall g \quad (7)$$

and  $g$  is the set of regions,  $i$  is the set of crops, and  $j$  is the set of production factors. The decision variable is  $X_{gij}$ , which is the amount of resources  $j$  allocated for production of crop  $i$  in region  $g$ . The parameters  $v_{gi}$  and  $Y_{gi}$  are prices and yields in region  $g$  and crop  $i$ . Land cost is represented by an exponential area response function with intercept and elasticity parameters  $\delta_{gi}$  and  $\gamma_{gi}$ . Resource costs are represented as  $\omega_{gij}$ .

Equation 6 represents the CES production function which models  $Y_{gi}$  using parameters  $\beta$ ,  $\tau$ ,  $v$ ,  $\rho$ .

Equation 7 is the resource constraint that defines the boundary for applied water  $W$  in region  $g$  according to a particular water source  $ws$  (local diversions, state or federal water projects, and groundwater).

We conducted three SWAP model runs to obtain shadow values of water from the water resource constraint (Equation 7). We employed base observed water availability for the pre-drought year of 2010, the drought year of 2014, and a climate scenario for 2050 with a warm-dry form of climate change following Medellín-Azuara, Howitt, MacEwan and Lund [29].

### 5.2.3 Public Costs

Assuming responsible brine management, the human health and environmental externalities of agricultural water desalination will be dominated by the air emissions associated with powering desalination technologies. To quantify these damages, we estimated energy consumption and associated criteria pollutant and greenhouse gas emissions of three desalination technologies: (1) solar powered, grid

supplemented, multi-effect distillation (MED) (Solar Thermal or ST); (2) natural gas powered, grid supplemented MED (Gas Thermal or GT); and (3) grid powered reverse osmosis (RO). We estimated the energy consumption of MED desalination at 125 MJ / m<sup>3</sup> supplemented with 1.5 kWh / m<sup>3</sup> of grid energy, and the energy consumption of membrane pretreatment and RO of 5 kWh / m<sup>3</sup>. These energy estimates are sourced from the literature for small-scale systems with high (>90%) recovery and are constructed to include pretreatment, treatment, and brine disposal [14, 17, 19]. Using these technologies, we then estimate the emissions associated with grid electricity using CA state-level average emissions factors for CO<sub>2</sub>, NO<sub>x</sub> and SO<sub>2</sub> in 2012 derived from the EPA's Emissions & Generation Resource Integrated Database (eGRID)[34]. The eGRID database does not monitor PM<sub>2.5</sub>, so we instead used CA state-level average emissions factors in 2011 from the EPA's National Emissions Inventory [35]. We estimate emissions from the combustion of primary fuel in small scale natural gas boilers using US EPA AP-42 Compilation of Air Pollution Emission Factors [36]. Further detail is available in Section 11.2 in Appendix D.

We estimate the damages for NO<sub>x</sub>, SO<sub>2</sub> and PM<sub>2.5</sub> associated with air emissions from primary fuel and electricity consumption using the Air Pollution Emissions Experiments and Policy Version 2 (AP2) model for each county in California [37, 38]. Damages from emissions sourced from primary fuel are placed in the county which they occur, while damages associated with emissions sourced from grid locations are localized by assigning generation to each plant in proportion to their estimated relative contribution to the California grid (see Section 11.2 in Appendix D). Damages to human health are typically high in those locations with large populations and poor existing ambient air quality. For CO<sub>2</sub> emissions, we assumed a social cost of carbon of \$41 per metric ton in 2014 USD [39].

#### *5.2.4 Public Benefits*

Agricultural drainage water desalination and concentrate disposal would reduce the amount of selenium, boron, nitrate, TDS and other contaminants in environmental systems. The diversity of methods for valuing ecosystem services, however, makes estimating the public benefits highly uncertain [40]. Instead,

we select environmentally sensitive areas (ESAs) in the CV that are highly impaired by agricultural drainage and estimate ecosystem valuation that would be required for drainage water desalination to confer positive net benefits at a societal level. This required valuation is termed the “benefit gap.”

To estimate the benefit gap, we subtract private and public costs from private benefits of water desalination within the ESAs. ESAs are selected using EPA’s Healthy Watershed program by first selecting those HUC12 watersheds that contain both agriculture and artificial drainage areas, and sub-selecting the watersheds with rank normalized median summer conductivity greater than 0.8 (Figure S2 in Appendix D). The at-risk zone is determined to include 88 watersheds, or 21% of the cropped area in the study. Private costs are likely to vary depending on local electricity prices, brine disposal options, and regulations. In this analysis, we adopt a uniform midpoint estimate of 1 \$/m<sup>3</sup> for all systems. Private benefits and public costs are determined at the field level or county level as described above.

### **5.3 Results**

We estimate the private and public costs and benefits of agricultural water desalination to assess independent technology adoption as well as the potential role for policy intervention. Desalination adoption is determined by the net private benefits of the technology for the grower, estimated as the additional revenues associated with lower irrigation water salinity and augmented water supply, minus the additional costs associated with system fixed and variable costs. In addition to the benefits and costs of desalination for agricultural producers, the adoption of widespread desalination confers benefits and imposes costs to the public at large. The balance of these public costs and benefits determine the socially optimal level of technology adoption and the policy interventions that may be warranted to encourage or discourage desalination. We explore the role for policy by quantifying the human health impacts of reduced air quality associated with higher energy use and exploring the requisite breakeven benefits of reduced drainage on downstream ecosystems.

### *5.3.1 Private Benefits of Improved Water Quality*

We estimate the marginal value of reducing the salinity of CV irrigation water to zero while holding the volume of water applied constant. The average marginal value of improved quality is \$0.01 per m<sup>3</sup> (5<sup>th</sup> percentile \$0.00; 50<sup>th</sup> percentile \$0.00; 95<sup>th</sup> percentile \$0.08) and is highest in areas with high crop value, high salinity levels, low crop water needs, and high crop salt sensitivity (Figure 5-1A). Areas with a higher marginal value of desalinated water are clustered in the southern and western CV, where salinity values are highest. Almonds, pistachios, alfalfa and grapes report the highest crop revenue gains from decreasing the salinity of applied irrigation water, and these crops accounted for 2.2 million planted acres (or approximately 45% of planted acreage in the CV) in 2014.

### *5.3.2 Private Benefits of Improved Water Supply*

Desalination technology also offers the possibility of increasing water supply by treating impaired water sources such as brackish groundwater or agricultural drainage water. This additional water has an economic value to agricultural producers that increases with increasing water scarcity. We model the additional value of water by using the shadow price as determined by training the SWAP model to 2010 (pre-drought), 2014 (drought), and 2050 (climate change) scenarios for each of the 27 SWAP regions in the CV. The average regional difference in value between the pre-drought and drought years is \$250 per acre-ft, but varies between \$0 and \$880 per acre-ft depending on SWAP region. The 2050 warm-dry climate change scenario, by contrast, increases the average regional difference by only \$4.20 per acre-ft, or 3.1%. The increase in value between non-drought and drought years is concentrated in the southern CV where water scarcity is highest (Figure 5-1B and 5-1C).

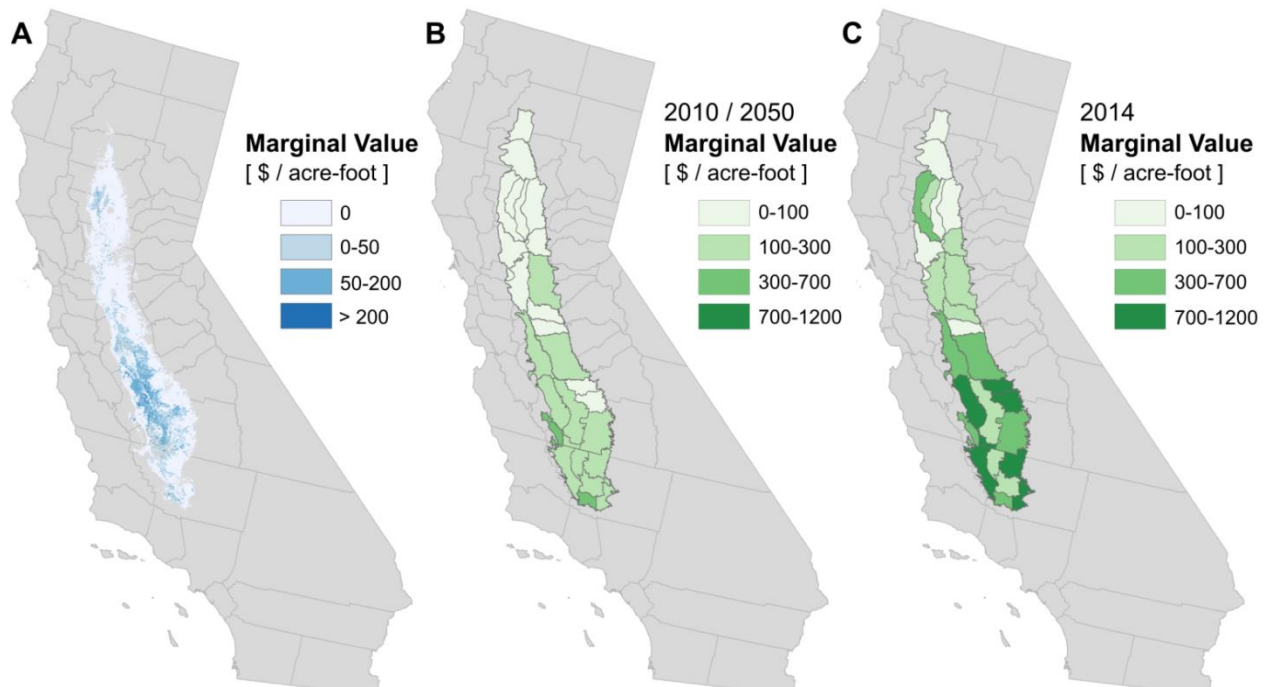


**Figure 5-1. Marginal value of improved water quality and additional water supply. A) Marginal value of removing dissolved solids from a cubic meter of irrigation water, while holding the volume of irrigation water constant. B) Marginal value of an additional acre-ft of irrigation water at salinities equivalent to current irrigation water (490 ppm TDS)[1] under pre-drought (2010) and future climate (2050) scenarios. C) Marginal value of an additional cubic meter of irrigation water under drought scenarios represented by water availability in 2014. One acre-ft is equivalent to 1233 m<sup>3</sup>.**

Figure 5-2A plots the marginal values in Figure 5-1 as a cumulative density function (CDF). The marginal values of augmented water supply for 2010 and 2014 are summed with estimates for the value of water quality to calculate a single combined value of water quality and quantity. This value can be interpreted as the farmer's willingness to pay for desalinated water from untapped sources. The average value is \$0.12 per m<sup>3</sup> (5<sup>th</sup> percentile \$0.02; 50<sup>th</sup> percentile \$0.09; 95<sup>th</sup> percentile \$0.26) in 2010 and \$0.30 (5<sup>th</sup> percentile \$0.02; 50<sup>th</sup> percentile \$0.26; 95<sup>th</sup> percentile \$0.75) in 2014. Under drought conditions, just 4% of land area receives a value of desalinated water within the \$0.78-\$1.33 per m<sup>3</sup> range of inland desalination costs reported in the literature. Absent drought, however, very little land is likely to receive net private benefits from installing desalination technologies.

### 5.3.3 *Public Air Emissions Costs*

Desalination processes consume primary fuel or electricity and may increase emissions of criteria air pollutants and greenhouse gasses. We find that air emission damages to human health and the environment associated with desalinating agricultural water vary considerably depending on technology and power source. Solar thermal (ST) desalination systems consume only a small amount of electricity for pumping and therefore generate the fewest air emission damages per volume of desalinated water at \$0.05 per m<sup>3</sup>, or 58.40 per acre-ft. Electricity driven reverse osmosis (RO) desalination technologies impose significantly larger damages of \$0.16 per m<sup>3</sup>, or \$196 per acre-ft. The damages from electricity-driven desalination technologies are estimated using generation-normalized average emissions factors for the CA electricity grid and, thus, the spatial distribution and proportion of damages from each pollutant are constant. The estimated damages from criteria air pollutant and CO<sub>2</sub> emissions are approximately equal, though the exact proportion depends on the specific technology (Figure 5-2B).

Gas thermal (GT) systems impose significantly larger human health and environmental damages of \$0.36 per m<sup>3</sup>, or \$449 per acre-ft. The estimated air emission damages vary based on the county in which desalination activity occurs, and range between \$404 and \$550 per acre-ft. Nearly two-thirds of these damages are attributed to CO<sub>2</sub> emissions, a value that is substantially higher than that of ST or RO (Table S1 in Appendix D).

### 5.3.4 *Public Benefits of Agricultural Drainage Treatment*

Capturing and desalinating agricultural tile drainage will reduce the ecosystem damages associated with current leaching practices. To circumvent the uncertainty associated with estimating marginal ecosystem services conferred by reduced agricultural water treatment, we instead assess the minimum value of ecosystem services necessary for policy interventions incentivizing technology adoption to be worthwhile from a public perspective.

The required value of ecosystem services depends on both the desalination process and the water availability in a given year. In both drought (2014) and non-drought (2010) years, the ST system had the highest combined net social benefits, followed by grid-powered reverse osmosis, and finally natural gas powered thermal systems. In non-drought years, the benefit gap for solar thermal is  $-\$0.94$  per  $m^3$  or  $-\$1160$  per acre-ft for the median acre, indicating that nearly the entire private system cost would need to be supplied by the public. During drought years this benefit gap for the median acre drops to  $-\$0.69$  per  $m^3$  or  $-\$850$  per acre-ft, and for the top 25<sup>th</sup> percentile the benefit gap drops to just  $-\$0.35$  per  $m^3$  or  $-\$436$  per acre-ft. Very few acres report net positive benefits, suggesting that policy interventions would be necessary to close the benefit gap and incentivize technology adoption.

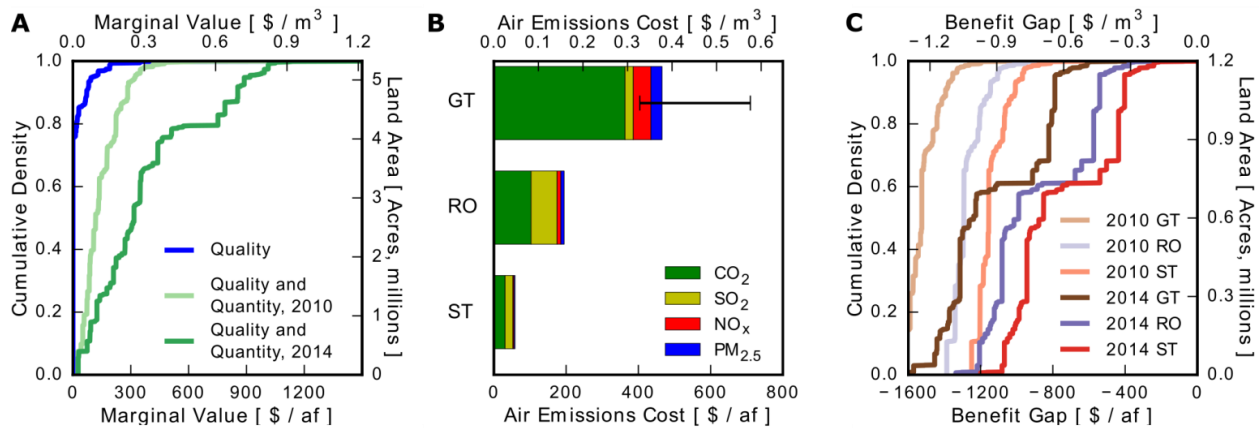


**Figure 5-2. Private and public benefits and costs by crop and land area. A) CDF of private benefits for improved water quality and summed benefits of improved water quality and augmented supply in 2010 and 2014. B) Estimated air emission damages per unit of desalinated water for the gas powered thermal (GT), grid-powered reverse osmosis (RO), and solar-powered thermal systems (ST). C) CDF of private benefits minus social costs (the benefit gap) for GT, RO, and ST systems for 2010 and 2014 values of augmented supply. This benefit gap represents the minimum ecosystem valuation required for desalination technologies to have net societal benefits.**

## 5.4 Discussion

Desalination technologies confer benefits and costs to agricultural producers as well as society at large. In this study we quantify those benefits and costs to assess desalination adoption and the potential role of policy in stimulating societally optimal outcomes. This analysis suggests that water desalination by

private growers is unlikely to be widely adopted in the CV, as the costs of small-scale desalination units under current policy and regulatory frameworks exceed the benefits that growers are likely to realize from improved water quality or augmented water supply.

Desalination technologies also generate benefits and impose costs to outside parties beyond agricultural producers. Water treatment technologies can be energy intensive and may lead to human health and climate impacts. If growers installed desalination capacity to treat a quarter of the agricultural water applied to most economically beneficial 10% of the CV, annual air emission damages would range between \$97 and \$726 million. Desalination technology and system location explain this variation in the magnitude of public costs, with solar powered MED reported damages nearly an order of magnitude smaller than on-site natural gas combustion driven MED systems. These damages are significant with respect to the private costs to growers, varying between 4.7% and 36% of the system's estimated private cost.

Given the human health and climate damages associated with air emissions from water desalination, considerable ecosystem service benefits from reduced agricultural loading to the environment would be necessary to justify policy incentives for technology adoption. During non-drought periods, we find the net public benefits associated with implementing desalination technologies will only be positive if ecosystem service benefits are on the order of the cost of the technology itself. This implies that the private benefits are essentially entirely offset by public air emission damages. For technology implementation to occur, this benefit gap could be closed by policy in the form of either a subsidy or a tax.

The conclusions of this study are qualified by several assumptions delineated in the methods section. First, the benefits of desalinated water to the growers are quantified using economic modeling in marginal terms, meaning that non-marginal effects (such as crop switching) are not included. The marginal assumption is likely to be more important for land currently cultivating low revenue crops (e.g. corn, wheat, rice, alfalfa, cotton), which may increase revenue by switching to high-revenue crops. The

decision to switch from low value to high value crops is complex – for instance, while we observe that 42% of the land area in our study correspond to low value crops, 52% of these low-value crops already have salinity below the threshold where yields of salt-sensitive almonds would be completely unimpaired. While salinity is no doubt important for crop selection, a wide variety of other variables including market factors, capital and operational expenses, risks exposure associated with perennial crops, water availability (both groundwater and surface water), soil fertility, applicability of irrigation technologies, and availability of drainage dictate what growers will ultimately cultivate. While not accounting for crop switching may cause us to underestimate the value of desalinated water in some areas, resolving salinity does not imply that salt-sensitive high value crops will yield significantly higher revenue.

Second, we assume that growers are rational agents with good information on water resources. In reality, many perennial crop farmers were surprised by the drought and paid significantly more than the average costs for water modeled in this study.

Third, agricultural water is assumed to have a fixed concentration of dissolved solids of 490 ppm, estimated in previous work [1]. We make this assumption in the absence of spatially resolved data on the salinity of the applied irrigation water, which is dependent upon the site-specific mix of groundwater, surface water, rainwater, and tile drainage water that a grower chooses to apply. A grower using higher salinity sources may realize significantly greater value from implementing desalination technologies than reported in this study. On the other hand, growers applying less saline sources would realize even less value.

Fourth, each desalination system is assumed to have amortized costs of \$0.78–\$1.33 per m<sup>3</sup>, regardless of desalination technology, energy inputs, or system recovery. In reality, there may be a tradeoff between public and private costs of different technologies, a tradeoff that could be explored with further research into theoretical energy requirements and more precise cost estimation. Finally, the present analysis does not value the human health, environmental, or climate damages associated with brine disposal

technologies or the environmental externalities associated with manufacturing the capital equipment for water desalination.

Despite the absence of strong economic or policy drivers for agricultural water desalination, there are several technological, economic, regulatory, and climate factors likely to evolve over the next two decades that may increase the net benefits of agricultural water desalination for growers in the CV. The costs of water desalination could decrease as a result of research, development, deployment, and standardization of distributed brackish water desalination technologies. In addition, CV growers are transitioning toward high value, perennial tree crops with higher capital costs and longer payback periods on the order of 30 years [42]. These crops reduce the elasticity of water demand during drought years, and may increase grower willingness to pay under future drought conditions. Recent regulatory action limiting groundwater withdraws, which currently provide ~40% of the California water supply in a non-drought year and much more in a drought year [43], may further increase the price of water in the CV above the SWAP predictions and thereby encourage on-farm water reuse efforts. At the same time, restricting state-issued discharge permits and the provision of in-basin drainage management may limit the discharge of agricultural drainage to vulnerable ecosystems. Finally, recent climate models predict that the western United States will become drier and more drought prone. Despite these expected changes in water availability, we find that desalination is still not likely to offer significant net benefits to growers in an average, non-drought year circa 2050. Since system capital costs are amortized over decades, economic assessments based upon conditions from short drought periods may be overly optimistic.

Policy makers will need to consider a range of environmental, economic, and sociological factors when evaluating policy interventions affecting agricultural desalination in the CV. Examples include alternative water sourcing costs; the value of the agricultural sector outputs; technology impacts to marginalized groups; expected changes in ecological impacts; and the hydrological implications of pumping saline groundwater [44]. Policy interventions could take the form of a subsidy or a tax, with taxes either incentivizing adoption or forcing farm closure.

In conclusion, we find that the primary private benefits of agricultural water desalination are derived from increased water availability under drought scenarios. A small percentage of planted acreage in the CV may independently adopt desalination technologies if extreme drought conditions were forecast to persist over two decades, but the median acre is unlikely to experience adoption under the modelled drought or climate scenarios without significant policy intervention. Under current and foreseeable technological and economic conditions the major role for desalination technology, if there is one, is confined to ecosystem protection.

## References

- [1] Welle P and Mauter M High-Resolution Model for Estimating the Economic and Policy Implications of Agricultural Soil Salinization in California *Environmental Research Letters* Under Review
- [2] Wang G 2005 Agricultural drought in a future climate: results from 15 global climate models participating in the IPCC 4th assessment *Climate dynamics* **25** 739-53
- [3] Huang J P, Yu H P, Guan X D, Wang G Y and Guo R X 2016 Accelerated dryland expansion under climate change *Nature Climate Change* **6** 166-171
- [4] Cook B I, Ault T R and Smerdon J E 2015 Unprecedented 21st century drought risk in the American Southwest and Central Plains *Science Advances* **1** e1400082
- [5] Ghassemi F, Jakeman A J and Nix H A 1995 *Salinisation of land and water resources: human causes, extent, management and case studies* (Oxfordshire: CAB international)
- [6] Howitt R, Kaplan J, Larson D, MacEwan D, Medellín-Azuara J, Horner G and Lee, N 2009 *The economic impacts of Central Valley salinity: Final Report to the State Water Resources Control Board*
- [7] Sabo J L, Sinha T, Bowling L C, Schoups G H, Wallender W W, Campana M E, Cherkauer K A, Fuller P L, Graf W L, Hopmans J W, Kominoski J S, Taylor C, Trimble S W, Webb R H and Wohl E E 2010 Reclaiming freshwater sustainability in the Cadillac Desert *P Natl Acad Sci USA* **107** 21263-70
- [8] Tilman D, Balzer C, Hill J and Befort B L 2011 Global food demand and the sustainable intensification of agriculture *P Natl Acad Sci USA* **108** 20260-4
- [9] Wichelns D and Oster J D 2006 Sustainable irrigation is necessary and achievable, but direct costs and environmental impacts can be substantial *Agricultural Water Management* **86** 114-27
- [10] Schwabe K A, Kan I and Knapp K C 2006 Drainwater management for salinity mitigation in irrigated agriculture *Am J Agr Econ* **88** 133-49
- [11] Ohlendorf H M 1989 Bioaccumulation and effects of selenium in wildlife *Selenium in Agriculture and the Environment* 133-77
- [12] Chang A C and Brawer Silva D 2014 *Salinity and drainage in San Joaquin Valley, California*
- [13] Schoups G, Hopmans J W, Young C A, Vrugt J A, Wallender W W, Tanji K K and Panday S 2005 Sustainability of irrigated agriculture in the San Joaquin Valley, California *P Natl Acad Sci USA* **102** 15352-6
- [14] Stuber M D 2016 Optimal design of fossil-solar hybrid thermal desalination for saline agricultural drainage water reuse *Renewable Energy* **89** 552-63

- [15] McCool B C, Rahardianto A, Faria J, Kovac K, Lara D and Cohen Y 2010 Feasibility of reverse osmosis desalination of brackish agricultural drainage water in the San Joaquin Valley *Desalination* **261** 240-50
- [16] Brame J, Li Q and Alvarez P J 2011 Nanotechnology-enabled water treatment and reuse: emerging opportunities and challenges for developing countries *Trends in Food Science & Technology* **22** 618-24
- [17] McCool B C, Rahardianto A, Faria J I and Cohen Y 2013 Evaluation of chemically-enhanced seeded precipitation of RO concentrate for high recovery desalting of high salinity brackish water *Desalination* **317** 116-26
- [18] Rahardianto A, McCool B C and Cohen Y 2008 Reverse osmosis desalting of inland brackish water of high gypsum scaling propensity: kinetics and mitigation of membrane mineral scaling *Environmental science & technology* **42** 4292-7
- [19] Karagiannis I C and Soldatos P G 2008 Water desalination cost literature: review and assessment *Desalination* **223** 448-56
- [20] Yermiyahu U, Tal A, Ben-Gal A, Bar-Tal A, Tarchitzky J and Lahav O 2007 Rethinking Desalinated Water Quality and Agriculture *Science* **318** 920-1
- [21] National Agricultural Statistics Service, U.S. Department of Agriculture 2015 *California Agricultural Statistics 2013 Annual Bulletin*
- [22] California Department of Water Resources 2015 *Groundwater Sustainability Program, Draft Strategic Plan*
- [23] Medellín-Azuara J, MacEwan D, Howitt R E, Koruakos G, Dogrul E C, Brush C F, Kadir T N, Harter T, Melton F and Lund J R 2015 Hydro-economic analysis of groundwater pumping for irrigated agriculture in California's Central Valley, USA *Hydrogeol J* **23** 1205-16
- [24] Draper A J, Jenkins M W, Kirby K W, Lund J R and Howitt R E 2003 Economic-engineering optimization for California water management *Journal of water resources planning and management* **129** 155-64
- [25] Quinn N W, Ortega R, Rahilly P J and Royer C W 2010 Use of environmental sensors and sensor networks to develop water and salinity budgets for seasonal wetland real-time water quality management *Environmental Modelling & Software* **25** 1045-58
- [26] Reddy K and Ghaffour N 2007 Overview of the cost of desalinated water and costing methodologies *Desalination* **205** 340-53
- [27] Mickley M C 2006 Membrane Concentrate Disposal: Practices and Regulation, Desalination and Water Purification. pp 1-303
- [28] Johnson W R, Tanji K K and Burns R T 1997 Drainage Water Disposal (Rome, Italy: Food and Agricultural Organization of the United Nations)
- [29] Medellín-Azuara J, Howitt R E, MacEwan D J and Lund J R 2011 Economic impacts of climate-related changes to California agriculture *Climatic Change* **109** 387-405
- [30] Maas E V and Hoffman G J 1977 Crop salt tolerance - current assessment *Journal of the irrigation and drainage division* **103** 115-34
- [31] Hoffman G J and Van Genuchten M T 1983 Soil properties and efficient water use: water management for salinity control *Limitations to efficient water use in crop production* 73-85
- [32] Howitt R E 1995 Positive Mathematical-Programming *Am J Agr Econ* **77** 329-42
- [33] Howitt R E, Medellín-Azuara J, MacEwan D and Lund J R 2012 Calibrating disaggregate economic models of agricultural production and water management *Environmental Modelling & Software* **38** 244-58
- [34] Environmental Protection Agency 2016 Emissions & Generation Resource Integrated Database (eGRID) <https://www.epa.gov/energy/egrid>
- [35] Environmental Protection Agency 2012 2011 National Emissions Inventory (NEI) Data <https://www.epa.gov/air-emissions-inventories/national-emissions-inventory-nei>
- [36] Environmental Protection Agency 1998 Emission Factor Documentation for AP-42 Section 1.4 Natural Gas Combustion.

- [37] Muller N Z and Mendelsohn R 2007 Measuring the damages of air pollution in the United States *Journal of Environmental Economics and Management* **54** 1-14
- [38] Muller N Z 2011 Linking policy to statistical uncertainty in air pollution damages *The BE Journal of Economic Analysis & Policy* **11**
- [39] Interagency Working Group (IWG) on Social Cost of Carbon 2013 Technical update on the social cost of carbon for regulatory impact analysis-under executive order 12866
- [40] Young R A and Loomis J B 2014 *Determining the economic value of water: concepts and methods*
- [41] Environmental Protection Agency 2016 Healthy Watersheds: Protecting Aquatic Systems through Landscape Approaches <https://www.epa.gov/hwp>
- [42] Lobell D B and Field C B 2011 California perennial crops in a changing climate *Climatic Change* **109** 317-33
- [43] California Department of Water Resources 2014 *California Water Plan Update 2013*. (Sacramento, CA: State of California)
- [44] Haddad B M 2013 A case for an ecological-economic research program for desalination *Desalination* **324** 72-8

## **Chapter 6: Assessing the Feasibility of Remote Sensing of Soil**

### **Salinity at Global Scale**

This chapter is currently in preparation for publication. It is being co-authored with Meagan Mauter, Siamak Ravanbakhsh, and Barnabás Póczos.

#### **6.1 Introduction**

Soil salinity is a problem which affects agricultural production in arid regions across the globe, and yet, current monitoring programs are not capable of providing high quality data necessary for economic and policy analysis. An estimated 76 million hectares of agricultural land is thought to be salt-affected [1], although available global estimates rely heavily on expert judgement and are several decades out of date. Comprehensive monitoring programs are available in some parts of the world, such as the United States Department of Agriculture (USDA) National Resource Conservation Service's (NRCS's) Soil Surface Geographic Database (SSURGO) [2]. Programs like SSURGO translate field measurements into regional maps, and must maintain the balance between program cost and data fidelity. High-density sampling (through both time and space) is costly, and program managers must weigh the cost of sampling against the accuracy of the estimates provided for those areas not directly measured. Often these field campaigns provide the only data available for economic and policy analysis of soil salinization on agriculture. Recent work has shown that soil salinity levels are a key uncertainty in assessing the impact of salinization [3], highlighting the need for higher resolution data.

Remote sensing through the use of orbital sensors offers an alternate approach for salinity monitoring. There are 373 active satellites whose primary purpose is earth observation or earth science as of March 29, 2017 [4]. Many of these sensors image continuously at a global scale, generating a rich set of data. If measured outgoing radiation can be accurately related to soil salinity using scientific and/or statistical

techniques, it may be possible to conduct salinity monitoring simultaneously over large spatial scales, with high resolution, and at low cost.

There have been two general approaches for detecting soil salinity through remote sensing – the direct approach and the indirect approach. The direct approach refers to the practice of detecting saline soils by observing the surface of bare soil [5-7]. Many salts commonly found in agricultural soils are highly reflective with absorption features across the visible-near infrared (VNIR), shortwave infrared (SWIR), and thermal infrared (TIR) spectral ranges [8, 9]. Using both the increased reflectivity and absorption features offers a method of distinguishing saline soils from their non-saline counterparts [7], even in the presence of confounding factors such as soil moisture [10]. However, mapping surface salinity is of limited use in agriculture, since plants are affected by salinity in the rootzone [11] and surface-level salinity does not always correlate well with rootzone salinity [12]. In irrigated agricultural regions, those regions most often affected by salinity, salts typically accumulate in the lower root-zone making them difficult to detect using reflectance profiles observed at the surface.

The indirect approach instead relies on observing vegetation and inferring the levels of soil salinity based on plant type and status. In this way, vegetation can act as an indicator for salinity throughout the rootzone. Recent successes with this approach have been predicated on the observation that soil salinity is relatively stable in the short term (5-7 years), and thus multiyear compositing techniques may be employed to decrease noise in satellite observations [13]. Lobell et al. [13] was the first analysis that found a reliable signal in a multi-year averaging approach. Following on this advance, Wu et al. [14] used a multi-year maximum, compositing satellite images by taking a 3-years of vegetation indices. Likewise, Scudiero et al. [15] and Scudiero et al. [16] attempted to predict salinity in the central valley of California by first averaging within year, and then applying a multi-year maximum over vegetation indices. These successful predictions at the regional scale renewed interest in sensing salinity using vegetation as an indicator.

The publications which have followed the indirect multi-year compositing approach share a number of other design parameters. First, they often employ on-the-ground electromagnetic sensors to measure apparent electrical conductivity ( $EC_a$ ), which can be related to electrical conductivity of the soil extract ( $EC_e$ ) with high accuracy [17]. Following this approach many observations can be taken at a single field and scaled to the resolution of the satellite using geostatistical techniques. This ensures that the salinity values used as the dependent variable accurately represent the salinity over the broader spatial scale in which they are linked. Second, the modelling techniques employed usually involve simple regression approaches, in which vegetation indices such as the normalized difference vegetation index (NDVI) or enhanced vegetation index (EVI) are related linearly to salinity. Third, the data is often collected over regional ( $10 - 10^5 \text{ km}^2$ ) domains. This is critical because spatial extent often serves as a proxy for data variability. Data collected over small spatial domains may include similar types of soils or crops, making the prediction task easier but making generalizability to other regions more difficult.

Accuracy can be difficult to compare across prediction efforts, due to reliance on different performance metrics as well as the inability of certain performance metrics (i.e.  $R^2$ ) to reliably compare results between datasets with large differences in the range of the dependent variable (see [18] for details). This is especially important for development of soil salinity prediction algorithms whose primary application is in agricultural settings, since very high levels of salinity do not generally occur on land that is actively being cultivated. Complimenting measures such as  $R^2$  with mean-squared error (MSE) or mean average error (MAE) allows for a more comprehensive comparison of model results between studies.

With the increasing application of cloud computing to satellite applications it is less difficult to scale regional methods to global data sets, which may increase sample sizes and allow for methods which avoid the pitfalls of parametric model choice. Since  $EC_e$  is relatively inexpensive to measure, it is often assessed alongside other soil samples. Ensemble datasets combined from multiple sources can increase the number and spatial range of samples included in an analysis. The construction of larger data sets may also support more complex non-parametric methods, such as neural networks, which require less strict assumptions on

how the independent variables must interact [19, 20]. Artificial neural networks (ANNs) can be estimated using conventional regression databases. They are organized in a hierarchical manner, and are thus able to account for complex nonlinear interactions between variables. Convolutional neural networks (CNNs) have traditionally been used for image classification, and are thus able to incorporate entire images as explanatory data to predict a single outcome. In the context of salinity, CNNs can thus take in an image of a field and use information from all pixels to estimate the salinity at its center. Neural networks have been successfully employed on satellite data across applications, including poverty [21], rainfall [22, 23], solar radiation [24, 25], oil spills [26], roads [27], vehicles [28] and scene classification [29, 30].

However, increasing the spatial extent of the dataset may bring in other confounding factors. A greater spatial range will likely be correlated with greater variability in climate, soil properties, cropping patterns and management techniques, economic and demographic data, as well as other factors. Moreover, it is less likely that ensemble salinity datasets will contain  $EC_a$  data, meaning there will be less certainty whether an individual point estimate accurately reflects the salinity of the surrounding area. Addressing whether successes in predicting soil salinity at regional scales can be scaled up to global datasets is an important research question, because success at larger scales will increase the cost-effectiveness of these technologies and contribute valuable sources of information for researchers and land managers.

In this study, we analyze a global data set of salinity measurements with 3672 observations spanning 27 years. Using Google Earth Engine, we download an array of satellite images for each individual observation. First, we analyze these data according to the multi-year compositing approach first implemented by Lobell et al. [13] in order to determine whether the conventional approaches can be successfully applied to a dataset with larger spatial extent. Next, we apply two other modelling approaches - artificial neural networks (ANNs) and convolutional neural networks (CNNs) to test whether we see an improvement in fit by using machine-learning techniques. We report the predictive capacity of each of these techniques on a subset of withheld testing data in order to compare the efficacy of the different approaches.

## 6.2 Methods

### 6.2.1 Overview

The goal of this study is to apply various modelling approaches to predict soil salinity at global scale. Soil salinity data include rootzone salinity measurements sourced from the National Cooperative Soil Survey (NCSS). These salinity measurements are point estimates taken from field sampling campaigns. We attempt to predict these measurements using a set of independent variables, including satellite data, temperature, precipitation, and factors related to elevation and slope. Figure 6-1 provides a visual schematic of the data.

Three modelling approaches are employed in this study. The first involves fitting an ordinary least squares (OLS) model using design parameters from other regional-scale analyses. The second approach applies an ANN on the same regression database constructed for the OLS model. The third approach applies a CNN on a larger set of image data in order to predict salinity at the image's center. The increase in modelling complexity from OLS to ANN and ANN to CNN allows the models to avoid the need for parametrically choosing how the outcome is related to the explanatory variables. However, with a finite data sample it becomes more difficult to precisely estimate the more complex models, which may in turn yield poorer predictive capacity.

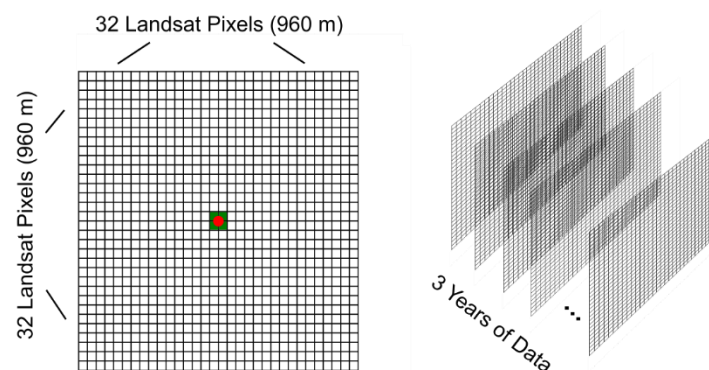


**Figure 6-1. Visual representation of data preparation. Around the original salinity measurement (red dot) a grid of 32 x 32 Landsat 5 pixels are taken. This is done for all Landsat images taken within three years of the observation. The green squares indicate the data used in the ordinary least**

**squares and artificial neural network approach, while the entire image is used in the convolutional neural network approach.**

## 6.2.2 *Data*

### 7.2.2.1 *Surface Reflectance Data – Landsat 5*

Landsat 5 was the fifth satellite for earth observation in the Landsat series and has the distinction of being the longest operating earth observing satellite. Its Thematic Mapper (TM) collected data between 1984 and 2011. In this study we use the surface reflectance product, which corrects top of atmosphere radiation to surface reflectance using the Landsat Ecosystem Disturbance Adaptive Processing System (LEDAPS) [31]. After correction, the surface reflectance for six bands are available – blue, green, red, near-infrared (NIR), SWIR 1, and SWIR 2.

### 7.2.2.2 *Elevation*

Elevation, slope, and aspect are calculated from USGS’s Global Multi-resolution Terrain Elevation Data 2010 (GMTED), which reports data on elevation at a global scale by combining multiple data sources including the Shuttle Radar Topography Mission, Canadian elevation data, and data from the Ice, Cloud, and Land Elevation Satellite (ICESat) [32].

### 7.2.2.3 *Temperature*

Temperature data are sourced from the National Centers for Environmental Prediction (NCEP) / National Center for Atmospheric Research (NCAR) Reanalysis Data. The data have a spatial resolution of 2.5 degrees with 6-hour temporal resolution. We aggregate temperature up to monthly averages before including it in the model.

#### *7.2.2.4 Precipitation*

Precipitation data are collected from Climate Hazards Group InfraRed Precipitation with Station (CHIRPS) [33]. These data are available quasi-globally (50°S-50°N at all longitudes) at a spatial resolution of 0.05 degrees.

#### *7.2.2.5 Land Cover*

Land cover data are sourced from the Global Land Cover Map (GlobCover), satellite-derived land use map constructed with data from ENVISAT's Medium Resolution Imaging Spectrometer (MERIS) [34]. GlobCover provides land classification according to 22 land cover classes defined by the United Nations (UN) Land Cover Classification System (LCCS). In some versions of the model we use the classes pertaining to farmland to divide the salinity data into subsets.

#### *7.2.2.6 NCSS Salinity Data*

The NCSS is a program that operates under the auspices of the United States Department of Agriculture's (USDA's) National Resources Conservation Service (NRCS). The NCSS coordinates efforts from across departments within the US federal government to standardize the collection, processing and dissemination of soils data. The database contains information collected from 1925 to present. Data include latitude, longitude, as well as the values of various soil parameters through the soil column, and are mapped in Figure S1 of Appendix E. Following the specification in Lobell et al. [13], soil salinity is defined as the weighted average of salinity for those horizons in the top 1.5 meters.

In selecting Landsat 5 as the source of our reflectance data, we limit the possible data to the years of its operation – 1984 to 2012. There are 3,672  $EC_e$  values within this data range, and 1,064  $EC_e$  data points once the available data are subsetted to those points that exist in agricultural areas according to the GlobCover 2010 dataset. Both datasets are used in prediction, and model performance is assessed based on a withheld subset of 20% of the data. Additionally, only those points with salinity less than 20 dS/m

were included in order to maintain relevancy of the prediction to agricultural settings. A histogram of the distribution of salinity is provided in Figure 6-2.

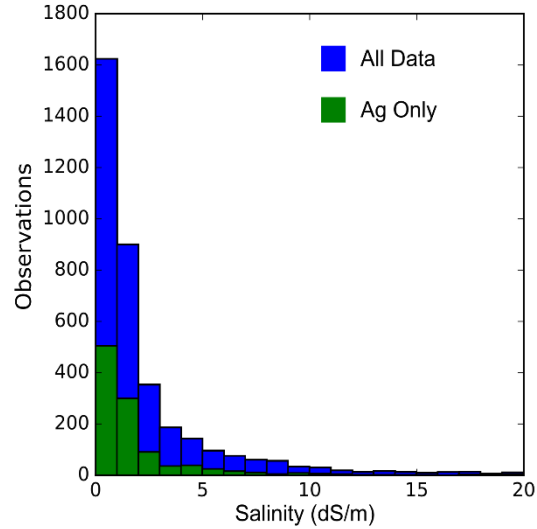


**Figure 6-2. Histogram of salinity observations. Blue bars represent all salinity values (n=3672) and green bars represent the agriculture only subset (n=1064).**

### 7.2.3 Modelling Approaches

#### 7.2.3.1 Ordinary Least Squares

The OLS approach attempts to predict salinity values using vegetation indices and ancillary data. For the purpose of this study we select four commonly used indices – the Normalized Difference Vegetation Index (NDVI), the Enhanced Vegetation Index (EVI), the Canopy Response Salinity Index (CRSI), and the Soil Adjusted Vegetation Index (SAVI). Each of these indices attempt to measure plant health, and are thus likely related to salinity levels. The indices are defined in Equations 1–4.

$$NDVI = \frac{NIR - RED}{NIR + RED} \quad (1)$$

$$EVI = G \cdot \frac{NIR - RED}{NIR + C_1 \cdot RED - C_2 \cdot BLUE + L_{EVI}} \quad (2)$$

$$CRSI = \sqrt{\frac{NIR \cdot RED - GREEN \cdot BLUE}{NIR \cdot RED + GREEN \cdot BLUE}} \quad (3)$$

$$SAVI = (1 + L) \cdot \frac{NIR - RED}{NIR + RED + L_{SAVI}} \quad (4)$$

In the equations above, the constants are set to the following parameters:  $G = 2.5$ ,  $C_1 = 6$ ,  $C_2 = 7.5$ ,  $L_{EVI}=1$ , and  $L_{SAVI}=0.5$ . *BLUE*, *GREEN*, *RED*, and *NIR* refer to Landsat 5 bands 1-4, respectively.

The above indices are used to predict salinity in single and multi-variate regressions, according to Equations 5 and 6, in which *VI* represents one of the four vegetation indices defined in Equations 1–4.

$$\text{Log}(EC_i) = \beta_0 + \beta_1 VI_i + \varepsilon_i \quad (5)$$

$$\text{Log}(EC_i) = \beta_0 + \beta_1 VI_i + \beta_2 \text{Precip}_i + \beta_3 \text{Temp}_i + \beta_4 \text{Elev}_i + \beta_5 \text{Slope}_i + \beta_5 \text{Aspect}_i + \varepsilon_i \quad (6)$$

Since multiple years of satellite data are collected for each point, it is necessary to create data composites in order to estimate the coefficients in Equations 5 and 6. Two approaches are implemented –multi-year maximum and multi-year average. First, we take a subset of the satellite data which only contains cloud-free summer imagery. Next, a vegetation index is calculated for each image. Lastly, the average and maximum of the resultant vegetation indices is calculated across all images.

We conduct the multivariate and univariate regression for each of the vegetation indices for the two compositing techniques. We perform this analysis on the full set of soil salinity data, as well as the data agriculture only subset, resulting in a total of 32 regressions.

### 7.2.3.2 Artificial Neural Networks

The approach implemented for the OLS models relies on selecting the “best” parametric formulation of the satellite data as represented by the vegetation indices. These indices require strong assumptions on how the band data are related to salinity. To avoid these assumptions, we train an ANN on the same datasets prepared for the OLS approach. The model is trained on all six of the surface reflectance bands,

as well precipitation, temperature, elevation, aspect, and slope. Four ANNs are trained – one for each compositing method on the agriculture only subset as well as the full dataset.

The ANN used in this analysis has two hidden layers with 256 and 128 nodes, respectively, and uses a rectified linear unit (ReLU) activation function. The total number of parameters implied with this architecture is 36,097, including bias terms.

### *7.2.3.3 Convolutional Neural Networks*

In order to implement the OLS and ANN models, we must create data composites through time. The CNN, however, is trained on the entire set of satellite imagery over the preceding 3 years. Moreover, as indicated in Figure 6-1, the entire Landsat image is incorporated in the prediction rather than only the center pixels. The data for each observation together thus form a set, in that there are many unordered observations which will be used to predict outcome salinity at each observation.

The CNN is trained using deep residual learning, a strategy which allows deeper neural networks to be trained while avoiding the vanishing gradient problem [35]. In this model, we take the set of data at each observation and implement 48 successive convolutional layers. We then use max pooling across the sets to arrive at an activation layer with 512 features, an approach described in Ravanbakhsh et al. [36].

Lastly, the 512 features are fed through a single dense layer to yield a point estimate of salinity. There are a total of 1,388,777 trainable parameters in the described modelling architecture.

## **6.3 Results**

### *7.3.1 Ordinary Least Squares*

The OLS modelling approach attempts to recreate the methods employed by Lobell et al. [13] on a global dataset. Of the regressions performed, we display the results from four in Figure 6-3 representing the best performing (as measured by out of sample  $R^2$ ) for the univariate and multivariate models trained on the full and agriculture only datasets. Each of the chosen regressions thus have the possibility of employing

either multi-year maximum or multi-year average compositing, as well as utilizing each of the four vegetation indices. We examine which of the parametric modelling choices results in the best fit.

Figures 6-3A and 6-3C report the results from the best univariate models on the agriculture only subset and the full data set, respectively. When plotting the salinity against the vegetation index we see a downward sloping trendline, indicating that a higher vegetation index is correlated with lower salinity as would be expected. The two selected models make use of separate compositing techniques – with the multiyear maximum being used on the subset and the multiyear average being used on the full data. CRSI is selected as the best performing vegetation index in both data sets, although model fit is generally poor. For the agriculture only subset, out of sample  $R^2$  is 0.0018. For the full data, out of sample  $R^2$  is 0.022.

Figures 6-3B and 6-3D report the results of the multivariate modelling efforts for the agriculture-only subset and the full data, respectively. As with the univariate modelling, models are selected based on performance on a withheld out of sample dataset. The  $y$  and  $x$  axes of these figures show the actual and predicted Log EC values, while the 1:1 trend line shows what would be a perfect fit. Model performance is highest with the CRSI vegetation index, and both models use multiyear max compositing. While the out of sample  $R^2$  values increase in the multivariate modelling scenario, they remain low. The agriculture only subset reports an  $R^2$  of 0.0081, while the full data reports an  $R^2$  of 0.051.

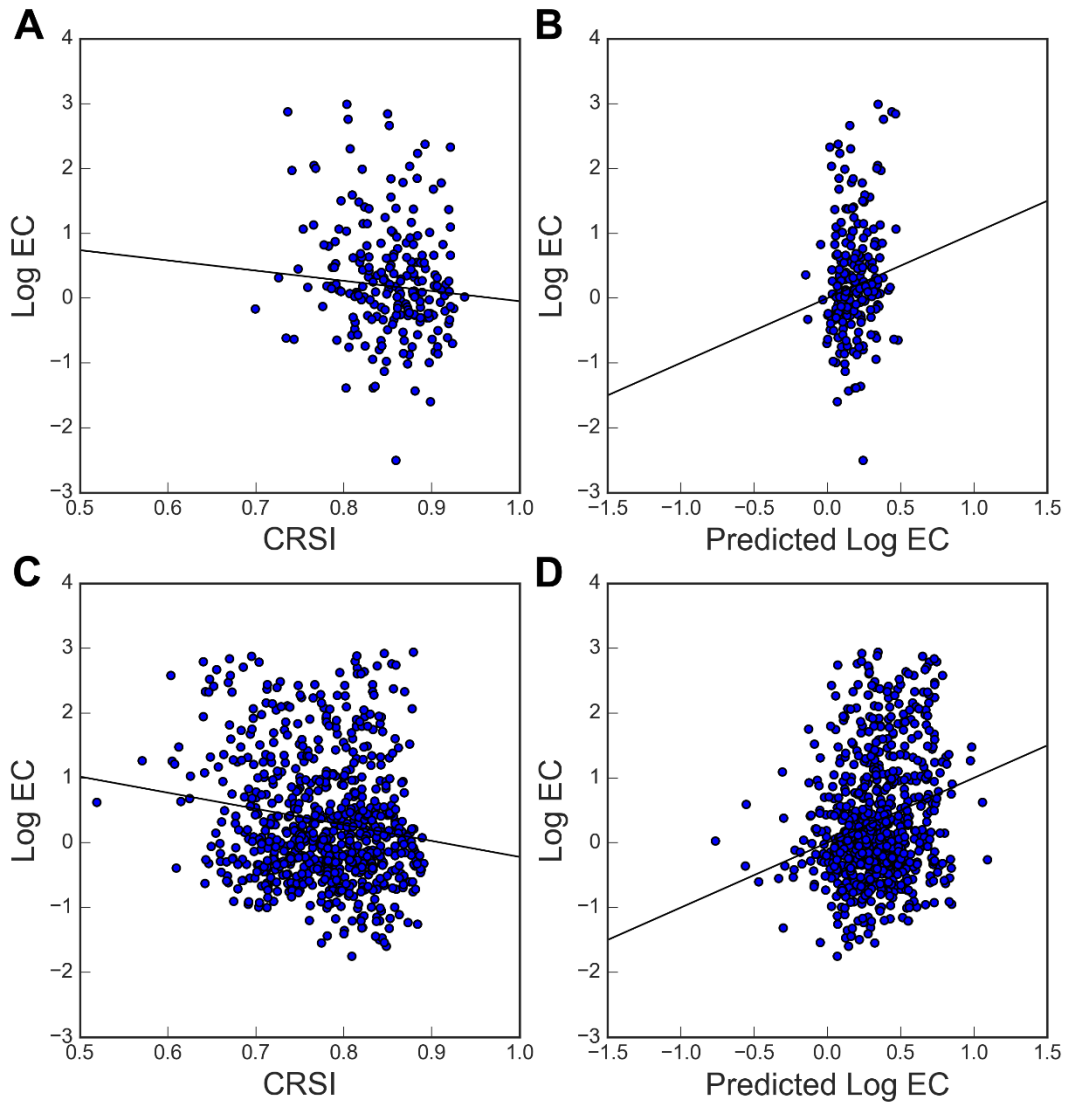


**Figure 6-3. Out of sample results from the ordinary least squares approach. A and B show the results from the agriculture only subset, while C and D show the results from all of the data. A and C show the regression of the natural log of electrical conductivity on Canopy Response Salinity Index (CRSI) using a univariate regression. B and D show the results of the multivariate regression using all parameters. CRSI performed best as measured by out of sample  $R^2$  for each regression.**

### 7.3.2 Neural Networks

The results from the ANN and CNN approaches are reported in Figures 6-4A and 6-4B. Since both models are multivariate the Figures report the actual and predicted Log EC values reported alongside a perfect 1:1 trendline.

Four ANNs were trained in total – multi-year maximum compositing technique on full data, multi-year maximum compositing technique on agriculture only subset, multi-year average compositing technique on full data set, and multi-year average compositing technique on the agriculture only subset. Figure 6-4A shows the results from the best performing ANN as measured by out of sample  $R^2$ , which utilizes the average compositing technique on the full set of data. The reported out of sample  $R^2$  for the best performing model was 0.15. Figure 6-4B shows the result from the single CNN trained on the full set of data, which reports an out of sample  $R^2$  of 0.069

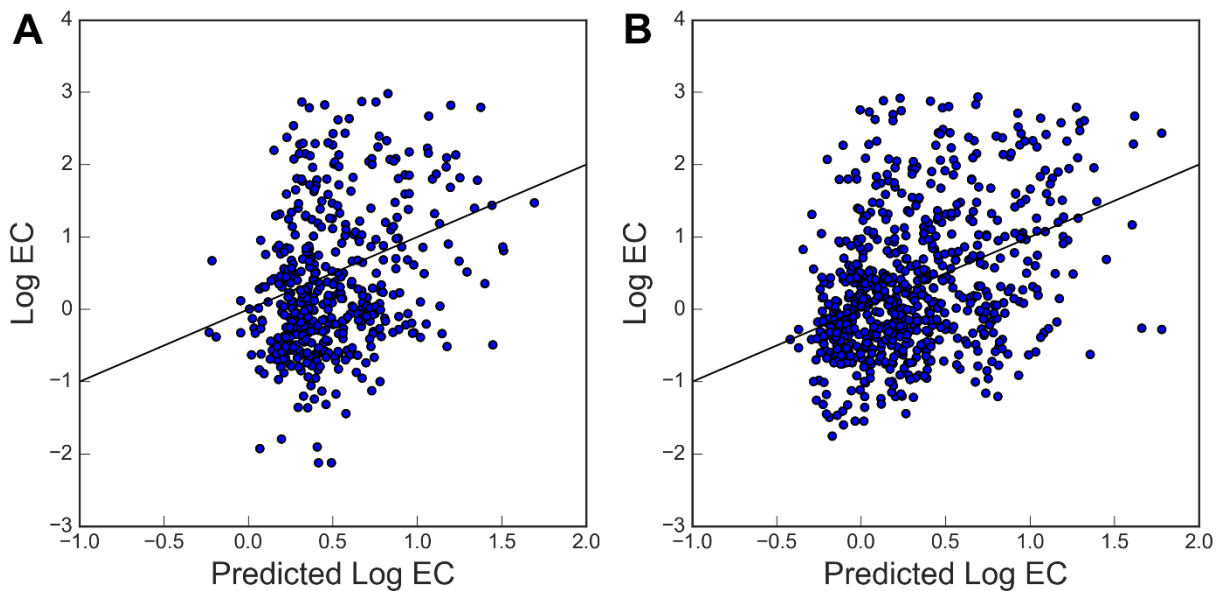


**Figure 6-4. Out of sample results from the artificial neural network (A) and the convolutional neural network (B). In A, the results from the best-performing ANN which utilized all of the data and the ‘average’ formulation. Blue line represents perfect prediction.**

### 7.3.3 Model Comparison

The OLS, ANN, and CNN models employed in this study vary significantly in their complexity. The more complex neural networks risk overfitting, so when comparing the models it is necessary to compare their out of sample performance. Results are reported in Table 6-1.

For the agriculture only subset, the OLS model outperforms the ANN in all metrics of fit, though the results are qualitatively similar. The CNN is not trained on the agriculture only subset due to its limited sample size.

For the full dataset, the ANN outperforms both the OLS model and the CNN in all measures of fit. Full results from all models are presented in Appendix E.

**Table 6-1. Out of sample measures of fit for OLS, ANN, and CNN models for full dataset.**

	AGRICULTURE ONLY SUBSET			FULL DATA		
	Mean Squared Error (MSE)	Mean Average Error (MAE)	R <sup>2</sup>	Mean Squared Error (MSE)	Mean Average Error (MAE)	R <sup>2</sup>
OLS	0.78	0.65	0.0081	0.94	0.78	0.051
ANN	0.79	0.67	0.0029	0.80	0.70	0.150
CNN	N/A	N/A	N/A	0.89	0.78	0.069

## 6.4 Discussion

In this study, we sought to test techniques traditionally used to predict soil salinity at regional scales on a global dataset, as well as apply more sophisticated statistical modelling. The techniques used to model regional-scale salinity processes rely on collecting exhaustive satellite imagery, weather data, and other auxiliary parameters over multiple years in order to predict rootzone salinity. These techniques are now easily ported to global datasets due to cloud computing services with access to satellite archives, such as

google earth engine. With the increased sample size it becomes feasible to implement more complex models, such as ANNs and CNNs.

Our results showed that these methods cannot be easily scaled to global data, either due to increased variability in the samples or the lack of accompanying  $EC_a$  data. Expanding the spatial domain of the sample increases variability in the climatic conditions, soil parameters, cropping patterns, management practices, ecological circumstances, among other variables. While global datasets will likely have larger sample size, extracting the signal from the noise amongst increased variability is likely to be a major challenge. Likewise, while  $EC_e$  is likely to be assessed in many soil surveys, such point estimates of salinity may misrepresent the salinity of a wider spatial domain. Relating the point estimate to the gridded Landsat data, therefore, likely introduces error. Recent studies at the regional scale all made use of  $EC_a$  data which produces a dataset with a much denser salinity mapping, allowing the researcher to be more confident that the salinity indicated at a particular location is representative of the entire satellite pixel [13, 37, 38]. While it is likely that many disparate datasets exist which contain  $EC_e$  samples, it is less likely that there are many such full field assessments using noncontact  $EC_a$  sensors.

We found some evidence in our results that the parametric vegetation index choice criteria can be supplanted by more complex neural networks. Studies in the literature often focus on testing several parametric combinations of satellite data, when it may be possible to avoid such strict assumptions using nonlinear models, such as neural networks. While the OLS modelling techniques outperforms the ANN in the sparser data sample, when using the full dataset the ANN performs best in out of sampling testing. The size of the data is important in all models, with improved out of sample prediction occurring in the larger data sets across techniques. The predictive capacity of the CNN is qualitatively similar to that of the OLS models, indicating that our sample size of 3,672 observations may be too small for the most complex imaging processing techniques. The optimal approach for our dataset lies in the middle path between an approach that uses parametrically imposed domain knowledge and one that employs completely data-driven modelling techniques.

Within the OLS approach, the models all employed the same vegetation index but different compositing techniques. The Canopy Response Salinity Index (CRSI) performed best across all models and datasets. While there has been some debate on the applicability of multiyear maximum versus multiyear average, our results do not offer strong evidence in either direction. The multiyear average performed better for the univariate model trained on the agriculture only subset, while the multiyear maximum performed better for the univariate agriculture only subset as well as the multivariate model on both datasets.

While the fit reported in this study is below that which would be useful for researchers and land managers, there is evidence to suggest the techniques employed in this study might serve to enhance prediction in other contexts. First, it was seen that prediction increased in larger sample sizes. All of the salinity data included in this study are sourced from one survey program, though it may be possible to collect an ensemble dataset by aggregating across national projects. Second, our study uses Landsat 5 data, and future studies may be able to make use of more advanced orbital sensors. Hyperspectral sensors and multispectral sensors with higher radiometric resolution can bring in more information than our available in our six-band data. Neural networks as applied in this study offer an approach for incorporating data from multiple satellites, something that cannot be done easily with the vegetation index approach. Third, there is an increasing amount of ancillary data at the global scale. For example, researchers are developing techniques to generate satellite-based crop classifiers at a global scale [39, 40], data which is not available in the modelling results presented in this study. Lastly, we have shown that applying neural networks may be superior to the vegetation index approach, a finding which may support efforts to predict salinity at the regional scale.

## References

- [1] Oldeman L 1994 *Soil Resilience and Sustainable Land Use*, ed D J Greenland and I Szabolcs (Wallingford, UK: CAB International) pp 99–118
- [2] Natural Resources Conservation Service, U.S. Department of Agriculture 2015 Soil Survey Geographic (SSURGO) Database <http://sdmdataaccess.nrcs.usda.gov/> (accessed September 10, 2015)
- [3] Welle P and Mauter M High-Resolution Model for Estimating the Economic and Policy Implications of Agricultural Soil Salinization in California *Environmental Research Letters* Under Review
- [4] Grimwood T 2011 Union of Concerned Scientists satellite database. <http://www.ucsusa.org/nuclear-weapons/space-weapons/satellite-database>
- [5] Goldshleger N, Ben-Dor E, Benyamini Y, Agassi M and Blumberg D G 2001 Characterization of soil's structural crust by spectral reflectance in the SWIR region (1.2-2.5  $\mu$  m) *Terra Nova* **13** 12-7
- [6] Metternicht G I 1998 Fuzzy classification of JERS-1 SAR data: an evaluation of its performance for soil salinity mapping *Ecol Model* **111** 61-74
- [7] Csillag F, Pásztor L and Biehl L L 1993 Spectral band selection for the characterization of salinity status of soils *Remote Sens Environ* **43** 231-42
- [8] Farifteh J, van der Meer F, van der Meijde M and Atzberger C 2008 Spectral characteristics of salt-affected soils: A laboratory experiment *Geoderma* **145** 196-206
- [9] Lane M D and Christensen P R 1998 Thermal infrared emission spectroscopy of salt minerals predicted for Mars *Icarus* **135** 528-36
- [10] Xu C, Zeng W Z, Huang J S, Wu J W and van Leeuwen W J D 2016 Prediction of Soil Moisture Content and Soil Salt Concentration from Hyperspectral Laboratory and Field Data *Remote Sensing* **8** 42
- [11] Maas E V and Hoffman G J 1977 Crop salt tolerance - current assessment *Journal of the irrigation and drainage division* **103** 115-34
- [12] Zare E, Huang J, Santos F A M and Triantafilis J 2015 Mapping Salinity in Three Dimensions using a DUALEM-421 and Electromagnetic Inversion Software *Soil Sci Soc Am J* **79** 1729-40
- [13] Lobell D, Lesch S, Corwin D, Ulmer M, Anderson K, Potts D, Doolittle J, Matos M and Baltes M 2010 Regional-scale assessment of soil salinity in the Red River Valley using multi-year MODIS EVI and NDVI *Journal of environmental quality* **39** 35-41
- [14] Wu W C, Al-Shafie W M, Mhaimed A S, Ziadat F, Nangia V and Payne W B 2014 Soil Salinity Mapping by Multiscale Remote Sensing in Mesopotamia, Iraq *Ieee J-Stars* **7** 4442-52
- [15] Morari F, Meggio F, Lunardon A, Scudiero E, Forestan C, Farinati S and Varotto S 2015 Time course of biochemical, physiological, and molecular responses to field-mimicked conditions of drought, salinity, and recovery in two maize lines *Front Plant Sci* **6** 314
- [16] Scudiero E, Skaggs T H and Corwin D L 2016 Comparative regional-scale soil salinity assessment with near-ground apparent electrical conductivity and remote sensing canopy reflectance *Ecol Indic* **70** 276-84
- [17] Corwin D L and Lesch S M 2005 Apparent soil electrical conductivity measurements in agriculture *Comput Electron Agr* **46** 11-43
- [18] Scudiero E, Corwin D L, Anderson R G and Skaggs T H 2016 Moving forward on remote sensing of soil salinity at regional scale *Frontiers in Environmental Science* **4** 65
- [19] Lek S and Guégan J F 1999 Artificial neural networks as a tool in ecological modelling, an introduction *Ecol Model* **120** 65-73
- [20] Mas J F and Flores J J 2008 The application of artificial neural networks to the analysis of remotely sensed data *International Journal of Remote Sensing* **29** 617-63
- [21] Jean N, Burke M, Xie M, Davis W M, Lobell D B and Ermon S 2016 Combining satellite imagery and machine learning to predict poverty *Science* **353** 790-4

- [22] Grimes D I F, Coppola E, Verdecchia M and Visconti G 2003 A Neural Network Approach to Real-Time Rainfall Estimation for Africa Using Satellite Data *Journal of Hydrometeorology* **4** 1119-33
- [23] Sorooshian S, Hsu K-L, Gao X, Gupta H V, Imam B and Braithwaite D 2000 Evaluation of PERSIANN System Satellite-Based Estimates of Tropical Rainfall *Bulletin of the American Meteorological Society* **81** 2035-46
- [24] Yadav A K and Chandel S S 2014 Solar radiation prediction using Artificial Neural Network techniques: A review *Renewable and Sustainable Energy Reviews* **33** 772-81
- [25] Şenkal O 2010 Modeling of solar radiation using remote sensing and artificial neural network in Turkey *Energy* **35** 4795-801
- [26] Frate F D, Petrocchi A, Lichtenegger J and Calabresi G 2000 Neural networks for oil spill detection using ERS-SAR data *Ieee T Geosci Remote* **38** 2282-7
- [27] Mokhtarzade M and Zoj M J V 2007 Road detection from high-resolution satellite images using artificial neural networks *Int J Appl Earth Obs* **9** 32-40
- [28] Chen X, Xiang S, Liu C L and Pan C H 2014 Vehicle Detection in Satellite Images by Hybrid Deep Convolutional Neural Networks *Ieee Geosci Remote S* **11** 1797-801
- [29] Hu F, Xia G-S, Hu J and Zhang L 2015 Transferring Deep Convolutional Neural Networks for the Scene Classification of High-Resolution Remote Sensing Imagery *Remote Sensing* **7** 14680
- [30] Nogueira K, Penatti O A B and dos Santos J A 2017 Towards better exploiting convolutional neural networks for remote sensing scene classification *Pattern Recognition* **61** 539-56
- [31] Schmidt G, Jenkerson C, Masek J, Vermote E and Gao F 2013 Landsat ecosystem disturbance adaptive processing system (LEDAPS) algorithm description. *Open-File Report* p 27
- [32] Danielson J J and Gesch D B 2011 Global multi-resolution terrain elevation data 2010 (GMTED2010) *Open-File Report*
- [33] Funk C, Peterson P, Landsfeld M, Pedreros D, Verdin J, Shukla S, Husak G, Rowland J, Harrison L, Hoell A and Michaelsen J 2015 The climate hazards infrared precipitation with stations—a new environmental record for monitoring extremes **2** 150066
- [34] Arino O, Ramos Perez J J, Kalogirou V, Bontemps S, Defourny P and Van Bogaert E 2012 Global Land Cover Map for 2009 (GlobCover 2009)
- [35] He K, Zhang X, Ren S and Sun J 2016 Deep residual learning for image recognition. *Proceedings of the IEEE conference on computer vision and pattern recognition*, pp 770-8
- [36] Ravanbakhsh S, Schneider J and Poczos B 2016 Deep learning with sets and point clouds *arXiv preprint arXiv:1611.04500*
- [37] Scudiero E, Skaggs T H and Corwin D L 2014 Regional scale soil salinity evaluation using Landsat 7, western San Joaquin Valley, California, USA *Geoderma Regional* **2** 82-90
- [38] Scudiero E, Skaggs T H and Corwin D L 2015 Regional-scale soil salinity assessment using Landsat ETM plus canopy reflectance *Remote Sens Environ* **169** 335-43
- [39] You L Z, Wood S, Wood-Sichra U and Wu W B 2014 Generating global crop distribution maps: From census to grid *Agr Syst* **127** 53-60
- [40] King L, Adusei B, Stehman S V, Potapov P V, Song X-P, Krylov A, Di Bella C, Loveland T R, Johnson D M and Hansen M C 2017 A multi-resolution approach to national-scale cultivated area estimation of soybean *Remote Sens Environ* **195** 13-29

## Chapter 7: Conclusions

The advent of remotely sensed data provides a new avenue for informed, quantitative policy analysis. These new data often have increased temporal resolution as well as both increased spatial extent and resolution compared to traditional sources. This confers two chief advantages – (1) the increase in resolution prevents the reliance on regional averages and thus increases the accuracy of policy analysis and (2) the increase in extent and resolution from survey/field sources makes certain analyses possible that would not have been otherwise.

There are, however, key challenges inherent to remotely sensed data. Often, as is the case with land use classifiers, there will be errors in the satellite accuracy and it will be necessary to correct these data with ground-truth estimates. Residual monitoring programs are thus necessary to maintain high accuracy of usability of the data products. Likewise, the uncertainty in remotely sensed data call for the application of traditional policy analysis tools such as simulation and uncertainty analyses. Many of these techniques do not scale efficiently to very large datasets, making treatment of uncertainty a key difficulty in making use of the data.

In this dissertation, I present the results of 5 policy analyses which make use of remotely sensed data sources for policy. Through these five chapters, I explore the complexity of employing high resolution satellite data sources for application in agricultural and environmental systems while treating the uncertainty inherent in the data.

In Chapter 2, I assessed coral response to temperature in an effort to assess the impacts of climate change on coral reefs. Coral cover has been declining in recent decades due to increased temperatures and environmental stressors. However, the extent to which different stressors contribute both individually and in concert to bleaching and mortality is still uncertain. I developed a regression approach which uses non-linear parametric models that control for unobserved time invariant effects to estimate the effects on coral bleaching and mortality due to temperature, solar radiation, depth, hurricanes and anthropogenic stressors

using historical data from a large bleaching event in 2005 across the Caribbean. Two separate models were created, one to predict coral bleaching, and the other to predict near-term mortality. A large ensemble of supporting data was assembled to control for omitted variable bias and improve fit, and a significant improvement in fit was observed from univariate linear regression based on temperature alone. The results suggest that climate stressors (temperature and radiation) far outweighed direct anthropogenic stressors (using distance from shore and nearby human population density as a proxy for such stressors) in driving coral health outcomes during the 2005 event. Indeed, temperature was found to play a role ~4 times greater in both the bleaching and mortality response than population density across their observed ranges. The empirical models tested in the study have large advantages over ordinary-least squares – they offer unbiased estimates for censored data, correct for spatial correlation, and are capable of handling more complex relationships between dependent and independent variables. The models offered a framework for preparing for future warming events and climate change; guiding monitoring and attribution of other bleaching and mortality events regionally and around the globe; and informing adaptive management and conservation efforts.

In Chapter 3, I introduced a generalizable approach for estimating the field-scale agricultural yield losses due to soil salinization. When integrated with regional data on crop yields and prices, this model provided high-resolution estimates for revenue losses over large agricultural regions. The methods accounted for the uncertainty inherent in model inputs derived from satellites, experimental field data, and interpreted model results. I applied this method to estimate the effect of soil salinity on agricultural outputs in California, performing the analysis with both high-resolution (i.e. field scale) and low-resolution (i.e. county-scale) data sources to highlight the importance of spatial resolution in agricultural analysis. The model estimated that soil salinity reduced agricultural revenues by \$3.7 billion (\$1.7 - \$7.0 billion) in 2014, amounting to 8.0 million tons of lost production relative to soil salinities below the crop-specific thresholds. When using low-resolution data sources, I found that the costs of salinization are

underestimated by a factor of three. These results highlight the need for high-resolution data in agro-environmental assessment as well as the challenges associated with their integration.

In Chapter 4, I assessed the evidence for crop switching as a behavioral response to salinity levels by growers in the Central Valley of California using a regression approach. Since the Central Valley of California only intersects 19 counties, I employed a spatial disaggregation technique to downscale land use data to 56,043 soil polygon regions. The spatial disaggregation technique, cross-entropy minimization, utilizes county data as well as high-resolution satellite imagery to compile information at an intermediate scale. Additionally, I constructed a rich set of explanatory variables for each soil polygon including salinity, other soil parameters, temperature, precipitation, topographical features, crop prices, expenses, as well as spatial fixed effects which demarcate local administrative boundaries. The regression results indicated that while growers behave in a manner consistent with agronomic data regarding crop tolerance, their response to salinity levels is relatively small in magnitude. Lastly, I conducted policy exercises to compare the results of damages from soil salinization for two models – one which allowed for farmer crop switching in accordance with the regression results and another which fixed cropping patterns at 2015 levels. Results from the policy analyses indicated that the effect of crop switching was much smaller than uncertainty inherent in the data.

In Chapter 5, I assessed water desalination as a proposed solution for mitigating the effects of drought, soil salinization, and the ecological impacts of agricultural drainage. An integrated modelling framework was used to estimate the public and private costs and benefits of distributed desalination in the Central Valley (CV) of California. I employed environmental and economic models to estimate the value of reducing the salinity of irrigation water; the value of augmenting water supply under present and future climate scenarios; and the human health, environmental, and climate change damages associated with generating power to desalinate water. It was found that water desalination is only likely to be profitable in 4% of the CV during periods of severe drought, and that current costs would need to decrease by 70-90% for adoption to occur on the median acre. Fossil-fuel powered desalination technologies also

generate air emissions that impose significant public costs in the form of human health and climate change damages, although these damages vary greatly depending on technology. The ecosystem service benefits of reduced agricultural drainage would need to be valued between \$800 and \$1200 per acre-foot, or nearly the full capital and operational costs of water desalination, for the net benefits of water desalination to be positive from a societal perspective.

In Chapter 6, I assessed the feasibility of monitoring soil salinity at the global scale using satellite-based remote sensing. Several studies have been successful relating soil salinity to satellite-based vegetation indices at regional scales using ordinary least squares (OLS) regression. Using google earth engine and a salinity dataset containing 3,672 observations of electrical conductivity of the soil extract ( $EC_e$ ), I compiled a global dataset of salinity measurements, satellite data, weather data, and information related to elevation and slope. I applied to this dataset the methods employed in regional-scale studies, namely multivariate OLS of salinity on vegetation indices and ancillary data. Next, I applied both artificial neural networks (ANNs) and convolutional neural networks (CNNs) to the same data, and compare models based on performance on a withheld portion of the data. While the predictive capacity is below that that would be useful to create an operational data product, I found that using neural networks may lead to better prediction of salinity than OLS approaches. Further research may benefit by compiling a broader set of ancillary data, as well as using datasets with a higher density of measurements, such as those with measurements of apparent electrical conductivity ( $EC_a$ ) collected by noncontact sensors.

Through each of these case studies, satellite-based remote sensing provided key information. The analyses in Chapter 2 (assessment of climate change on corals), Chapter 4 (assessment of farmer's behavioral response to salinity) and Chapter 6 (prediction of soil salinity) would have been not feasible without key satellite inputs. The analyses in Chapter 3 (assessment of salinity on California revenues) and Chapter 5 (assessment of desalination technologies) would have been feasible in theory, though the accuracy and reliability of the results would have been greatly reduced.

Each of the above analyses suggest further research. The assessment of coral response in Chapter 2 to climate change could be coupled with climate predictions for the coming decades in order to better understand the implication of coral decline. The approach utilized for assessing the costs of salinization in Chapter 3 could be extended to include empirical techniques to account for likely shifts in the commodity pricing and crop switching techniques of growers. The methodology in Chapter 4 could be extended to multiple years of data in order to more accurately estimate the effects of salinity. And the modelling approaches implemented to predict salinity in Chapter 6 might be tested using more technologically advanced orbital sensing on more recently collected salinity data.

The policy analyses explored in these case studies help to illuminate the benefits and challenges associated with high-resolution satellite data sources, as well as indicate possible avenues for improvement. While the technology which predicts land use data for agriculture has matured, many other key agricultural data are not available. Factors related to price and cost data may never be available at high resolution, but other factors such as water use, irrigation type, and yields would likely significantly improve the ability to model farmer behavioral response to climate change or policy. As these data products become increasingly available, policy analyses are likely to become more accurate and applicable for policy makers seeking to manage agricultural and environmental systems.

## APPENDIX A: Chapter 2

### 8.1 Spatial Distribution

Figure S1 shows the spatial distribution of the observations. The temporal distribution can be found in Figure 3 of the main text. There were three main concentrations of data: Belize/Mexico (~44%), The Florida Keys (~14%), and the eastern Caribbean (~25%).

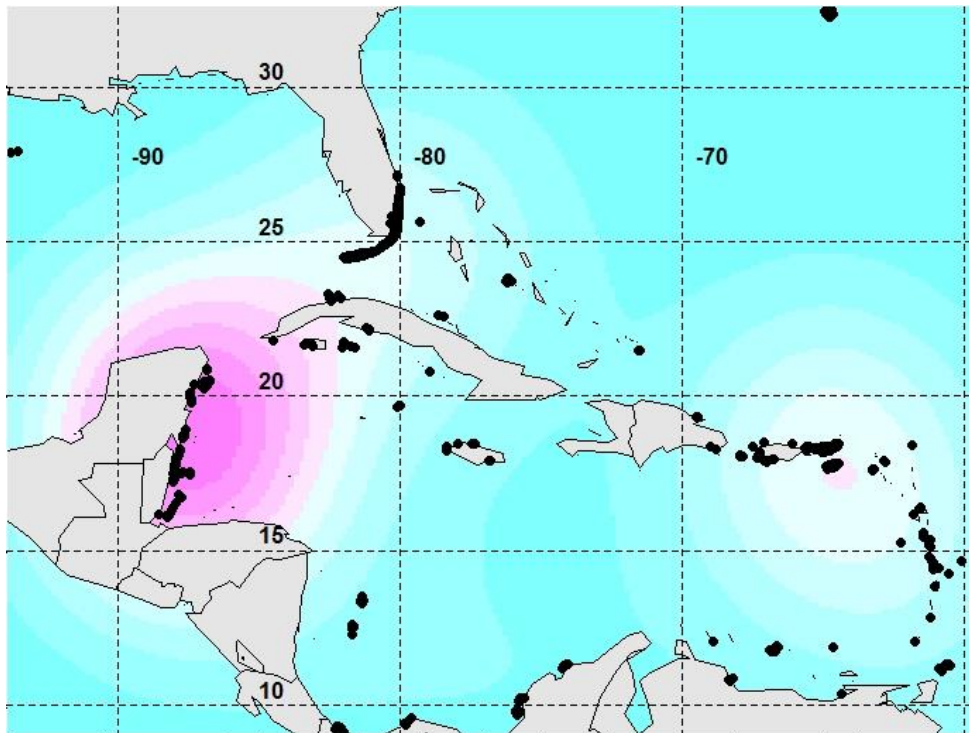


**Figure S1. Spatial distribution of observations. This figure shows spatial observations distributed over the Caribbean. Each black circle is an observation. The colors represent observation density, with pink showing high density and turquoise showing low.**

### 8.2 Addressing Multi-Collinearity

When dealing with multiple measures in a regression analysis it is necessary to be careful to avoid constructing models with problems of multicollinearity, or high correlation between independent variables. Correlated independent variables result in large standard errors making statistical inference difficult. While multicollinearity does not bias the estimates directly, it can magnify biases caused by

omitted variables or other causes. To avoid this, each of the models tested only includes one measure of each stressor (for instance maximum DHW or observed DHW, not both), with the presumption that different formulations of the same stressor will display high correlation. Table S1 shows the correlations between all variables, and indeed it can be seen that different formulations of the same stressor report correlation. Correlations across stressors (e.g. maximum DHW and maximum PAR anomaly) are generally low.

**Table S1. Correlations between stressors. The upper-right triangle contains sample correlation coefficients.**

	Maximum DHW	Observed DHW	Maximum PAR Anomaly	Observed PAR Anomaly	Distance From Shore	Population Density	Wind	Depth
Maximum DHW		0.67***	0.19***	0.11***	0.06***	-0.08***	-0.04*	0.15***
Observed DHW			-0.06***	-0.33***	0.03*	-0.09***	-0.07***	0.15***
Maximum PAR Anomaly				0.36***	-0.02	0.32***	0.06***	-0.10***
Observed PAR Anomaly					-0.11***	-0.01	-0.14***	0.00
Distance From Shore						-0.02	0.13***	0.10***
Population Density							0.05**	-0.09***
Wind								-0.13***
Depth								

P-values for statistical significance of indicated correlation coefficients:  
 \*\*\* p<0.01, \*\* p<0.05, \* p<0.1

### 8.3 Functional Forms for the Regressions

In Tables S2 and S3, a series of models are presented along with measures of fit. The marginal effect of temperature is reported alongside to show the robustness of effect to model choice. For the purposes of these tables, two stressor forms are considered:

Univariate:

$$Bleaching_i = f(ObsDHW_i)$$

$$Mortality_i = f(MaxDHW_i)$$

Multivariate:

$$Bleaching_i = f(ObsDHW_i, ObsPAR\ Anomaly_i, Depth_i, DFS_i, PopDens_i, Wind_i, ObsDHW_i \times Depth_i, ObsPAR\ Anomaly_i \times Depth_i)$$

$$Mortality_i = f(MaxDHW_i, MaxPAR\ Anomaly_i, Depth_i, DFS_i, PopDens_i, Wind_i, MaxDHW_i \times Depth_i, MaxPAR\ Anomaly_i \times Depth_i)$$

The functional forms used are OLS, Tobit, and Fractional Logit. OLS, while being a common modeling strategy due to its simplicity, can have limitations under certain circumstances. It is not an appropriate choice for a censored dependent variable and will yield biased results. The model's linear formulation of independent variables can be misleading if the true data-generating process is not linear. Tobit allows for a censored dependent variable while maintaining the linear form of independent variables. Lastly, Fractional Logit would be more appropriate for modeling censored dependent variables with non-linear effects.

#### 8.4 Using k-fold Cross-Validation to Identify the Best Model

We used a *k*-fold cross-validation for model selection. Cross-validation allows for simulation of out of sample prediction by withholding part of the data as a training set and uses part as testing set. In this study *k* was set equal to 5, meaning 80% of the data was iteratively used to predict the remaining 20%. Cross-validated R<sup>2</sup> and cross-validated MSE allow us to simulate which model is predicting best out of sample. The fractional logit model that controls for spatial effects performs best for both mortality and bleaching.

**Table S2: Mortality models and results.**

Model	Description	Univariate /Multivariate	Spatial Control	Average Marginal Effect for Temperature	Cross-Validation R <sup>2</sup>	Cross-Validation MSE
OLS	Standard linear regression	Univariate	None	0.660	0.15	38.59
OLS	Standard linear regression	Multivariate	None	0.666	0.20	36.32
OLS	Standard linear regression	Multivariate	Spatial Dummies	0.502	0.28	32.69
Tobit	Linear regression which accounts for censored dependent variable	Univariate	None	1.530	0.15	38.59

<b>Tobit</b>	Linear regression which accounts for censored dependent variable	Multivariate	None	1.680	0.18	37.23
<b>Tobit</b>	Linear regression which accounts for censored dependent variable	Multivariate	Spatial Dummies	1.861	0.08	41.77
<b>Fractional Logit</b>	Sigmoid which allows for non-linear effects	Univariate	None	0.594	0.17	37.68
<b>Fractional Logit</b>	Sigmoid which allows for non-linear effects	Multivariate	None	0.614	0.30	31.78
<b>Fractional Logit</b>	Sigmoid which allows for non-linear effects	Multivariate	Spatial Dummies	0.050	0.32	30.87

**Table S3. Bleaching models and results.**

Model	Description	Univariate /Multivariate	Spatial Control	Average marginal effect for Temperature	Cross-Validation R <sup>2</sup>	Cross-Validation MSE
<b>OLS</b>	Standard linear regression	Univariate	None	3.22	0.18	701.1
<b>OLS</b>	Standard linear regression	Multivariate	None	3.09	0.21	675.5
<b>OLS</b>	Standard linear regression	Multivariate	Spatial Dummies	3.28	0.25	641.3
<b>Tobit</b>	Linear regression which accounts for censored dependent variable	Univariate	None	3.54	0.18	701.1
<b>Tobit</b>	Linear regression which accounts for censored dependent variable	Multivariate	None	3.33	0.20	684.0
<b>Tobit</b>	Linear regression which accounts for censored dependent variable	Multivariate	Spatial Dummies	3.56	0.24	649.8
<b>Fractional Logit</b>	Sigmoid which allows for non-linear effects	Univariate	None	2.89	0.18	701.1
<b>Fractional Logit</b>	Sigmoid which allows for non-linear effects	Multivariate	None	2.70	0.23	658.4
<b>Fractional Logit</b>	Sigmoid which allows for non-linear effects	Multivariate	Spatial Dummies	2.99	0.27	624.2

## 8.5 Within-Region Correlation Tables

**Table S4. Correlations between stressors in the Reference Region - Joint Northern Gulf / Western Caribbean.**

	Maximum DHW	Observed DHW	Maximum PAR Anomaly	Observed PAR Anomaly	Distance From Shore	Population Density	Wind	Depth
Maximum DHW		0.31***	-0.09	-0.09	-0.11	-0.02	0.08	0.04
Observed DHW			-0.11	-0.25***	0.06	-0.05	-0.09	0.01
Maximum PAR Anomaly				0.23***	-0.26***	0.73***	-0.73***	-0.10
Observed PAR Anomaly					-0.19***	0.34***	-0.22***	0.13
Distance From Shore						-0.37***	0.54***	0.03
Population Density							-0.68***	0.13
Wind								-0.15**
Depth								

P-values for statistical significance of indicated correlation coefficients: \*\*\* p<0.01, \*\* p<0.05, \* p<0.1

**Table S5. Correlations between stressors in the Bermuda Region.**

	Maximum DHW	Observed DHW	Maximum PAR Anomaly	Observed PAR Anomaly	Distance From Shore	Population Density	Wind	Depth
Maximum DHW		1.00***	-0.16	-0.33	-0.06	NA	NA	0.45**
Observed DHW			-0.16	-0.33	-0.06	NA	NA	0.45**
Maximum PAR Anomaly				0.91***	-0.38	NA	NA	-0.48**
Observed PAR Anomaly					-0.43**	NA	NA	-0.50**
Distance From Shore						NA	NA	-0.23
Population Density							NA	NA
Wind								NA
Depth								

P-values for statistical significance of indicated correlation coefficients: \*\*\* p<0.01, \*\* p<0.05, \* p<0.1

**Table S6. Correlations between stressors in the Bahamian Region.**

	Maximum DHW	Observed DHW	Maximum PAR Anomaly	Observed PAR Anomaly	Distance From Shore	Population Density	Wind	Depth
Maximum DHW		0.76***	-0.43***	-0.04	-0.03	0.95***	-0.49***	0.34**
Observed DHW			-0.31**	-0.62***	0.00	0.71***	-0.42**	0.26
Maximum PAR Anomaly				0.06	0.65***	-0.48***	0.20	-0.55***
Observed PAR Anomaly					0.06	-0.04	0.08	-0.09
Distance From Shore						-0.19	-0.06	-0.39**
Population Density							-0.48***	0.39**
Wind								-0.27
Depth								

P-values for statistical significance of indicated correlation coefficients: \*\*\* p<0.01, \*\* p<0.05, \* p<0.1

**Table S7. Correlations between stressors in the Eastern Caribbean.**

	Maximum DHW	Observed DHW	Maximum PAR Anomaly	Observed PAR Anomaly	Distance From Shore	Population Density	Wind	Depth
Maximum DHW		0.14***	0.14***	0.22***	-0.07	-0.10*	0.14***	-0.14***
Observed DHW			-0.56***	-0.71***	-0.06	-0.19***	-0.14***	0.11*
Maximum PAR Anomaly				0.59***	0.02	0.07	0.34***	-0.20***
Observed PAR Anomaly					-0.06	0.03	0.03	-0.14***
Distance From Shore						-0.21***	0.29***	0.13***
Population Density							0.01	-0.01
Wind								-0.06
Depth								

P-values for statistical significance of indicated correlation coefficients: \*\*\* p<0.01, \*\* p<0.05, \* p<0.1

**Table S8. Correlations between stressors in the Greater Antilles.**

	Maximum DHW	Observed DHW	Maximum PAR Anomaly	Observed PAR Anomaly	Distance From Shore	Population Density	Wind	Depth
Maximum DHW		0.83***	0.01	-0.03	-0.11	0.09	-0.22	0.22
Observed DHW			-0.05	-0.30**	-0.09	0.22	-0.27**	0.09
Maximum PAR Anomaly				0.23	0.03	0.12	0.23	-0.05
Observed PAR Anomaly					0.01	0.05	-0.30**	-0.01
Distance From Shore						0.30**	0.22	-0.08
Population Density							-0.08	-0.11
Wind								0.07
Depth								

P-values for statistical significance of indicated correlation coefficients: \*\*\* p<0.01, \*\* p<0.05, \* p<0.1

**Table S9. Correlations between stressors in the Southern Caribbean.**

	Maximum DHW	Observed DHW	Maximum PAR Anomaly	Observed PAR Anomaly	Distance From Shore	Population Density	Wind	Depth
Maximum DHW		0.97***	0.17	-0.54***	-0.11	-0.06	0.83***	0.09
Observed DHW			0.20	-0.54***	-0.09	-0.11	0.77***	0.06
Maximum PAR Anomaly				0.21	0.19	0.08	-0.01	0.00
Observed PAR Anomaly					-0.06	0.41***	-0.64***	-0.07
Distance From Shore						-0.19	0.07	0.01
Population Density							0.07	-0.13
Wind								0.09
Depth								

P-values for statistical significance of indicated correlation coefficients: \*\*\* p<0.01, \*\* p<0.05, \* p<0.1

**Table S10. Correlations between stressors in the Southwestern Caribbean.**

	Maximum DHW	Observed DHW	Maximum PAR Anomaly	Observed PAR Anomaly	Distance From Shore	Population Density	Wind	Depth
Maximum DHW		0.31***	-0.01	0.30***	0.00	0.41***	-0.41***	-0.19
Observed DHW			-0.38***	-0.07	0.00	0.18	-0.51***	-0.19
Maximum PAR Anomaly				0.51***	-0.27***	-0.42***	-0.03	-0.17
Observed PAR Anomaly					-0.10	-0.26***	-0.26***	-0.17
Distance From Shore						-0.01	0.07	0.21*
Population Density							0.14	0.16
Wind								0.44***
Depth								

P-values for statistical significance of indicated correlation coefficients: \*\*\* p<0.01, \*\* p<0.05, \* p<0.1

**Table S11. Correlations between stressors in the Floridian region.**

	Maximum DHW	Observed DHW	Maximum PAR Anomaly	Observed PAR Anomaly	Distance From Shore	Population Density	Wind	Depth
Maximum DHW		0.31***	-0.09	-0.09	-0.11	-0.02	0.08	0.04
Observed DHW			-0.11	-0.25***	0.06	-0.05	-0.09	0.01
Maximum PAR Anomaly				0.23***	-0.26***	0.73***	-0.73***	-0.10
Observed PAR Anomaly					-0.19	0.34***	-0.22***	0.13
Distance From Shore						-0.37***	0.54***	0.03
Population Density							-0.68***	0.13
Wind								-0.15**
Depth								

P-values for statistical significance of indicated correlation coefficients: \*\*\* p<0.01, \*\* p<0.05, \* p<0.1

## APPENDIX B: Chapter 3

### 9.1 Data for Case Study

A map is provided in Figure S1 as a spatial reference for various geographic features of interest in California.

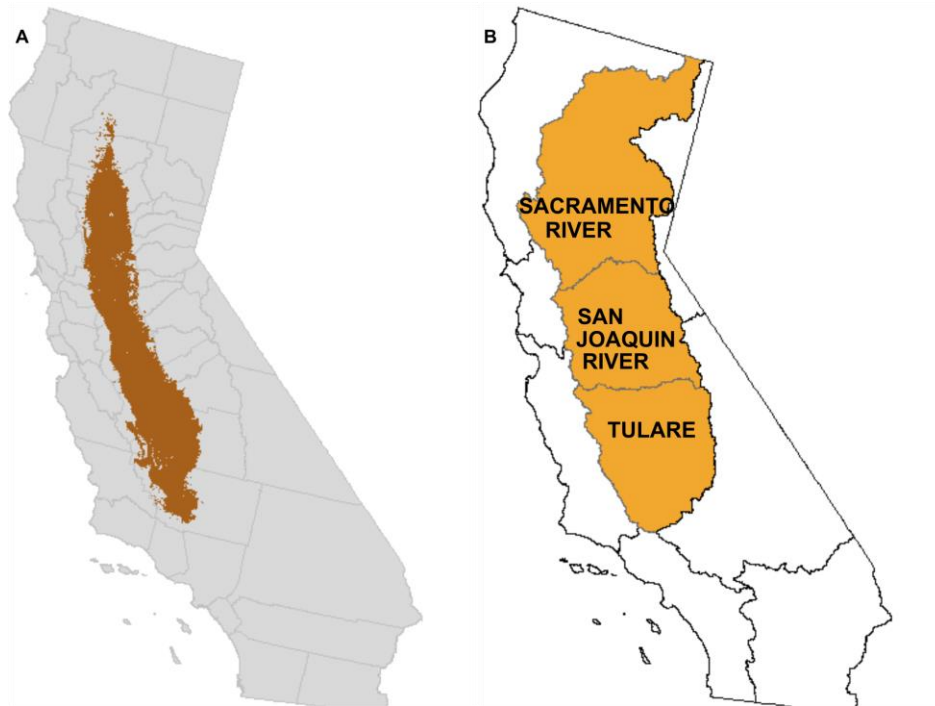


**Figure S1. Cropped area in the Central Valley of California (A) and major relevant hydrologic regions in California (B).**

#### 9.1.1 NASS County Commissioner Data

Table A1 reports the crops assessed in this study. These 20 crops correspond to those crops with highest revenues as outlined in the statewide 2013 crop report [1]. Together, they correspond to over 95% of the revenues generated by the non-livestock agricultural sector.

Yields and prices are obtained from the NASS County Agricultural Commissioner's Data [2]. These data are published yearly and report statewide crop yields and prices at county-level resolution. In Table S2, the crop names used in this study are paired with their corresponding NASS names and commodity codes.

If multiple NASS crops are listed for a single study crop, we calculate the weighted average of the yields and prices.

If no yield or price data was available for a particular crop in a particular county, the values reported for “Sum of Others” was used in its stead. For a single crop (Walnuts) no values were available for “Sum of Others,” and instead we substituted state averages. All reported values are for 2013.

Alongside the crop in Table S1 we display the threshold and slope parameters for the yield reduction model (4). These parameters are collected from a number of studies carried out in the mid-twentieth century that were first summarized in Maas and Hoffman [3] and subsequently updated and republished. While presented in numerous publications in varying degrees of completeness, we found no discrepancies between the values reported in the different articles and reports [3-6]. Where possible, we use values in more recent publications. For three crops (walnuts, pistachios, and oranges), no direct threshold and slope parameters were given. Rather, they were categorized into one of several tolerance groupings (sensitive, moderately sensitive, moderately tolerant, and tolerant). For each of these categories, a representative threshold and slope parameter were chosen based on graphical representations reported in Hoffman [6] and other publications.

In order to use the agricultural county commissioner’s data, we first match the 20 study crops with NASS commodities codes [2]. The crops corresponded to NASS commodities with a ‘one-to-many’ relationship. Table S2 reports the mapping used in this study. Once mapped, we develop county and state level datasets containing information on yield, prices, and revenue per acre. These datasets inform key parameters in our study.

### *9.1.2 NASS Cropland Data Layer:*

NASS produces the Cropland Data Layer (CDL) satellite-based crop classifier [7]. The CDL distinguishes between 132 distinct crops with an overall accuracy rating of 84.9%. Table S3 relates crops in this study to CDL object identifiers and provides the producer and user accuracy for each crop. Producer accuracy

represents the number of ground-truth points accurately classified in generating the map, representing the likelihood that a random crop will be correctly rendered. User accuracy represents the likelihood that a given pixel on the map is actually what is found in the field. These ground-truth points are used to remove bias from the estimates, as discussed previously. All reported values are for 2014.

### *9.1.3 Gridded Soil Survey Geographic (gSSURGO) Database*

SSURGO is a nationwide dataset developed from the National Cooperative Soil Survey (NCSS). NCSS is a collaboration between federal, state, and private institutions with the goal of disseminating information about the state of soils across the country led by the U.S. Department of Agriculture (USDA) and the National Resource Conservation Service (NRCS). SSURGO map scale is between 1:12,000 and 1:63,360 and is the most detailed soil survey product available from the program [8].

The FY2015 gSSURGO database is a December 1, 2014, snapshot of the soil data mart database released in the Environmental Systems Research Institute, Inc. (ESRI) file geodatabase format at the state level. Vector data are released as map units, including the 456,249 map units spanning California that have a median area of 0.12 km<sup>2</sup> and average area of 0.92 km<sup>2</sup>. Vector data is converted to raster format to improve computational performance.

Electrical conductivity (EC) is measured at the ‘component’ level, a unit of soil classification smaller than map units. No spatial data are available for components, and so to connect the EC measurements to a specific geographic location each component is first referenced to the map unit in which it is contained. Next, the map unit EC value is calculated by taking the weighted average (weights determined by area) of the component level data, then calculating a second weighted average through the A and B soil horizons. In order to arrive at the EC estimate for the component, SSURGO aggregates many local measurements. While the individual measurements are not released, a reported representative value is accompanied by the top and bottom of the observed range, allowing us to account for uncertainty in the salinity estimate (Figure S2).

The SSURGO dataset is derived from field measurements and is continuously updated to reflect changing soil conditions. The labor intensity of measuring soil quality parameters and spatial extent of the dataset limit the frequency of resurveying, with most measurements occurring in regions with the greatest rate of soil quality change. To account for uncertainty in soil quality estimates, we vary the SSURGO data in a sensitivity analysis in Section 9.3.

**Table S1. Crop Salt Tolerance Parameters.**

Crop	Threshold	Slope	Source
Almonds	1.5	19.0	Hoffman 2010
Grapes	1.5	9.6	Hoffman 2010
Strawberries	1.0	33.0	Maas 1993
Walnuts*	1.5	15.4	Hoffman 2010
Lettuce	1.3	13.0	Maas 1993
Alfalfa	2.0	7.3	Hoffman 2010
Tomatoes	2.5	9.9	Hoffman 2010
Pistachios*	3.0	7.7	Maas 1993
Broccoli	2.8	9.2	Maas 1993
Rice	3.0	12.0	Maas 1993
Oranges*	1.7	16.0	Maas 1993
Cotton	7.7	5.2	Maas 1993
Carrots	1.0	14.0	Maas 1993
Celery	1.8	6.2	Maas 1984
Peppers	1.5	14.0	Maas 1993
Lemons	1.5	12.8	Maas 1993
Peaches	1.7	21.0	Maas 1993
Wheat	6.0	7.1	Hoffman 2010
Cherries*	1.5	15.4	Maas 1993
Corn	1.7	12.0	Hoffman 2010

\*Indicates that no direct data was available. Instead category level data (tolerant, moderately tolerant, moderately sensitive, sensitive) were translated to values using graphical representations in Hoffman [6].

**Table S2. Mapping Between Study Crops and NASS Commodity Data**

Study: Name	NASS: Name	NASS: Commodity Code	2013 State Average Yield per Acre [tons]	2013 Prices [\$/ton]	2013 Revenue per acre [\$/acre]
Alfalfa	HAY ALFALFA, SEED ALFALFA	181999, 172119	3.85	227.29	875.07

Almonds	ALMONDS ALL	261999	1.12	5681.86	6363.68
Broccoli	BROCCOLI FOOD	307189,			
	SERVICE, BROCCOLI	307199,			
	FRESH MARKET,	307299,			
	BROCCOLI	307919	7.29	813.91	5929.33
	PROCESSING,				
	BROCCOLI				
	UNSPECIFIED				
Carrots	CARROTS FOOD	313189,			
	SERVICE, CARROTS	313199,			
	FRESH MARKET,	313299,			
	CARROTS	313999	23.8	250.00	5957.50
	PROCESSING,				
	CARROTS				
	UNSPECIFIED				
Celery	CELERY FOOD	316189,			
	SERVICE, CELERY	316199,			
	FRESH MARKET,	316999	36.6	433.93	15886.18
	CELERY UNSPECIFIED				
Cherries	CHERRIES SWEET	213199	2.6	3817.60	10002.11
Corn	CORN GRAIN, CORN	111991,			
	POPCORN, CORN	192999,			
	SILAGE, CORN SWEET	111992,	11.0	66.64	731.71
	ALL	323999			
Cotton	COTTON LINT PIMA,	121229,			
	COTTON LINT	121299,			
	UNSPECIFIED,	121219	0.9	2709.14	2411.13
	COTTON LINT				
	UPLAND				
Grapes	GRAPES RAISIN,	216399,			
	GRAPES TABLE,	216199,	11.2	896.62	10060.08
	GRAPES WINE	216299			
Lemons	LEMONS ALL	204999	16.5	758.06	12492.83
Lettuce	LETTUCE HEAD,	340999,			
	LETTUCE LEAF,	342999,			
	LETTUCE ROMAINE,	341999,	17.3	480.05	8314.47
	LETTUCE	339999			
	UNSPECIFIED				
Oranges	ORANGES NAVEL,	201119,			
	ORANGES	201999,			
	UNSPECIFIED,	201519	15.6	556.67	8689.62
	ORANGES VALENCIA				
Peaches	PEACHES	212399,			
	CLINGSTONE,	212199,			
	PEACHES FREESTONE,	212999	12.8	620.84	7928.13
	PEACHES				
	UNSPECIFIED				
Peppers	PEPPERS BELL,	363999,			
	PEPPERS CHILI HOT	364999	18.0	735.28	13205.63
Pistachios	PISTACHIOS	268079	1.2	4695.91	5822.93
Rice	RICE MILLING, RICE	106199,			
	SEED, RICE WILD	171069,	3.2	418.69	1331.43
		198199			
Strawberries	BERRIES	237199,			
	STRAWBERRIES	237299,	29.8	1867.59	55728.89
	FRESH MARKET,	237999			

	BERRIES				
	STRAWBERRIES				
	PROCESSING, BERRIES				
	STRAWBERRIES				
	UNSPECIFIED				
Tomatoes	TOMATOES FRESH	378199,			
	MARKET, TOMATOES	378299,			
	PROCESSING,	378999	36.4	96.90	3528.13
	TOMATOES				
	UNSPECIFIED				
Walnuts	WALNUTS ENGLISH	263999	1.9	3432.90	6316.54
Wheat	WHEAT ALL, WHEAT	101999,			
	SEED	171019	2.4	264.11	639.15

#### 9.1.4 Computing

The total analysis was performed in 20 hours of processing time using a combination of Python 2.7.11, ESRI ArcGIS 10.2.2 accessed through ArcPy, NumPy 1.10.1 [9], and IPython 4.0.1 [10]. All plots were made using Matplotlib 1.5.0 [11]. Regression analyses were performed in R 3.1.1 using mgcv package 1.8.0 [12]. The analysis was run on a desktop computer with an Intel i7 3.4 GHz processor with 16GB of installed RAM.

## 9.2 Bias Removal

The approaches taken in both models utilized in the main paper make use of field-scale estimates of crop type sourced from a satellite-based crop classifier and combines this estimated crop type with soil maps of salinity and region-level information on management practices, crop water-use, yields, and prices. Small differences in classifier accuracy between different crop types can introduce a large bias into the estimate, even if the classifier on aggregate produces highly accurate results [13]. This bias can be systematically removed using accurate, though sparse, ground measurements to correct widely available, though biased, satellite classification. While several approaches for removing bias have been discussed in the literature, in this study we make use of a direct estimator due its straightforward implementation and relative efficiency [14].

To remove bias, a confusion matrix is constructed from ground truth data that indicates both the probability that a pixel is correctly classified and the probability that a pixel is misclassified as each of the other possible categories. From this, an arbitrary value  $Z_{p,c}$  calculated using crop-specific information is compiled into a pixel estimate of the same quantity  $Z_p$  by using the following transformation:

$$Z_p = \sum_c P_{c^*,c} Z_{p,c} \quad (1)$$

where the subscript  $c$  indicates crop, the subscript  $p$  indexes the pixel, and  $P_{c^*,c}$  is the probability that given the classifier indicates that a pixel contains a particular crop  $c^*$ , the pixel actually contains crop  $c$ .

### 9.3 Uncertainty Analysis

The key parameter in our study is the total revenues lost due to salinity, calculated at \$3.7 billion annually. There are key uncertainties in this calculation which should be tested in order to assess the robustness of our estimate. First, the spatially resolved 30 m pixel salinity data generated by the SSURGO project contains considerable smoothing. A single point estimate of soil electrical conductivity is generated for each ‘map unit.’ Map units have a median area of 0.12 km<sup>2</sup>, meaning that this median map unit is comprised of 4000 pixels each reporting the same value of salinity. Since salinity as a process can vary in relatively short distances, this smoothing introduces uncertainty into our estimate.

SSURGO reports a low and high value for each parameter alongside the representative value. We assess the uncertainty parametrically by repeating the analysis using ‘low’, ‘medium’, and ‘high’ salinity values. The medium salinity value scenario is identical to the analysis in the main paper, while for the low and high analyses we apply the low and high electrical conductivity values respectively.

Additional uncertainty arises from county level estimates of prices and yields. While likely very accurate for the 2013 crop year, it is possible that this crop year was an anomaly in either yields or prices for some of the crops in the study. To assess the likelihood of anomalies driving our result, we collect ten years of

crop data (2004 – 2013) and calculate the standard error on the trendline [2]. Specifically, we calculate the following regressions for each crop:

$$p_i = \beta_0 + \beta_1 \cdot Year_i + \varepsilon_i \quad (2)$$

$$y_i = \beta_0 + \beta_1 \cdot Year_i + \varepsilon_i \quad (3)$$

where each observation  $i$  corresponds to a single year's data. The dependent variables,  $p_i$  and  $y_i$ , are state average prices and yields. The standard error of prices and yields is calculated by taking the root mean squared error of the residual.

As with salinity, we calculate a 'low', 'medium', and 'high' scenario with both prices and yields. The medium scenario is calculated as in the main paper, while the low and high scenarios are calculated by subtracting and adding the de-trended standard error to the 2013 estimates, respectively.

In addition to rerunning the analysis with each individual parameter set at its low, medium, and high values, we perform a final analysis with all parameters set at their low, medium, and high values. While setting all values simultaneously low or high is likely to be unduly pessimistic or optimistic, it is a useful step in understanding if total uncertainty is driven primarily by a single parameter or by the combination of parameters.

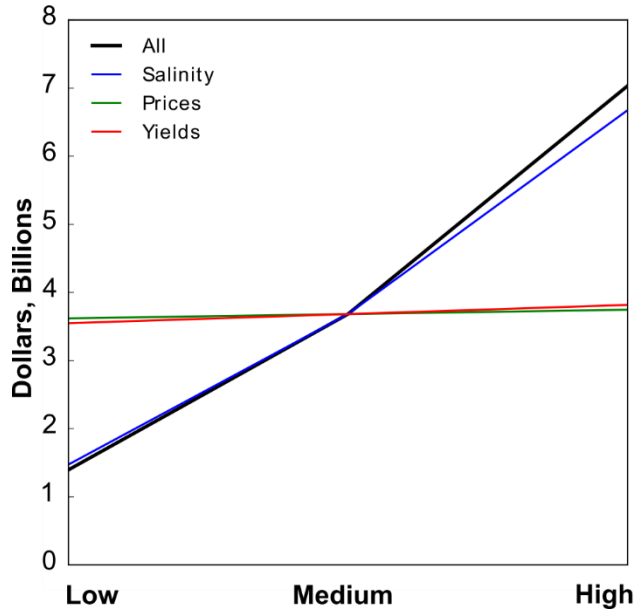


**Figure S2. Revenue losses under low, medium, and high scenario cases for each parameter used in this study. For each line, the other variables are held at their best guess, with the exception of the ‘All’ line, in which each parameter is set at low, medium, and high.**

In Figure S2, the low, medium, and high scenarios are reported. The year to year variation of prices and yields makes little impact on the final analysis, as indicated by the relatively similar estimates of revenue loss. Uncertainty in the salinity data, on the other hand, drives a relatively large variation. The low and high scenarios for salinity correspond to estimates of revenue lost of \$1.5 and \$6.7 billion, making up the majority of the \$1.7 - \$7.0 billion range.

#### **9.4 Performance of Crop Classifier**

The USGS conducts an internal assessment of its crop classifier by collecting ground truth estimates of actual cropping patterns and comparing them to predictions from the crop classifier. The accuracy can be quantified by using producer and consumer accuracy. User accuracy is the likelihood that, given a crop is classified in a pixel as  $c$ , it is actually  $c$  in the field. Producer accuracy is the likelihood that, given a crop is actually  $c$  in the field, it is classified correctly as  $c$  in the prediction. Producer and consumer accuracies for the 2014 CDL for California are reported in Table Se. Most crops have relatively high accuracies,

though, vegetable and fruit crops (e.g. broccoli, lettuce, strawberries) are identified less consistently than the field and tree crops. Celery in particular, is never selected by the classifier, and is thus omitted from this analysis.

**Table S3. Accuracy of Remotely Sensed Land Use Data**

Crop	CDL Crop Name	Producer's Accuracy	User's Accuracy
Alfalfa	Alfalfa	94.1%	90.7%
Almonds	Almonds	88.5%	90.7%
Broccoli	Broccoli	30.0%	61.8%
Carrots	Carrots	52.6%	72.6%
Celery	Celery	0%	NA
Cherries	Cherries	32.8%	54.3%
Corn	Corn, Sweet Corn	85.2% / 44.1%	86.8% / 43.0%
Cotton	Cotton	96.9%	92.5%
Grapes	Grapes	92.0%	86.4%
Lemons	Citrus	88.7%	90.9%
Lettuce	Lettuce	54.2%	58.1%
Oranges	Oranges	78.7%	81.3%
Peaches	Peaches	84.2%	45.2%
Peppers	Peppers	33.0%	62.9%
Pistachios	Pistachios	72.1%	85.3%
Rice	Rice	99.3%	99.3%
Strawberries	Strawberries	39.1%	56.6%
Tomatoes	Tomatoes	90.5%	87.7%
Walnuts	Walnuts	83.4%	84.2%
Wheat	Durum Wheat, Spring Wheat, Winter Wheat	83.4% / 67.5% / 73.6%	81.7% / 75.9% / 75.9%

All estimates in the study are unbiased using information from Table S3 as discussed in Methods.

In order to test the performance of the USGS crop classifier, we compare unbiased land estimates from the crop classifier with the land estimates from the NASS county commissioner data (Figure S3). If the ratio of these two values is above 1.0, the crop classifier is likely overestimating the representation of a particular crop, while if below 1.0 it is likely underestimating its representation. Even after removing bias, seven crops are not estimated within 30% of their true value. These crops are broccoli, carrots, celery, corn, lettuce, peaches and peppers. Comparing with Table S3, these crops generally report lower

accuracies than those crops more accurately identified. We aggregate these crops into a single category, Other High Uncertainty Crops (OHUC), when reporting their values in the main manuscript.

Important to note is the CDL is developed for crop year 2014 while the NASS data corresponds to 2013, meaning that some of the variation noted in Figure S3 may be due to temporal mismatch.

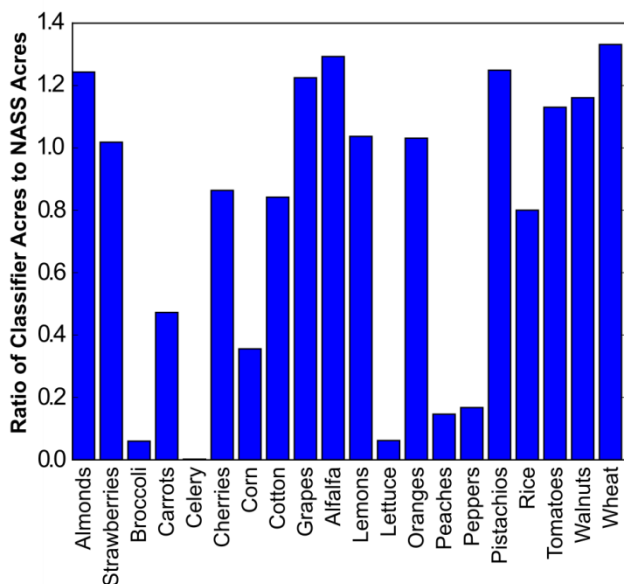


**Figure S3. Ratio of the acres predicted by the crop classifier compared with acres reported in NASS agricultural commissioner’s data. Values above one indicate that the classifier is over-predicting crop representation, while values below one indicate the classifier is under-predicting crop representation. All values are unbiased using crop assessment reported in table D1.**

## 9.5 Grower Adaptation

We observe that growers are likely modifying their crop choices in accordance with extant salinity values. In Figure S4B, crop salt tolerance is plotted spatially. It is quantified as  $Y_{50}$ , or the salinity value at which yields are expected to be 50% of maximum levels. Figure S4B shows that in the Central Valley, crop salt tolerance is qualitatively higher in the southern and western regions where salinity is elevated, suggesting that salinity may be a factor in crop selection. In the northern and southern extremes of the state crop salinity tolerance values are also high, driven largely by the large amounts of alfalfa grown in these regions.

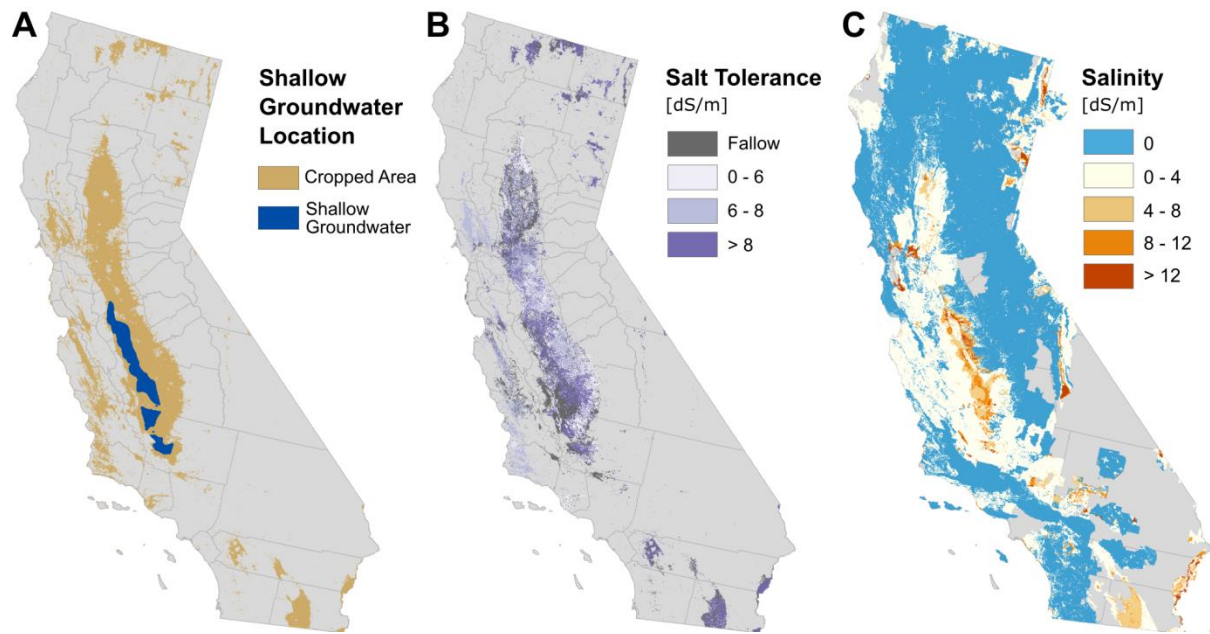


**Figure S4. (A) Location of areas with a shallow groundwater table, (B) salt tolerance values, (C) and extant salinity levels. Salt tolerance is quantified as Y50, or the salinity at which yield is expected to be reduced to 50%.**

We observe that the average soil salinity by crop and salt tolerance levels are positively correlated, while crop salt tolerance levels and marginal revenues are negatively correlated (Figure S5). These two facts illustrate the tradeoff experienced by agricultural producers – they can either produce lower value, high tolerance crops with high yields or high value, low tolerance crops with reduced yields.

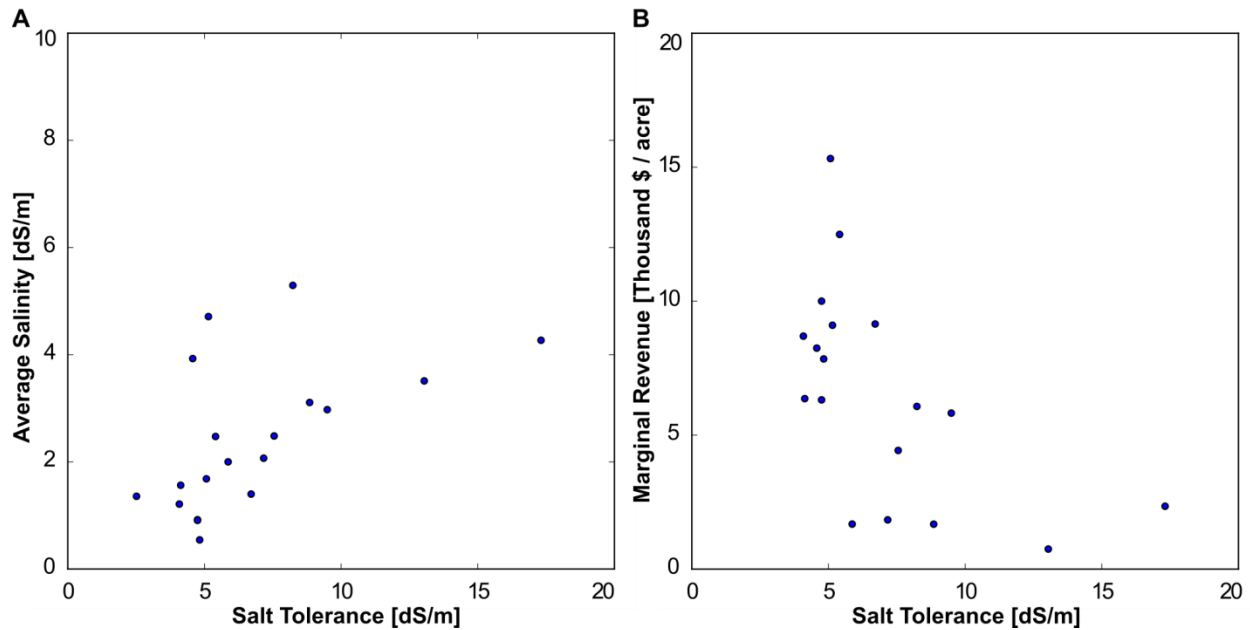


**Figure S5. (A) Salt tolerance vs average salinity for each crop and (B) salt tolerance values vs marginal revenue for each crop. Average salinity represents the mean salinity value across all pixels for each crop in the study. Marginal revenues are state averages.**

## 9.6 Estimating Calorie Losses Associated with Soil Salinization in California

While caloric losses are not of primary interest in the specialty crop dominated Californian agriculture system, we demonstrate here that the methods applied in the main paper can be used to analyze the loss in human nutrition as a result of land degradation.

Caloric losses were determined by multiplying the estimates of lost yield at the pixel level by the energy density in calories per ton for each crop. Energy density estimates were sourced from the FAO report on Food Composition for International Use [15]. Certain crops, such as Alfalfa and Cotton, are not typically consumed and are therefore assigned a caloric density of 0 calories·gram<sup>-1</sup> even though, in the case of alfalfa, the crop may contribute indirectly to human caloric intake.

We find that the majority of the calories lost are associated almonds and rice, due to a combination of their high acreage and high caloric density (Figure S6). The Other High Uncertainty Crops (OHUC)

category also features prominently, driven primarily by the inclusion of corn. Aggregate losses across all crops total 6.0 million person-years, assuming a 2000 calorie·day<sup>-1</sup> requirement.

We find that different crops are driving aggregate caloric losses than those that are driving aggregate revenue losses. Figure S6A makes this difference clear by plotting losses for each crop. Those crops towards the lower right quadrant have high calorie losses but low revenue losses (e.g. rice) while those in the upper left quadrant (e.g. strawberries) have relatively higher revenue losses in comparison with their calorie losses. Almonds, due largely to their large gross acreage, lead in both metrics.

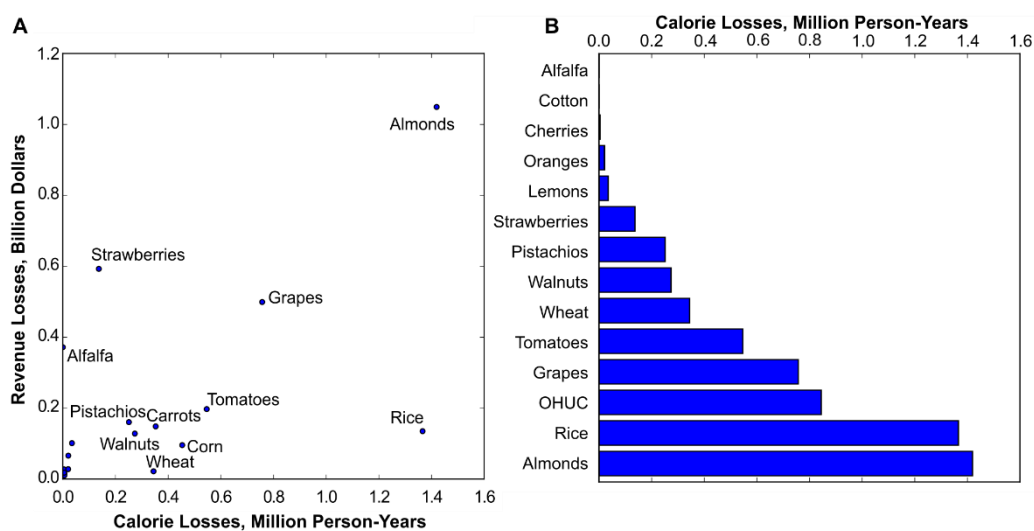


**Figure S6. (A) Calorie loss revenue loss tradeoff and (B) calorie losses by crop.**

## 9.7 Statistical Analysis

We performed a brief statistical analysis in order to determine the correlation between salinity and four parameters – crop marginal value, crop salt tolerance, estimated yield reduction, and estimated revenue losses per acre (Table S4). The goal of the analysis was to assess the relative magnitude of the correlation between salinity and the parameters of interest as well as test the correlation for significance.

The salinity data used in other parts of this study is stored in raster format to speed computation. It is, however, originally released as a vector file, with 456,249 individual polygons spanning California. In this section we revert to the polygon format so as to avoid artificially inflating our sample size. Our four

parameters of interest are each spatially averaged within the polygon to construct the dependent variable. After removing those polygons with no crops, we are left with a sample size of 296,987 data points.

Spatial data often violate the independent and identically distributed (IID) assumption of ordinary least squares (OLS) due to correlation in the error term. While the estimated OLS coefficients remain unbiased, inference testing becomes inappropriate as the standard errors are downward biased. Common approaches for handling this issue (e.g. generalized least squares, spatial lag model, spatial error model, spatial durbin model) typically require the estimation of the correlation structure codified in a spatial weights matrix  $W_{ij}$ . This matrix, if stored in a dense format, has size  $n \times n$  where  $n$  is the number of data points. While size constraints can be lessened by imposing cutoffs based on distance and storing data in a sparse format, we found it difficult to construct a weighting matrix with a reasonable structure given our large sample size.

Instead, we fit a generalized additive model (GAM) in an effort to control for spatial location. GAMs are non-parametric models that are used to estimate the effect of linearly independent covariates on a dependent variable. Since GAMs avoid specifying the parametric form of the regressors they are able capture complex nonlinear behavior.

We perform four regressions, each fitting on the four parameters of interest while controlling for location. Latitude and longitude are smoothed together using a thin plate spline regression, the parameters of which are fitted using generalized cross validation. The general form is given in Equation 4, where  $y_i$  represents a single observation  $i$  of one of the four parameters of interest and  $S_i^S$  is soil salinity.

$$y_i = \beta_0 + \beta_1 S_i^S + f(Lat, Lon) + \varepsilon_i \quad (4)$$

We find that both the  $\beta_0$  and the  $\beta_1$  parameter in each of the four regressions are highly significant. While we are primarily interested in the magnitude and significance of the effect of salinity ( $\beta_1$ ), the intercept ( $\beta_0$ ) is also informative since it can be interpreted as the estimated value of the parameter when there is no salinity present in the soils.

Regressing marginal revenue [\$/acre] on soil salinity [dS/m] results in a positive intercept of \$6245.44 and a negative slope of -\$304.46. Marginal revenue is calculated as simply the observed price per ton multiplied by the observed yield per acre, both resolved at the county level. The intercept indicates that crops being grown at locations with zero salinity have an expected value of \$6245.44, and that with each increasing unit salinity, the marginal value decreases by \$304.46. This effect is likely due to the observed trend that crops with higher marginal revenues exhibit lower salt tolerance (figure E2b).

Salt tolerance is calculated by solving for the salinity value at which crop yields would be reduced 50%. Regressing salt tolerance [dS/m] on salinity [dS/m] results in an intercept of 7.47 and a slope of 0.034. The positive slope indicates that, as salinity increases, farmers are observed planting more salt tolerant crop species. While the effect is statistically significant the slope is low in magnitude.

Relative yield and revenue losses are both estimated (not observed) parameters that take salinity as direct inputs (Equations 2 and 6 in Chapter 3), making it unsurprising that the regressions report statistically significant correlations. The slope in the relative yield [%] equation is negative, indicating that for each unit increase in soil salinity relative yield decreases by 5.38 percentage points. Revenue losses increase with soil salinity, registering a \$364.90 increase per unit increase in soil salinity. The intercepts of both regressions indicate a slight misspecification, with zero salinity registering 101.2% yield and -\$25.32 revenue losses. This misspecification is likely a result of the truncated nature of salinity response in Equation 2 in Chapter 3, and is relatively small in magnitude.

**Table S4. Regression Results**

	<b>Marginal Revenue</b>	<b>Salt Tolerance</b>	<b>Relative Yield</b>	<b>Revenue Losses</b>
<b>Salinity Coefficient</b>	-304.46*** (3.87)	0.034*** (0.0012)	-5.38*** (0.0048)	364.9*** (1.81)
<b>Intercept</b>	6245.44*** (10.14)	7.47*** (0.0031)	101.2*** (0.0126)	-25.32*** (4.76)
<b>Observations</b>	296987	296987	296987	296987
<b>Adjusted R<sup>2</sup></b>	0.53	0.55	0.853	0.186

## 9.8 Symbols

$Z$ :	Example parameter [unitless]
$P$ :	Probability that classifier is correct [unitless]
$Y^L$ :	Yield losses [tons / acre]
$F$ :	Fraction of maximum yield [unitless]
$Y^M$ :	Theoretical maximum yield [tons / acre]
$b$ :	Crop salt tolerance slope parameter [(dS/m) <sup>-1</sup> ]
$S^S$ :	Soil salinity [dS/m]
$a$ :	Crop salt tolerance threshold parameter [dS/m]
$Y^{TL}$ :	Total yield losses [tons]
$k$ :	Acre to pixel conversion factor [acre / pixel]
$R^L$ :	Revenue losses [\$ / acre]
$p$ :	Prices [\$ / ton]
$R^{TL}$ :	Total revenue losses [\$]
$A$ :	Crop acreage [acres]
$c^*$ :	Predicted crop
$c$ :	Observed crop
$p$ :	Pixel-scale measurement
$r$ :	Region-scale measurement
$0$ :	Initial value

## References

- [1] National Agricultural Statistics Service, U.S. Department of Agriculture 2015 *California Agricultural Statistics 2013 Annual Bulletin*
- [2] National Agricultural Statistics Service, U.S. Department of Agriculture 2013 County Ag Commissioners' Data Listing [http://www.nass.usda.gov/Statistics\\_by\\_State/California/Publications/AgComm/Detail](http://www.nass.usda.gov/Statistics_by_State/California/Publications/AgComm/Detail) (accessed August 15, 2015).
- [3] Maas E V, and Hoffman G J 1977 Crop salt tolerance - current assessment *J. Irrig. Drain. Div. ASCE* **103** 115-34.
- [4] Maas E 1984 Crop tolerance *California Agriculture* **38** 20-21.
- [5] Maas E 1993 Testing crops for salinity tolerance *Proc. Workshop on Adaptation of Plants to Soil Stresses* p 247.
- [6] Hoffman G J 2010 *Salt Tolerance of Crops in the Southern Sacramento-San Joaquin Delta*
- [7] National Agricultural Statistics Service, U.S. Department of Agriculture 2014 CropScape cropland data layer. <http://nassgeodata.gmu.edu/CropScape> (accessed September 2, 2015)
- [8] Natural Resources Conservation Service, U.S. Department of Agriculture 2015 Soil Survey Geographic (SSURGO) Database <http://sdmdataaccess.nrcs.usda.gov/> (accessed September 10, 2015)
- [9] Van Der Walt S, Colbert S C and Varoquaux G 2011 The NumPy array: a structure for efficient numerical computation *Comput. Sci. Eng.* **13** 22-30
- [10] Pérez F and Granger B E 2007 IPython: a system for interactive scientific computing *Comput. Sci. Eng.* **9** 21-9
- [11] Hunter J D 2007 Matplotlib: A 2D graphics environment *Comput. Sci. Eng* **9** 90-5
- [12] Wood S N 2011 Fast stable restricted maximum likelihood and marginal likelihood estimation of semiparametric generalized linear models *J. Roy. Stat. Soc. B.* **73** 3-36
- [13] Czaplewski R L 1992 Misclassification bias in areal estimates *Photogrammetric Engineering and Remote Sensing* **58** 189-92
- [14] Gallego F J 2004 Remote sensing and land cover area estimation. *International Journal of Remote Sensing* **25** 3019-47
- [15] Chatfield C 1949 Food composition tables for international use (Rome, Italy: Food and Agriculture Organization of the United Nations)

## APPENDIX C: Chapter 4

**Table S1. Tolerance and marginal revenue of crop categories. Tolerance is defined according to the salinity at which yields are estimated to be reduced by 50%, and marginal revenue is the estimated revenue per acre.**

	Tolerance	Marginal Revenue
Nuts, Sensitive	4.28	5891.46
Other Tree	4.68	10161.70
Nuts, Tolerant	9.49	3075.09
Grain	7.17	1536.35
Feed (Hay)	8.85	1065.16
Field	17.32	2305.19
Vineyard	6.71	6978.27
Veggie, Sensitive	2.52	61033.45
Veggie	5.16	10686.22
Veggie, Tolerant	7.73	5189.98

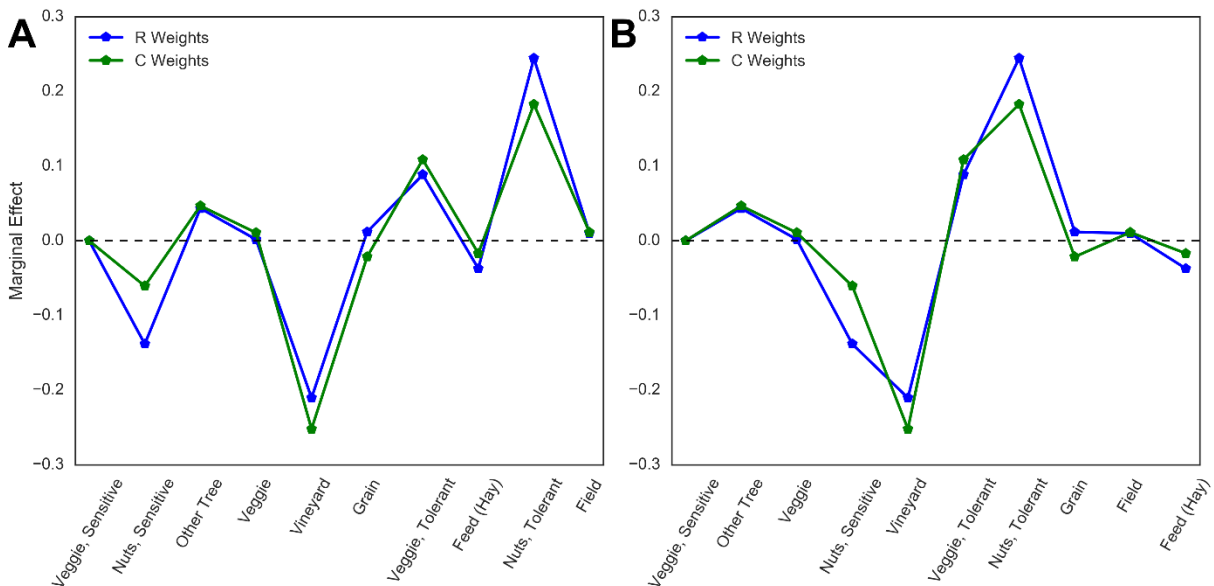


**Figure S1 Marginal effects for crop groups organized by increasing salinity tolerance (A) and decreasing marginal revenue reduction (B). Marginal revenue reduction is calculated by multiplying the slope parameter from Equation 9 by the price and yield of the each crop group. For both graphs, a positive slope indicates that the regression results agree with the agronomic data.**

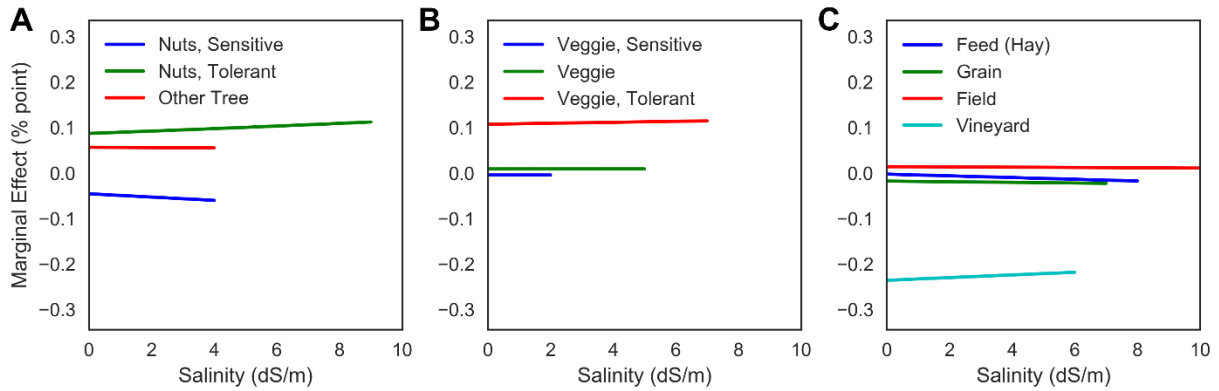


**Figure S2. Marginal effects across salinity domains for tree crops (A), vegetables (B), and other crops (C). Marginal effects are estimated by parametrically setting salinity according to values in the x-axis and assigning all other variables their mean value. Lines are plotted from 0 to the Yield<sup>Rel,50</sup> (the salinity value at which yields are reduced by half) of each crop.**

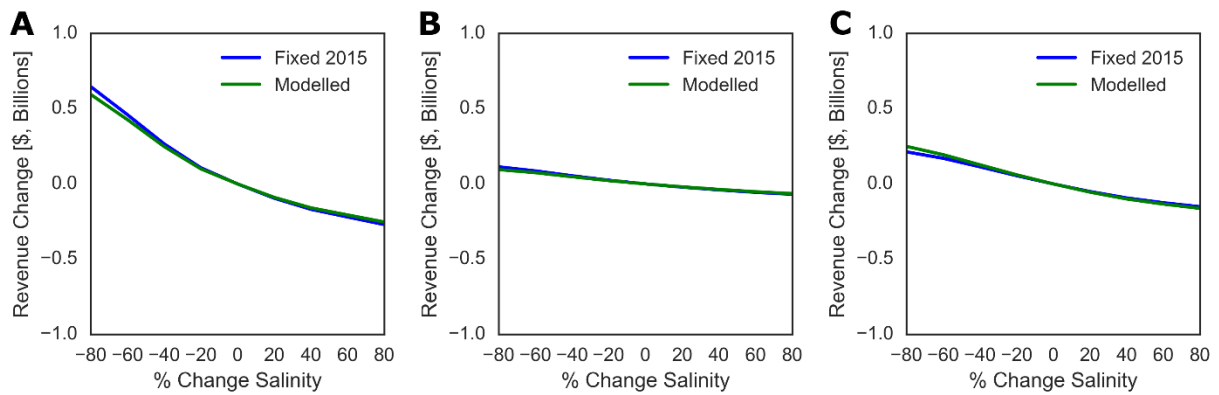


**Figure S3 Policy analysis for tree (A), vegetable (B) and other (C) crop clusters. Clusters are defined as in Figure S2.**

**Table S2 Average Fractional Coverage of Crop Groups.**

Crop Group	Average Fractional Coverage
Nuts, Sensitive	0.3455
Nuts, Tolerant	0.0560
Other Tree	0.0977
Feed (Hay)	0.1964
Grain	0.0774
Field	0.0220
Vineyard	0.1245
Veggie, Sensitive	0.0002
Veggie	0.0181
Veggie, Tolerant	0.0622

## APPENDIX D: Chapter 5

### 11.1 Air Emission Damage Analysis

In order to quantify public costs we value the damages associated with additional energy use, arriving at a value with units [\$/m<sup>3</sup>] or [\$/acre-ft]. We quantify the damages for three hypothetical systems – (1) solar powered, grid supplemented thermal desalination (ST); (2) gas powered, grid supplemented thermal desalination (GT); and (3) grid powered reverse osmosis (RO). The two thermal systems are assumed to use 125 MJ / m<sup>3</sup> for driving the desalination process and 1.5 kwh / m<sup>3</sup> of auxiliary grid electricity. The reverse osmosis system is assumed to be powered by 5 kwh / m<sup>3</sup> of grid electricity. In this study we focus on four key air pollutants: SO<sub>2</sub>, NO<sub>x</sub>, PM 2.5 (criteria air pollutants) and CO<sub>2</sub>.

The first step of the valuation methodology is to quantify the emissions associated with unit energy use. For grid electricity, we consider in state generation as well as imports from other regions. California generates roughly 66% of its energy use in-state, while 13% come from the northwest region (Alberta, British Columbia, Idaho, Montana, Oregon, South Dakota, Washington, and Wyoming) and 21% comes from the southwest region (Arizona, Baja California, Colorado, New Mexico, Nevada, Texas, and Utah)[1]. We assume each plant contributes to emissions in proportion to its share of annual generation by using a series of weights (Equations 1 and 2). Generation from out of country sources (Alberta and British Columbia) are omitted due to their relatively small contribution and limits in data availability.

$$EF_{i,p}^{Cal} = p_i \cdot EF_{i,p} \quad (1)$$

$$p_i = f_r \cdot \frac{G_i}{G_r} \quad (2)$$

In Equation 1,  $EF_{i,p}^{Cal}$  is the California specific emission factor which indicates the additional quantity of pollutant (subscript  $p$ ) is emitted at a particular plant (subscript  $i$ ) given an additional unit of energy used in California. This is calculated by multiplying the plant specific emission factor  $EF_{i,p}$  by the share of California's consumption produced at plant  $i$ ,  $p_i$ . The share of generation ( $p_i$ ) is calculated in Equation 2,

where  $G_i$  is the generation that occurs at plant  $i$ ,  $G_r$  is the generation that occurs in region  $r$ , and  $f_r$  is the fraction of generation in region  $r$  that is exported to California. We use plant data for all plants in states within the northwest, southwest, and Californian regions.

While annual generation and emission factors for  $\text{NO}_x$ ,  $\text{SO}_2$ , and  $\text{CO}_2$  are all available through CEMS, PM 2.5 is not included in this program. Data is instead incorporated from US EPA National Emissions Inventory (NEI)[2]. NEI reports gross emissions in tons at three year intervals. We acquire separate data for biomass, coal, natural gas, and oil at the state level for 2011. The gross emissions are divided by the total generation of each plant type in each state to estimate the emission rate. Once the emission rate for each plant is determined, the weighting structure specified in Equations 1 and 2 are applied.

In addition to grid emission, emissions from local natural gas generation for the GT system must be calculated. We estimate these emissions by using the US EPA AP-42 Compilation of Air Pollution Emission Factors, which reports that 120,000 lb / million standard cubic feet (mscf) of  $\text{CO}_2$ , 7.6 lb / mscf PM, 0.6 lb / mscf  $\text{SO}_2$ , 100 lb / mscf  $\text{NO}_x$  are emitted by small boilers in the generation process [3].

The second step in valuation is converting emissions to damages. For  $\text{CO}_2$ , a social cost of carbon of \$36 / metric ton (2007 dollars) is applied. For the three criteria air pollutants, damages depend on the location in which the pollutants are emitted. The emission rates are aggregated from the plant to the county level, and damages rates from the Air Pollution Emission Experiments and Policy (APEEP) model are applied [4]. APEEP quantifies human health impacts from air pollutants based on where the pollutants are emitted – areas with high population density report more aggregate damages than sparsely populated zones.

Grid emissions therefore have constant damages, since the emissions profile is identical regardless of the location of the desalination unit. For the GT system, however, the location of the desalination system is important. The closer the emissions are to population centers, the greater the estimate damages. Table S1 shows the magnitude of damages per unit of water treated for each system, with a range reported for the

GT system depending on which county the unit is located. Figure 11-1 shows the spatial variation of damages of the GT system for counties with agricultural production included in this analysis.

**Table S1. Estimated public damages of desalination in \$/acre-ft.**

[\$ / acre-ft]	Thermal (solar)	Reverse Osmosis	Thermal (natural gas)
<b>CO<sub>2</sub> Damages (county range)</b>	\$31.00	\$103.00	\$363.00
<b>SO<sub>2</sub> Damages (county range)</b>	\$21.60	\$71.90	\$22.70 (\$21.90 - \$24.40)
<b>NO<sub>x</sub> Damages (county range)</b>	\$3.15	\$10.50	\$39.90 (\$13.50 - \$102)
<b>PM 2.5 Damages (county range)</b>	\$2.75	\$9.10	\$23.40 (\$6.20 - \$62.20)
<b>Total Damages (county range)</b>	\$58.40	\$196.00	\$449.00 (\$404 - \$550)

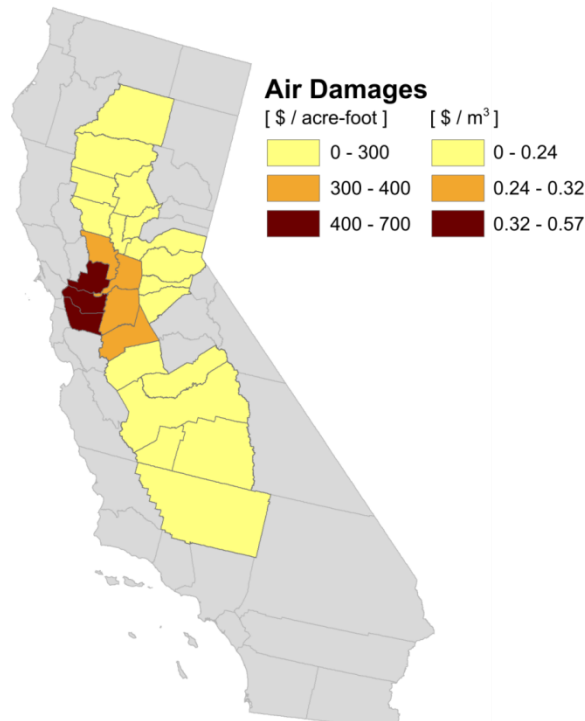


**Figure S1. Air damages from a gas-powered, thermal desalination unit varies depending on location. Damages from solar-powered, thermal desalination and grid-powered reverse osmosis (not shown) do not vary spatially.**

## 11.2 Defining Environmentally Sensitive Areas

Treating agricultural drainage at the farm level provides a mechanism for preventing harmful pollutants from arriving at environmentally sensitive areas (ESAs). This public benefit, while difficult to quantify, may be an important driver of adoption for desalination technologies. In the main text we analyze how large this public benefit would need to be in order to reap a net positive societal benefit.

ESAs are chosen using data from EPA's Healthy Watersheds Program [5]. [5] This mission of this program is to generate a series of aggregated indices that indicate watershed health, and to publish these indices in GIS format. ESAs are chosen by first selecting HUC12 watersheds that contain agriculture and artificial drainage areas, and from those selecting the watersheds with rank normalized median summer conductivity greater than 0.8. This method selects 88 watersheds which define our selected at-risk zone, together accounting for 21% of the cropped area in the study. Figure S2 shows the selected areas for the analysis.



**Figure S2. Subset of environmentally sensitive area included in the analysis.**

### 11.3 Irrigation Salinity Data

One of the key data limitations in our study is the lack of high-resolution data on the salinity of the applied water. This parameter will differ from field to field, pursuant to the grower's usage of groundwater and surface water as well as the quality of the available local sources. Additionally, the quality of each of these sources is likely to vary on annual time scales. As such, no data exists at sufficient resolution to quantify this parameter, and it must be estimated. The main analysis uses a single point estimate of water salinity of 490 mg/L. In this section we both detail the calculation that lead to this point estimate as well as discuss other possible approaches for estimating salinity of the applied irrigation water. We then use each of these estimates to analyze the sensitivity of our results to modelling choices surrounding this parameter.

#### 11.3.1 Modelling Water Salinity

The first approach for estimating the salinity of the applied water uses high-resolution data on soil salinity and converts this to implied irrigation water salinity using the same model presented in the main manuscript [6]. The conversion from soil salinity to water salinity can be accomplished through Equation 3.

$$S^W = \frac{S^S}{\frac{1}{L} + \frac{0.2}{L} \cdot \ln(L + (1 - L))e^{-5}} \quad (3)$$

In Equation C.1,  $S^W$  is the salinity of the applied water,  $S^S$  is the soil salinity, and  $L$  is the crop-specific leaching fraction.

The implied irrigation water salinity can be seen in Figure C.1A. When soils report salinity values of 0.0 mg/L total dissolved solids (TDS), the model implies that the grower is applying water with 0.0 mg/L TDS. This is likely an underestimate, as all irrigation water contains some quantity of dissolved solids. It can also be seen in Figure S3A that certain areas purport to use water salinity values of >4000ppm. These are likely overestimates which result from violations of a fundamental assumptions built into the model,

namely that the soil be well-drained. Much of the saline areas of California, however, are plagued by shallow groundwater tables (see Figure S3B).

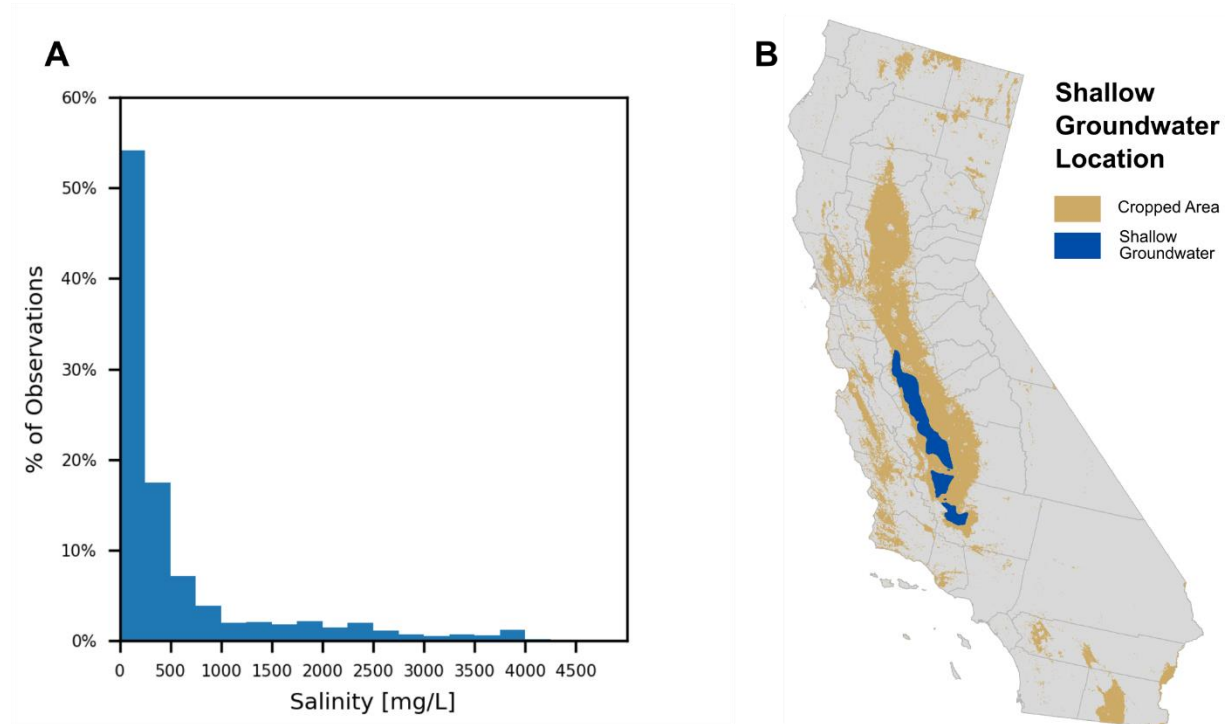


**Figure S3. Modelled salinity results (A) and locations affected by shallow groundwater table (B). The y-axis in A shows the percentage of total observations in each bin. For example, 54% of observations have salinity between 0 and 250 mg/L. Data for B from <https://water.ca.gov/drainage>.**

### 11.3.2 Averaged Modelling Results

Since the first approach likely overestimates the salinity of applied water in areas with high salinity and underestimates in areas with low salinity, an approach that avoids these shortcomings would be to use the average of the estimated modelling results outlined in the previous section. Applying this technique causes there to be a loss of spatial heterogeneity in the modelling of this parameter, but avoids error being introduced by outliers.

This can be accomplished in two ways. The first is averaging the modelling results across all pixels, which yields an estimate of TDS of 585 mg/L. Since the model is known to be inaccurate in areas with

shallow groundwater tables, however, a second approach would be to take a spatial average of all areas outside of the shallow groundwater zone (Figure S3B). This second average yields an estimate for TDS of 490 mg/L, and is the baseline approach taken in the main analysis.

### *11.3.3 Surface Water and Groundwater Estimates*

An alternative to deriving water salinity estimates from modelling results is to use information about the salinity of available surface and groundwater. While 38% of the California's net human water use is groundwater, this number varies drastically by year and location [7]. As such, we perform a bounding analysis, calculating reasonable point estimates by assuming that farms use either only surface water or only groundwater.

The quality of surface water imports is carefully monitored and managed through the use of electrical conductivity sensors in the major import canals. The California Aqueduct and Delta-Mendota canal, which supply irrigation water to much of the San Joaquin and Tulare Lake Basins, typically report salinity values between 300 and 350 mg/L [8]. While these values represent a large portion of the surface water imports in the south, other irrigation sources may have higher levels of salinity [9]. We apply the upper side of this range (350 ppm) to represent a farmer consuming surface water.

The quality of groundwater is much more variable. The Groundwater Ambient Monitoring and Assessment (GAMA) program assesses water quality across the state and produces publications as to the state of groundwater quality [10]. In reviewing the results from three such studies in the Sacramento, Tulare, and San Joaquin Basins it was found that groundwater quality could vary between 123 and 2670  $\mu\text{S}/\text{cm}$  (78 and 1708 mg/L), though the averages for all the wells in each study were in the range of 400-500 mg/L [11-13]. Since our earlier approaches already contain estimates in the range of the averages, and in the interest of conducting as broad of a sensitivity analysis as possible, we use the upper and lower range for groundwater conductivity (78 mg/L and 1708 mg/L, respectively) as two additional approaches. It should be noted, however, that these are aggressive ranges. The upper range (1708 mg/L) in particular,

assumes that the entire state applies irrigation levels well in excess of the 1000 mg/L upper secondary maximum contaminant level (SMCL-CA) set by the state of California [13].

#### *11.3.4 Sensitivity of Results to Modelling Choices*

The salinity of the applied irrigation water enters the analysis when modelling the private benefits of improved water quality, Equation 4 in the main manuscript. Since the salinity of applied water term enters linearly, for each approach we can calculate the change in the value of improved water quality relative to the baseline scenario by applying a simple ratio between the salinity of the new approach and the salinity of the baseline.

Improved water quality, however, does not make up the entirety of the private benefits. The second component is the value of augmented supply, which is not affected by the quality of existing irrigation water.

In Table C.1, we report the percentage change from the baseline scenario for improved water quality, total private benefits (assuming 2010 pre-drought values of water), as well as the share of cropped area with private benefit above the estimated cost of desalination, \$1 / m<sup>3</sup>. The more moderate assumptions of 350 and 585 mg/L show modest adjustments to total private benefits, but do not affect the result that no land is available that exceeds the current costs of desalination. While the more aggressive assumptions of 17 mg/L and 1708 mg/L change the computed private benefits more drastically, they still do not meaningfully adjust the amount of land in which total benefits exceeding system cost.

**Table S2. Sensitivity to Assumed Water Salinity Values. The total private benefits includes improved water quality as well as the value of augmented supply for 2010 (pre-drought conditions).**

	<b>Percentage Change, Improved Water Quality</b>	<b>Percentage Change, Total Private Benefits</b>	<b>Percentage Cropped Area with Private Benefit &gt; \$1/m<sup>3</sup></b>
<b>Baseline (490 mg/L)</b>	--	--	0%
<b>Modelled Salinity</b>	see Figure C.2A	see Figure C.2B	0%
<b>Average with Shallow Groundwater (585 mg/L)</b>	19.3%	6.7%	0%
<b>Surface Water (350 mg/L)</b>	28.6%	-9.8%	0%
<b>Groundwater, Low Estimate (17 mg/L)</b>	-96.5%	-29%	0%
<b>Groundwater, High Estimate (1708 mg/L)</b>	249%	86%	1.1%

The percentage change from baseline cannot be computed for the modelled water salinity results, as it will be different depending where in the distribution it is being assessed. Figure S4 shows the respective cumulative density functions with the modelled data. Since the baseline results use an average of the modelled results, the higher values are larger for the modelled results and the lower values are smaller. Despite being the higher values being larger than the baseline, 0% of the benefits exceed \$1 / m<sup>3</sup>, the estimated cost of desalination. We thus find, across a broad range of modelling assumptions, that our major conclusions are unaffected for reasonable values of the salinity of applied irrigation water.

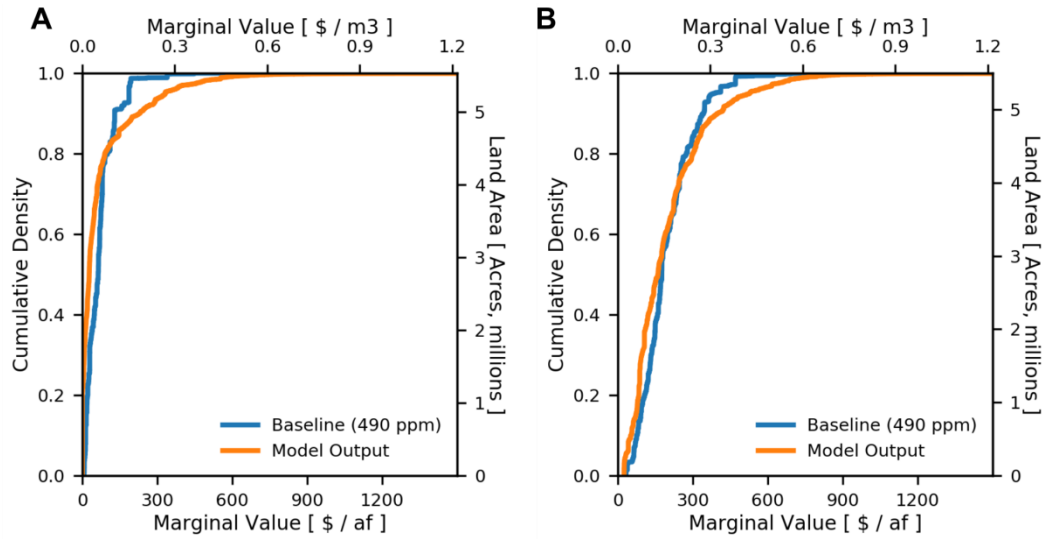


**Fig S4. Cumulative Density Function of Improved Water Supply (A) and Total Private Benefits (B) for baseline (490ppm) and spatially modelled output.**

## 11.4 List of Symbols

### 11.4.1 Variables

$R$ : Revenues

$S^S$ : Soil salinity

$b$ : Crop salt tolerance slope parameter

$p$ : Prices

$Y^M$ : Theoretical maximum yield

$L$  : Leaching fraction

$S^W$ : Water salinity

$W^T$ : Water treated

$\Pi$ : Profits

$W$ : Applied water

$v$ : Prices

$Y$ : Production  
 $\delta$ : Exponential response function intercept  
 $\gamma$ : Exponential response function elasticity  
 $X$ : Resources use  
 $\omega$ : Resource cost  
 $\tau$ : Factor productivity  
 $\beta$ : Resource coefficient  
 $\rho$ : CES elasticity parameter

#### *11.4.2 Subscripts:*

$g$ : Region  
 $i$ : SWAP crop group  
 $j$ : Resource  
 $ws$ : Water source (project water, surface diversion or groundwater)  
 $land$ : Land resource

## References

- [1] California Energy Commission (CEC) 2016 QFER CEC-1304 Power Plant Owner Reporting Database [http://energyalmanac.ca.gov/electricity/web\\_qfer/](http://energyalmanac.ca.gov/electricity/web_qfer/)
- [2] Environmental Protection Agency 2012 2011 National Emissions Inventory (NEI) Data <https://www.epa.gov/air-emissions-inventories/national-emissions-inventory-nei>
- [3] Environmental Protection Agency (EPA) 1998 Emission Factor Documentation for AP-42 Section 1.4 Natural Gas Combustion.
- [4] Muller N Z and Mendelsohn R 2007 Measuring the damages of air pollution in the United States *Journal of Environmental Economics and Management* **54** 1-14
- [5] Environmental Protection Agency 2016 Healthy Watersheds: Protecting Aquatic Systems through Landscape Approaches <https://www.epa.gov/hwp>
- [6] Hoffman G J and Van Genuchten M T 1983 Soil properties and efficient water use: water management for salinity control *Limitations to efficient water use in crop production* 73-85
- [7] California Department of Water Resources 2014 *California Water Plan Update 2013*. (Sacramento, CA: State of California)
- [8] Medellín–Azura J, Howitt R E, Lund J R and Hanak E 2008 The Economic Effects on Agriculture of Water Export Salinity South of the Delta Technical Appendix I *Comparing Futures for the Sacramento-San Joaquin Delta*. Public Policy Institute of California, San Francisco, CA
- [9] United States Geological Service (USGS) 2016b WaterQualityWatch <https://waterwatch.usgs.gov/wqwatch>
- [10] United States Geological Service (USGS), 2016a. Groundwater Ambient Monitoring and Assessment. <https://ca.water.usgs.gov/gama>
- [11] Bennett G L, Fram M S and Johnson T 2017 Groundwater-quality data in the Tulare Shallow Aquifer Study Unit, 2014-2015: Results from the California GAMA Priority Basin Project
- [12] Bennett P A, Bennett G L and Belitz K 2009 Groundwater quality data for the northern Sacramento Valley, 2007: Results from the California GAMA program
- [13] Burton C A and Belitz K 2008 Ground-Water Quality Data in the Southeast San Joaquin Valley, 2005-2006-Results from the California GAMA Program.

## APPENDIX E: Chapter 6

**Table S1. Univariate Out of Sample  $R^2$  values.**

	Agriculture Only Subset		Full Dataset	
	Maximum Composite	Average Composite	Maximum Composite	Average Composite
NDVI	-0.0092	-0.0082	0.0060	0.0085
EVI	-0.012	-0.010	0.0024	0.00055
CRSI	0.0018	0.0010	0.016	0.023
SAVI	-0.0092	-0.0082	0.0060	0.0085

**Table S2. Multivariate Out of Sample  $R^2$  values.**

	Agriculture Only Subset		Full Dataset	
	Maximum Composite	Average Composite	Maximum Composite	Average Composite
NDVI	-0.0013	-0.0027	0.037	0.019
EVI	-0.0050	-0.0050	0.022	0.0019
CRSI	0.0081	0.0068	0.051	0.035
SAVI	-0.0013	-0.0027	0.037	0.019
ANN	0.0030	-0.052	0.10	0.14

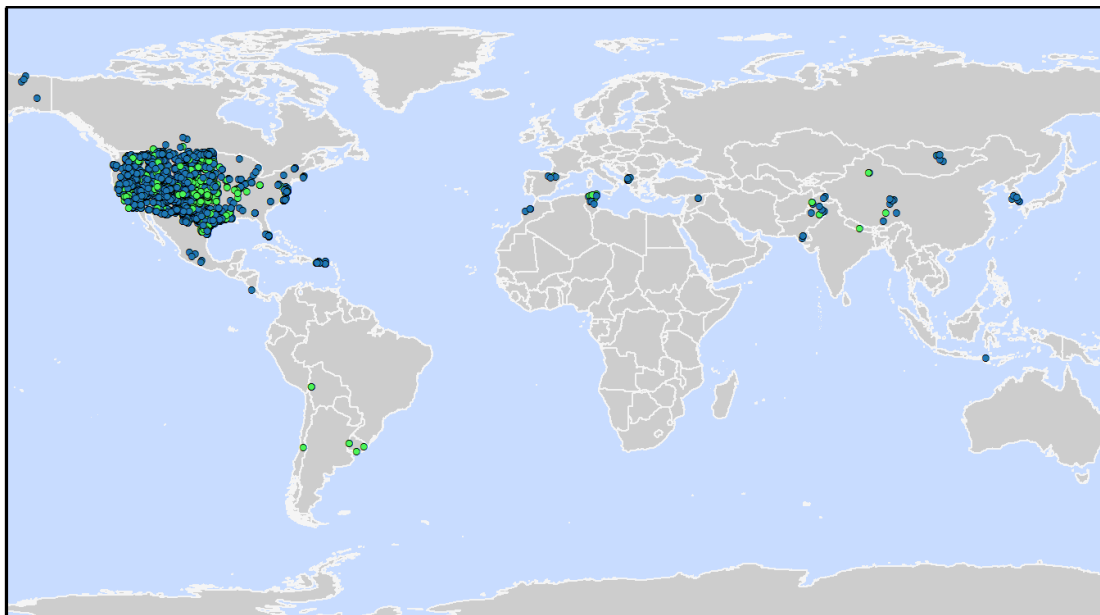


**Figure S1. Spatial Distribution of observations. Green dots represent observations on agricultural land as defined by GlobCover 2010, while blue dots represent observations on non-agricultural land.**